Static Resource Allocation in Space-division Multiplexing & Elastic Optical Networks

March ２０２０

Mingcong Yang

Static Resource Allocation in Space-division Multiplexing & Elastic Optical Networks

Graduate School of Systems and Information Engineering

University of Tsukuba

March ２０２０

Mingcong Yang

Contents

List of Figures

List of Tables

List of Acronyms

WDM	Wavelength-Division Multiplexing
RWA	Routing and Wavelength Assignment
SLE	Static Lightpath Establishment
VoD	Video-on-Demand
IoT	Internet of Things
EON	Elastic Optical Network
ITU-T	International Telecommunication Union Telecommunication
FS	Frequency Slice
CO-OFDM	Coherent Optical Orthogonal Frequency-Division Multiplexing
LAN	Local Area Network
DSB	Double-Side Band
ISI	Inter-Symbol Interference
ICI	Inter-Carrier Interference
N-WDM	Nyquist Wavelength-Division Multiplexing
DP	Dual-Polarization
BPSK	Binary Phase-Shift Keying
QPSK	Quadrature Phase-Shift Keying
8-QAM	8-ary Quadrature Amplitude Modulation
16-QAM	16-ary Quadrature Amplitude Modulation
BVT	Bandwidth Variable Transceiver
SDN	Software-Defined Network
ECC	Error-Correcting Code
ADC	Analog-to-Digital Conversation

DAC	Digital-to-Analog Conversation
Spe SpCh	Spectral Super-Channel
OXC	Optical Cross-Connect
BV-OXC	Bandwidth Variable Optical Cross-Connect
RSA	Routing and Spectrum Assignment
RMSA	Routing, Modulation, and Spectrum Assignment
RMSTA	Routing, Modulation, Spectrum, and Transceiver Assignment
TP	Transceiver Placement
ILP	Integer Linear Programming
MCLOD	Minimum Cost Lightpaths Assignment for Ordered Demands
KSP	K-Shortest Path
SMF	Single-Mode Fiber
SDM	Space-Division Multiplexing
SMFB	Single-Mode Fiber Bundle
MCF	Multi-Core Fiber
MMF	Multi-Mode Fiber
FMF	Few-Mode Fiber
FM-MCF	Few-Mode Multi-Core Fiber
ROADM	Reconfigurable Optical Add/Drop Multiplexer
SLC	Space Lane Change
RSSA	Routing, Spectrum, and Space Assignment
XT	Inter-Core Crosstalk
TA-MCF	Trench-Assisted Multi-Core Fiber
RSCA	Routing, Spectrum, and Core Assignment
MILP	Mixed Integer Linear Programming
CAPEX	Capital Expenditure
DSP	Digital Signal Processor
Spa SpCh	Spatial Super-Channel
Spa & Spe SpCh	Spatial and Spectral Super-Channel

Ind-Sw	Independent Switching
J-Sw	Joint Switching
FrJ-Sw	Fractional Joint Switching
WSS	Wavelength Selective Switch
RMSSGA	Routing, Modulation, Spectrum, Space, and Spatial Granularity Assignment
RR	Re-Routing
GVNA	Graph and Virtual Network-based Assignment
FF-SA	First-Fit Spectrum Allocation
PHBF	Product of the Hops and Bit-rate First
MRSA	Maximum Reuse Spectrum Allocation
LPF	Longest Path First
SimAn	Simulated Annealing
SCN	Spatial Channel Network

Acknowledgments

At first, special thanks to my advisor, professor Yongbing Zhang, for all his technical support and guidance, which make it possible in the realization of this thesis. His conscientious academic spirit and modest, open-minded personality inspire me not only in my academic study but also in my daily life.

I would like to thank Maiko Shigeno, the professor in Policy and Planning Sciences, the Graduate School of Systems and Information Engineering, University of Tsukuba, Japan, for her insightful and valuable comments, which helped me to improve my researches significantly.

I would like to thank Gangxiang Shen, the professor in the Graduate School of Electronics and Information, Soochow University, China, for his willingness to share his technical knowledge in this research field.

My heartiest thanks flow to my friends and my classmates who have given me their help in my daily life during the past three years.

I want to express my sincere gratitude to the *EPSON international scholarship foundation* for their financial support by means of a full scholarship. It would have been very hard to complete my Ph.D. course without their support.

Finally, my deep gratefulness to my beloved wife Jun Pi and my parents, for their love, great comprehension and support during these years, which are the key pillars to my Ph.D. degree.

Abstract

With the development and increasing popularity of cloud computing, video-on-demand, Internet of things, and other emerging Internet services, network traffic is growing at an extremely rapid rate. Therefore, from the deployment of the wavelength-division multiplexing-based optical network at the beginning of the 2000s, optical network architecture has undergone several significant evolutions to meet the rapid increase of network traffic. The first evolution from the conventional wavelength-division multiplexing-based optical network to elastic optical network induced by the introduction of orthogonal frequency-division multiplexing, Nyquist wavelength-division multiplexing, and distance-adaptive modulation technologies has prominently raised the spectral efficiency. Moreover, due to the capacity limits of conventional single-mode fibers, that is, the so-called nonlinear Shannon limit, the optical network architecture based on space-division multiplexing technology has been proposed to satisfy further growth of network traffic, which brought a further evolution to the optical network architecture.

From the perspective of network planning, the resource allocation problem has also changed several times to accord with the new features provided by every evolution of optical network architecture. Generally, resource allocation in optical networks is divided into two categories: the dynamic problem and the static problem. In the dynamic case which emerges during the network operation, it is assumed that connection requests are unknown in advance, and they arrive then disappear stochastically one-by-one. The resources required to establish the connection requests are assigned dynamically according to the current state of the network. The objective of the dynamic problem is to minimize the network blocking probability or to maximize the network throughput within an acceptable blocking probability (e.g., 1%). In the static case which mainly relates to the network planning phase, the traffic matrix containing a set of connection requests that must be established in the network is known in advance, and these connection requests must be assigned at the same time. In the static problem, the main objective is to minimize the number of used/required wavelengths or frequency slices in the network, considering the following reasons:

- Minimizing the number of used frequency slices is equivalent to maximizing the number of frequency slices that are not occupied in the network, which are available for future connec-

tion requests – assuming that the network scenario is semi-dynamic, we optimize the network by re-assigning the currently established connection requests as a static set, and the dynamic connection requests arrive in the network hereafter. Indeed, the semi-dynamic scenario also corresponds to the real-world scenario. In the real-world scenario, some lightpaths are pre-established between node pairs according to the predicted traffic volume matrix. Such established lightpaths will not be changed frequently, because an approximately 3.05 seconds setup time is required to establish a new lightpath. Therefore, minimizing the number of used frequency slices is to reduce the congestion level of the network, so as to satisfy more subsequent connection requests.

- Another reason is that there may exist different optical network systems. In general, one system with 320 frequency slices is much cheaper than the one with 640 frequency slices. Therefore, if we can reduce the number of required frequency slices smaller than 320 in the network planning phase, great cost-savings can be achieved.

In the wavelength-division multiplexing-based optical network, the resource allocation problem is called the routing and wavelength assignment problem. The spectrum on an optical fiber is divided into 80 numbers of available wavelengths which are fixed at 50 GHz in the typical wavelength-division multiplexing-based optical network. A lightpath and wavelength must be assigned to each connection request. The indices of these wavelengths must be consistent along the entire lightpath and non-overlapped on a common link. Such constraints are called wavelength continuity and no-overlapping.

Compared to the wavelength-division multiplexing-based optical network, the spectrum can be divided more flexibly in the elastic optical network, such as a division of 320 numbers of 12.5 GHz frequency slices or 640 numbers of 6.25 GHz frequency slices. The bandwidth variable transceivers and optical cross-connects enable us to meet connection requests with varying bit-rate and establishing lightpaths flexibly by using different numbers of frequency slices as needed, which can achieve higher spectral efficiency. However, as a negative effect, these frequency slices should be contiguous, which introduces an additional constraint of spectrum contiguity in resource allocation. Therefore, the resource allocation problem became to the routing and spectrum assignment problem in the elastic optical network.

Although the elastic optical network is a promising technology that leads to more efficient utilization of spectrum resource than does traditional wavelength-division multiplexing-based optical network, the growth in the transmission capacity of standard single-mode fiber has dramatically slowed because the transmission capacity per fiber is close to the nonlinear Shannon limit of the existing single-mode fiber, while the strongly continuous increasing future Internet traffic will inexorably reach this capacity limit. Therefore, in addition to the higher spectral efficiency achieved by

the elastic optical network, another way to overcome the capacity limitation is to get more available spectrum resources. The space-division multiplexing has emerged as a viable solution, whose basic concept is expanding the available optical transmission dimension of the space domain from the current one to multiple parallel dimensions. The expansion of the space domain will increase network capacity to higher orders of magnitude compared with what can be achieved with the single-mode fiber-based optical network infrastructure, enabling the network capacity to keep pace with traffic growth beyond the petabit-per-second level.

However, considering the expansion of spatial dimensions, it is necessary to choose appropriate spatial dimension(s) to each connection request simultaneously while allocating the spectrum and lightpath, which makes the resource allocation problem more complicated. In this case, the resource allocation problem is the so-called routing, spectrum, and space assignment problem. Of course, there also exist several extensions of this problem which considered additional features brought by the space-division multiplexing technology, such as cross-talk awareness, space lane change, and spatial granularity.

In summary, the evolutions of optical network architecture always introduce opportunities and challenges to the resource allocation in optical networks. The specially designed algorithms are essential to address the resource allocation problems owing to these evolutions. In this thesis, we detailedly discussed static resource allocation problems in recent years and summarized our contribution to this research field.

Chapter 1

Introduction

The application of optical transmission for the long-haul wired transmission system started from the nineteen eighty. Compared to the electrical transmission system, the time-division multiplexing-based optical transmission system achieved 10 times capacity up to 100 Gbps, and thanks to the wavelength-division multiplexing technology, the capacity of the optical transmission system increased up to 400 Gbps at the beginning of the 2000s. Due to the development of emerging Internet services, such as the internet of things, cloud computing, video on demand, 5G, internet traffic continuously grows in the past decade. The optical network has undergone significant changes to deal with this problem, from the earliest WDM-based optical networks to the elastic optical network, further to the space-division multiplexing network. However, the evolutions of the optical networks always introduce opportunities and challenges on resource allocation, and specially designed algorithms are essential to address the resource allocation problems to fit the features brought by the new network architecture.

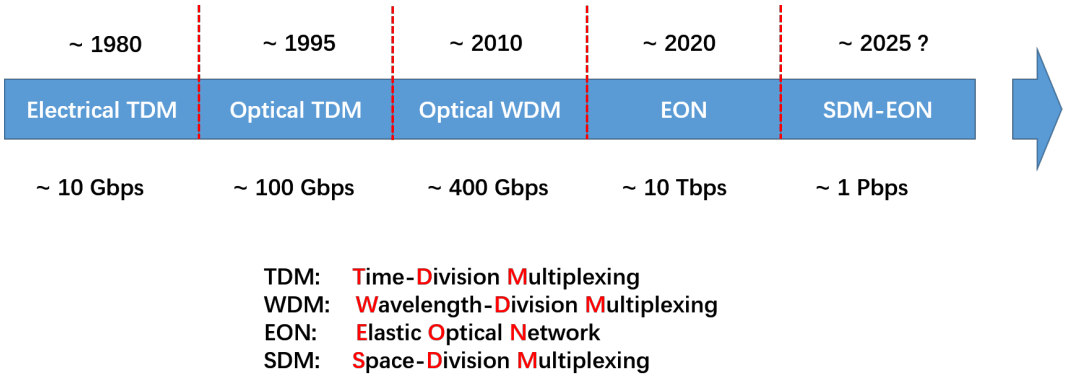

Figure 1.1: The evolutions of the long-haul wired terrestrial transmission system in the past few decades.

In this chapter, we begin with an introduction of the traditional wavelength-division multiplexing optical network, as well as the routing and wavelength assignment problem. Then, we make an overview of the relevant background technologies used in elastic optical network and the space-

division multiplexing optical network, as well as the routing and spectrum assignment problem and the routing, spectrum, and space assignment problem. In addition, we explain how these factors are related to the subject of our research problems listed as follows:

- The routing, modulation, spectrum, and transceiver assignment problem.
- The routing, spectrum, and core assignment with inter-core cross-talk management problem.
- The routing, modulation, spectrum, space, and spatial granularity assignment problem.

Moreover, we discuss the previous works related to resource allocation and clarify our contribution to this research field.

1.1 Wavelength-division multiplexing-based optical networks

1.1.1 Optical fiber transmission

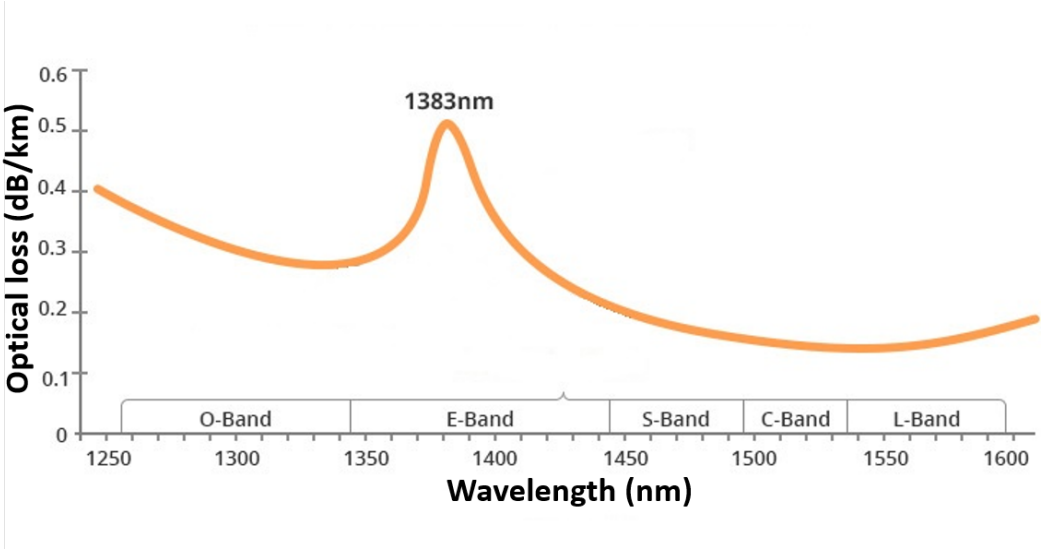

Figure 1.2: Wavelength bands in optical transmission: Optical loss (dB/km) V.S. wavelength (nm).

Compared to other wired physical transmission media, optical fiber transmission has been the unique option of the terrestrial transmission system currently, because of its wide available bandwidth and low loss. In the case of ensuring the optical loss of less than 0.5 dB/km, the total bandwidth of an optical fiber is approximately 400 nm. Generally, the available bandwidth is divided into several wavelength bands as shown in Fig. 1.2 [1, 2]. We can see that the band which achieves the minimum optical loss is the C-band which ranges from 1530 nm to 1565 nm. Besides, since the 1530 nm approximately corresponds to 196 THz, and 1565 nm corresponds to 192 THz, the available spectrum spanned by the C-band is about 4 THz. Consequently, due to the advantage of the low loss of the C-band, it is quite favorable for optical transmission with long-distance [1, 2].

1.1.2 Wavelength-division multiplexing transmission technology

The concept of wavelength-division multiplexing (WDM) was first presented in 1978, and be realized in the laboratory by 1980 [1]. As shown in Fig. 1.3, the WDM technology can multiply the capacity of a single optical fiber by multiplexing a number of optical carriers onto it. In other words, optical carriers can share a single optical fiber if different wavelengths are assigned to them.

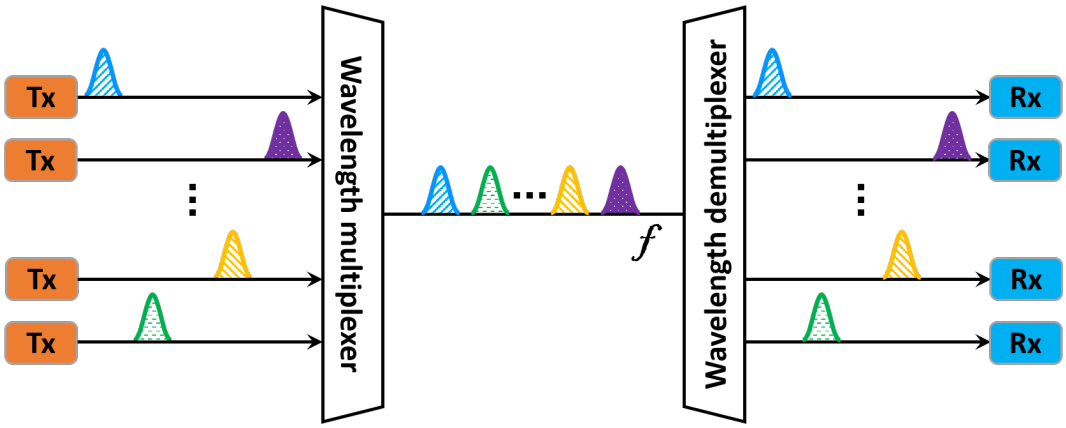

Figure 1.3: Illustration of wavelength-division multiplexing technology.

A typical WDM-based optical network uses the C-Band transmission window with 50 GHz channel spacing, that is, the total 4 THz spectrum on the C-band are divided into 80 numbers of available wavelengths, and each of which occupies 50 GHz spectrum [1–3]. In an optical channel, the spectrum used to carry the data is called the optical carrier, which should be less than 50 GHz, because a switching guard-band that occupies a certain spectrum is necessary between two optical carriers to achieve all-optical switching and routing. In general, the maximum supportable bit-rate of a single optical carrier is 40 Gbps (or 100 Gbps with shorter transmission reach) [3, 4]. In this case, for two connection requests with 60 Gbps and 90 Gbps traffic volume, the total spectrum requirement used to serve these two connection requests is 250 GHz, as illustrated in Fig. 1.4.

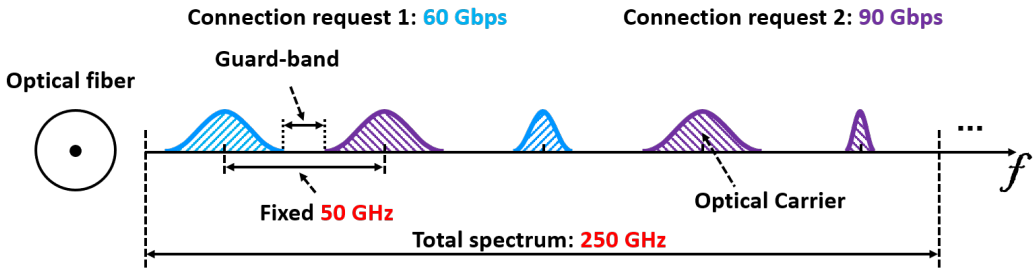

Figure 1.4: Illustration of WDM transmission for connection requests with 60 Gbps and 90 Gbps traffic volume.

1.1.3 Routing and wavelength assignment problem

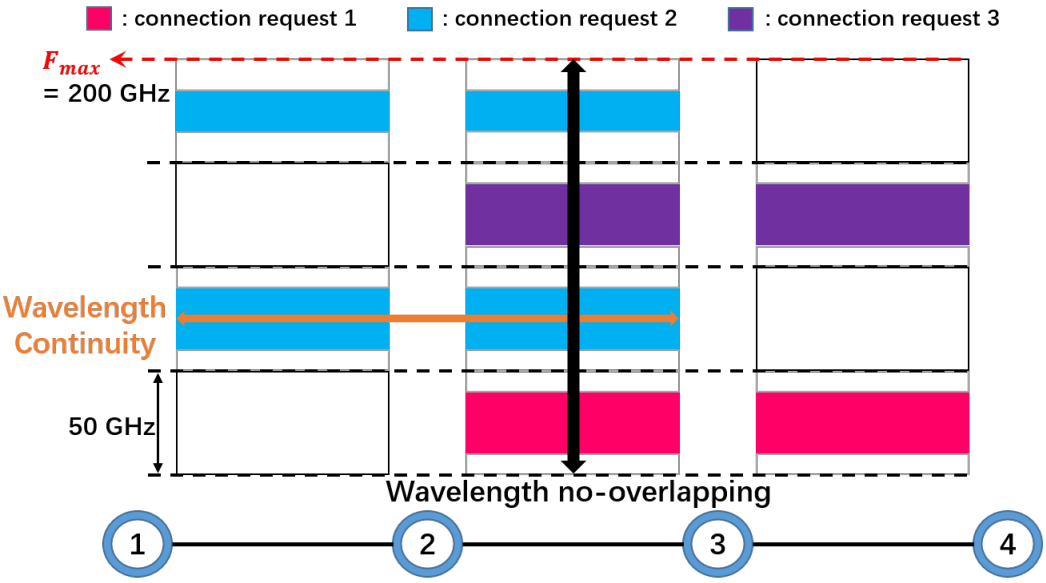

Figure 1.5: Illustration of wavelength continuity and no-overlapping constraints in RWA problem.

In this section, we introduce the routing and wavelength assignment (RWA) problem [5–8], which is also called as the static lightpath establishment (SLE) problem in some literature [5]. In (static) RWA problem, the network topology and connection requests are known in advance, and the typical objective is to minimize the spectrum usage (i.e., the required number of wavelengths) while a lightpath is assigned for each connection request. It is worth noting that wavelengths on all of the links along a lightpath must be the same to ensure all-optical transmission, as shown in Fig. 1.5. This constraint is the so-called wavelength continuity. Besides, another straightforward constraint called wavelength no-overlapping also should be considered when establishing lightpaths, which indicates that a single wavelength on a link is unable to be assigned to two lightpaths at the same time. The RWA problem has been proved to be an NP-hard problem [5, 9]. The approaches used to solve the RWA problem are usually the integer linear programming and the heuristic (greedy) algorithm, which have been widely investigated in many previous works [5–8].

1.2 Elastic optical networks

With the development and increasing popularity of cloud computing, video-on-demand (VoD), Internet of things (IoT) and other emerging Internet services, network traffic is growing explosively [10]. Traditional optical networks based on WDM technology allow a single wavelength to support a bit-rate of 40 Gbps. However, such a fixed frequency grid-based optical network suffers low spectral efficiency, resulting in a waste of spectrum resource as shown in Fig.2. This shortcom-

ing will eventually restrict data transmission services in the future.

To overcome the shortcoming above, the concept of elastic optical networks (EONs) has been proposed to achieve high spectral efficiency for the next-generation optical network [11, 12]. The key feature of EON is the much higher flexibility on the spectrum assignment. Conforming to the recommendation of the International Telecommunication Union Telecommunication (ITU-T) Standardization Sector G.694.1 [13], the total 4 THz spectrum resource can be divided into 320 numbers of 12.5 GHz frequency slices (FSs), and the central frequency granularity reduced to 6.25 GHz. Therefore, flexible optical channels that occupy different numbers of FSs with channel spacing equaling the integer multiple of 6.25 GHz can be created in EONs, resulting in much higher utilization of the spectral resource. In other words, flexible optical channels that carry different bit-rates can be created as needed to meet connection requests with varying traffic volumes. This flexibility is implemented by multiple advanced technologies which are detailed in the following.

1.2.1 Coherent optical orthogonal frequency-division multiplexing transmission technology

The coherent optical orthogonal frequency-division multiplexing (CO-OFDM) transmission technology [14–18] has been widely implemented in many other transmission systems - such as wireless local area network (LAN) [19] - before it is applied in the optical transmission as a solution to overcome the shortcoming of the traditional WDM-based transmission. As shown in Fig.1.6, in the CO-OFDM-based optical transmission, an optical carrier is composed of multiple sub-carriers, each of which carries a low data rate. The spectrum occupied by two adjacent subcarriers can overlap because they are orthogonally modulated, leading to high spectral efficiency.

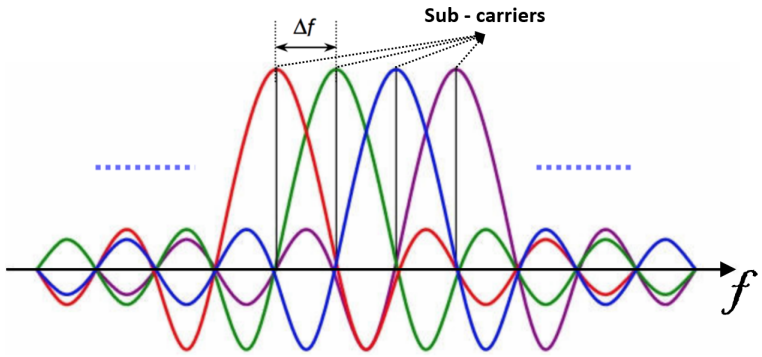

Figure 1.6: Illustration of CO-OFDM transmission technology.

Let us consider that a CO-OFDM optical carrier is composed of N numbers of sub-carriers with $\triangle_f$ spectrum occupation. Since the CO-OFDM is a double-side band (DSB) modulation technology [20], the maximumly supportable symbol-rate of the carried data for each sub-carrier is $0.5 \cdot \triangle_f$ Gbaud (baud: symbols per second). Therefore, the total spectrum occupied by this optical carrier

is $0.5 \cdot (N+1) \cdot \triangle_f$ GHz, and total supportable symbol-rate is $0.5 \cdot N \cdot \triangle_f$ Gbaud. Consequently, in theory, the supportable symbol-rate per Hertz of the CO-OFDM transmission technology is $\frac{N}{N+1}$ baud/Hz, which is close to the upper-bound of 1 baud/Hz (i.e., the Nyquist rate in the case of pass-band transmission) when N is large. However, this theoretical rate of the CO-OFDM transmission technology is difficult to reach in the real-world case, because of the inter-symbol interference (ISI) and inter-carrier interference (ICI) [1].

1.2.2 Nyquist wavelength-division multiplexing transmission technology

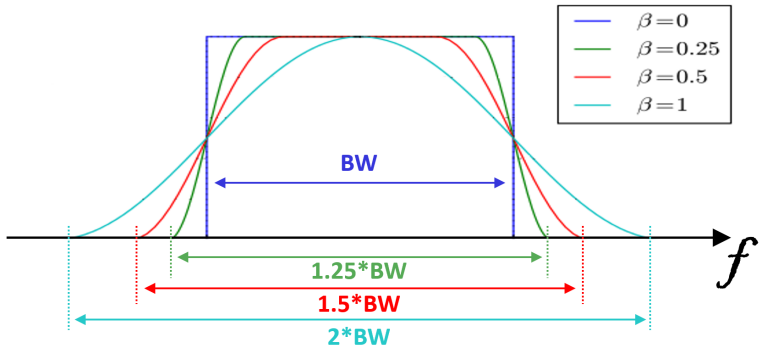

Figure 1.7: Illustration of Nyquist-WDM transmission technology.

As shown in Fig. 1.7, The Nyquist wavelength-division multiplexing (N-WDM) is a promising technology that can achieve high spectral efficiency by shaping the optical carrier into a square-like power spectrum [21–24]. In the ideal case, the occupied spectrum of a Nyquist-shaped optical carrier is identical with the symbol-rate of the carried data, that is, the supportable symbol-rate per Hertz of the N-WDM transmission technology can reach 1 baud/Hz. However, due to the resolution of a Nyquist-shaping filter is impossible to be infinitely fine in the real-world case, there is a certain spectral penalty that exists due to the imperfect shaping. If we assume that the BW is the spectrum occupation of the ideal Nyquist-shaped optical carrier, the real spectrum occupation will be $BW \cdot (1+\beta)$, where the β is the filter roll-off factor which is related to the resolution of the applied filter. Therefore, similar to CO-OFDM, the supportable symbol-rate per Hertz of the N-WDM is less than that of the ideal case (i.e., $\beta = 0$), and the Nyquist-shaped optical carrier is actually like a trapezoid.

1.2.3 Adaptive modulation transmission technology

In this thesis, four different modulation formats are considered, which are dual-polarization (DP) binary phase-shift keying (BPSK), quadrature phase-shift keying (QPSK), 8-ary quadrature amplitude modulation (8-QAM), and 16-ary quadrature amplitude modulation (16-QAM), respectively. The transmission reach and modulation levels (in bits per symbol) for these modulation formats are

shown in Table 1.1. It is worth noting that the transmission reach depends on many factors, such as design margins and fiber types, and many different reach models have been proposed in the literature. In our works, the transmission reach refers to the data proposed in Refs. [25–27] in the case of CO-OFDM-based optical networks, and refers to the data proposed in Refs. [28, 29] in the case of N-WDM-based optical networks.

Table 1.1: Transmission reach and modulation levels for different modulation formats.

Modulation formats		DP-BPSK	DP-QPSK	DP-8-QAM	DP-16-QAM
Transmission reach (km)	CO-OFDM	4000	2000	1000	500
	N-WDM	6300	3500	1200	600
Modulation level (bits/symbol)		2	4	6	8

From Table 1.1, we can see that a modulation format with a higher modulation level can support more bits per symbol but meanwhile has a shorter transmission reach. Therefore, for connection requests transmitted along lightpaths with different path-lengths, different modulation formats can be applied to offer different spectral efficiencies. For example, in the ideal case, the N-WDM-based transmission can maximumly support 1 baud/Hz (1 symbol/s/Hz), thus, offering spectral efficiency of 2 bit/s/Hz, 4 bit/s/Hz, 6 bit/s/Hz, and 8 bit/s/Hz under DP-BPSK, DP-QPSK, DP-8-QAM, and DP-16-QAM, respectively.

1.2.4 Flexible single-carrier transmission

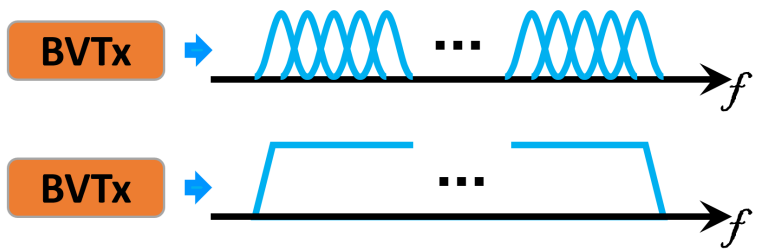

Figure 1.8: Illustration of bandwidth variable transceiver (BVT) & flexible optical carrier.

In EONs, the total 4 THz spectrum resource on the C-band is divided into 320 numbers of 12.5 GHz FSs. As shown in Fig. 1.8, the software-defined network (SDN)-based programmable bandwidth variable transceiver (BVT) [30–35] enables us to create a flexible optical carrier that occupies varying numbers of FSs by adjusting its symbol-rate adaptively to meet connection requests with different traffic volumes (i.e., bit-rate). For example, the adaptive symbol-rate of BVTs can be implemented by adjusting the number of the sub-carriers in the case of CO-OFDM, or by adjusting the width of the square-like power spectrum directly in the case of N-WDM. Moreover, in traditional WDM-based optical networks, changing the modulation format requires the use of a different

transceiver. In contrast, different modulation formats can be supported by a single BVT in EONs. Consequently, the flexible single-carrier transmission leads to much higher transmission flexibility than the traditional WDM-based transmission, leading to higher spectral efficiency.

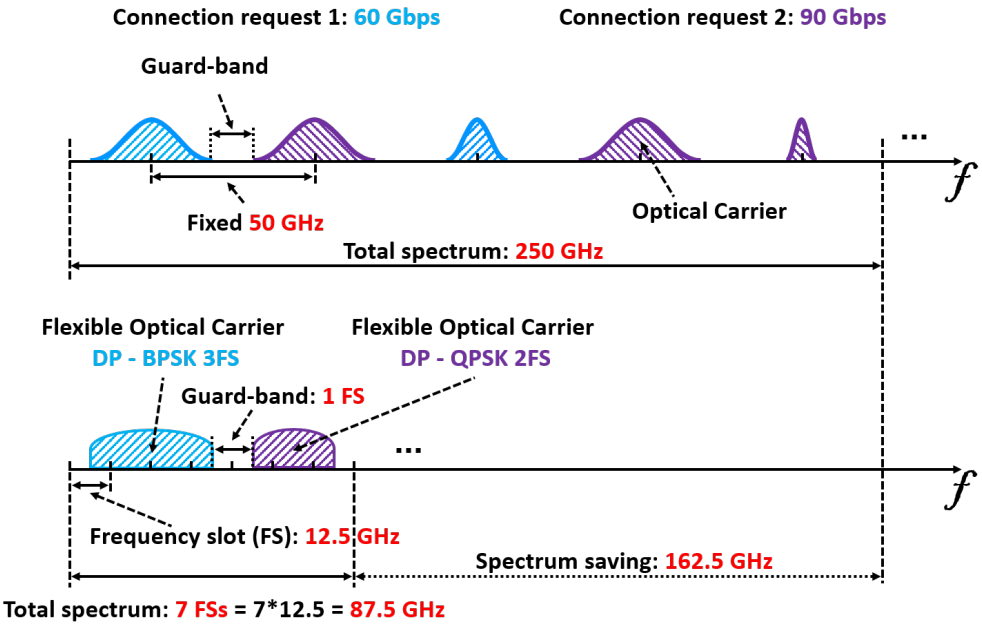

Figure 1.9: Illustration of WDM-based transmission V.S. flexible single-carrier transmission (the ideal case).

A simple example is shown in Fig. 1.9. The same with what is shown in Fig. 1.3 for WDM-based transmission, we assume that there are two connection requests with 60 Gbps and 90 Gbps traffic volume, whose lightpath lengths are 3800 km and 2400 km, respectively. According to Table 1.1, the DP-BPSK (modulation level: 2 bits/symbol) and DP-QPSK (modulation level: 4 bits/symbol) can be applied for them. The required symbol-rate of the BVT for each connection request is equal to the required bit-rate divided by the modulation level, which equals 60/2 = 30 Gbaud and 90/4 = 22.5 Gbaud, respectively. In the case of CO-OFDM-based transmission, we assume that each sub-carrier occupies $\triangle_f$ = 1 GHz spectrum, and support 0.5 Gbaud (i.e., the ideal case). Therefore, N = 60 and 45 numbers of sub-carriers are required, leading to 30.5 GHz and 23 GHz total spectrum requirement (refers to Section 1.2.1) for these two connection requests, respectively. On the other hand, the total spectrum requirement for N-WDM-based transmission is 30 GHz and 22.5 GHz, respectively, which are directly equal to the symbol rate (i.e., the ideal case). However, note that the spectrum granularity is 12.5 GHz in EONs, and therefore, in both the cases of CO-OFDM and N-WDM, the flexible optical carrier should occupy 37.5 GHz (3 FSs) and 25 GHz (2 FSs) for the two connection requests, respectively. Moreover, the same with the traditional WDM-based transmission, a certain width of switching guard-band should be allocated to sperate two flexible

optical carriers. A switching guard-band of 12.5 GHz (0.5 FS on both sides) is assumed in the example. Consequently, as shown in Fig. 1.9, the flexible single-carrier transmission achieves a significant saving of 162.5 GHz on the spectrum.

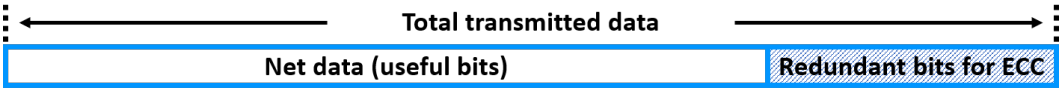

Figure 1.10: Illustration of error-correcting code (ECC).

Unfortunately, in the real-world case, there are many issues that influence the spectral efficiency in both the cases of CO-OFDM-based and N-WDM-based transmission, such as the physical issues we mentioned in Section 1.2.1 and Section 1.2.2, and the redundant bits for error-correcting code (ECC) [36] as shown in Fig.1.10 et al., resulting in more spectrum occupation compared to the ideal case as shown in Fig. 1.9. To be able to focus more on the resource allocation problems regardless of these complicated issues, there is a general assumption which is widely applied in the literature for flexible single-carrier transmission, that is, using the required number of FSs under a given modulation format directly to represent the traffic volume [Gbps] of the connection requests [37–42]. For example, considering the inevitable adverse issues above, we assume that the supportable bit-rate under DP-BPSK for a single FS spectrum (12.5 GHz) should less than the ideal 25 Gbps, which equals 15 Gbps. Under this assumption, the supportable bit-rate per FS will become 30, 45, and 60 Gbps for DP-QPSK, DP-8-QAM, and DP-16-QAM, respectively. Therefore, "connection requests with 60 Gbps and 90 Gbps traffic volume" can be represented by "connection requests required $\lceil 60/15 \rceil = 4$ FSs under DP-BPSK and $\lceil 90/30 \rceil = 3$ FSs under DP-QPSK", leading to a few additional spectrum occupations (as shown in Fig. 1.11) compared to the ideal case.

1.2.5 Spectral super-channel transmission

In the previous Section 1.2.4, we introduced flexible single-carrier transmission and compared its spectral efficiency with that of the traditional WDM-based transmission. Nevertheless, due to the limitation of the current analog-to-digital/digital-to-analog conversation (ADC/DAC) technology, the supportable symbol-rate of a BVT is unable to increase without bound, resulting in the flexible single-carrier transmission is more appropriate for low traffic volumes [30]. For example, to support a connection request with 400 Gbps traffic volume under DP-BPSK, we require a BVT that supports at least 200 Gbaud symbol-rate. Indeed, we require a higher symbol-rate in the real-world case because of the ECC. However, to the best of our knowledge, the transceiver with the currently highest symbol-rate was reported in Ref. [43], whose symbol-rate equals 107 Gbaud. Therefore, considering the large traffic volumes in the future, spectral super-channel transmission technology has been proposed to circumvent this limitation.

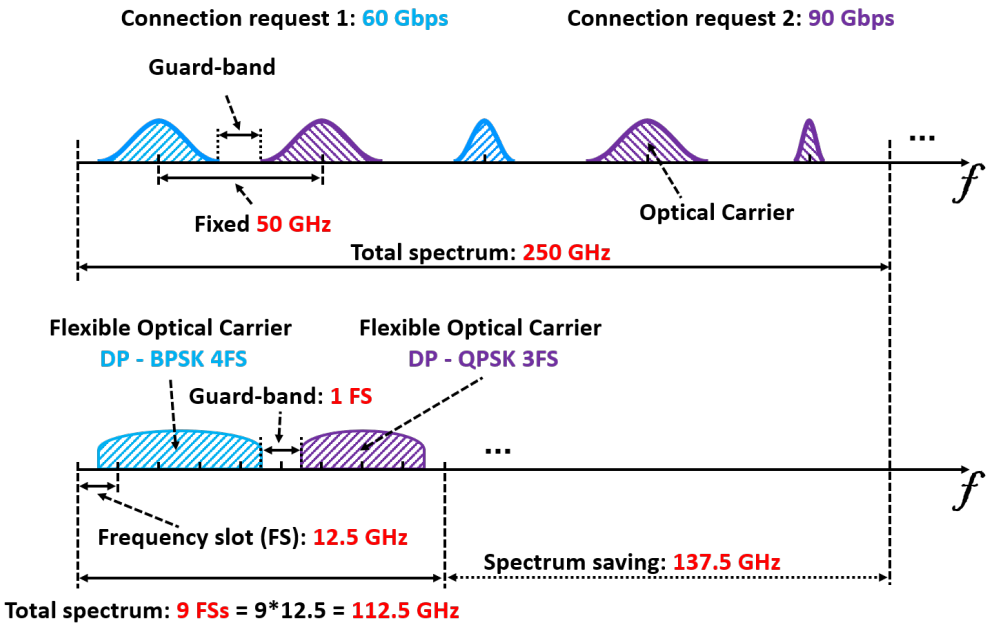

Figure 1.11: Illustration of WDM-based transmission V.S. flexible single-carrier transmission (the real-world case).

A spectral super-channel (Spe SpCh) [14, 18, 21, 23, 24, 44, 45] consists of multiple parallel adjacent optical carriers, each of which is generated by a transceiver with fixed symbol-rate. These N-WDM-based [21, 23, 24] or CO-OFDM-based [14, 18, 44, 45] optical carriers can be placed over the spectral domain without switching guard-bands between each other. Fig. 1.12 shows an Spe SpCh composed of 4 optical carriers placed in accordance with the ITU-T 12.5 GHz grid.

In Fig. 1.12, the symbol-rate of each transceiver is assumed to be 25 Gbaud, each of which generates an optical carrier supporting 50 Gbps traffic volume under DP-BPSK (i.e., without considering ECC). The resolution of the Nyquist shaping filters is assumed to be 3.125 GHz, leading to approximately 31.64 GHz spectrum occupation for each optical carrier [30]. Moreover, in accordance with the ITU-T 12.5 GHz spectrum granularity, the occupied spectrum of optical carriers should be the integer multiple of 12.5 GHz, that is, 3 FSs. Therefore, it is obvious that an N-WDM-based Spe SpCh composed of 4 optical carriers shown in Fig. 1.12 can support 200, 400, 600, and 800 Gbps traffic volume under DP-BPSK, DP-QPSK, DP-8-QAM, and DP-16-QAM, respectively, and occupies 13 FSs (162.5 GHz) total spectrum (including switching guard-bands).

Indeed, similar to the case of flexible single-carrier transmission, considering the inevitable redundant bits for ECC, we may need a transceiver with more than 25 Gbaud to support 50 Gbps net traffic volume under DP-BPSK. A general assumption for the symbol-rate of each transceiver is 28 Gbaud [26, 27] or 32 Gbaud [46], supporting 50 Gbps net traffic volume under DP-BPSK, that is, considering 3 GBaud and 7 GBaud for ECC, respectively. It is worth noting that there are

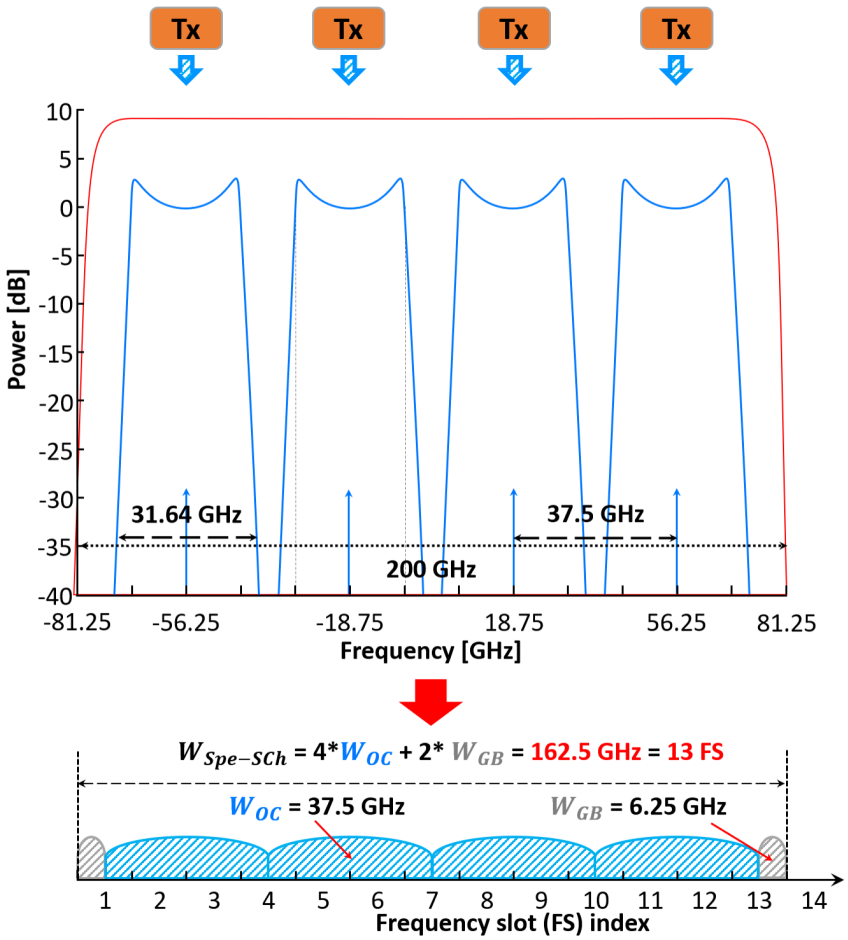

Figure 1.12: Illustration of a spectral super-channel composed of 4 Nyquist-shaped optical carriers spaced in accordance with the ITU-T 12.5 GHz grid.

many works that did not discuss the ECC in detail, such as the assumption of 32 Gbaud transceivers with 64 Gbps supportable traffic volume under DP-BPSK in Refs. [28, 47–50]. This indicates that the supportable traffic volume for each transceiver considered in these works actually does not represent the net traffic volume. Overall, although the symbol-rate of transceivers is varying in the previous works and there may also be different considerations of ECC, the spectrum occupations per optical carrier are the same in all previous works, that is, 3 FSs of 12.5 GHz. Consequently, for transceivers with different symbol-rates ranging from 25 Gbaud to 32 Gbaud, we consider that they are equivalent to what is shown at the bottom of Fig. 1.12.

As with the evaluation of the spectral efficiency in flexible single-carrier transmission, we show the spectrum occupation in the case of Spe SpCh in Fig. 1.13. Of course, two connection requests with the same 60 Gbps and 90 Gbps traffic volume are considered, and they are assumed to be transmitted under DP-BPSK and DP-QPSK with 50 Gbps and 100 Gbps supportable bit-rate per optical carrier. As shown in Fig. 1.13, in For the 60 Gbps connection request, we require $\lceil 60/50 \rceil$

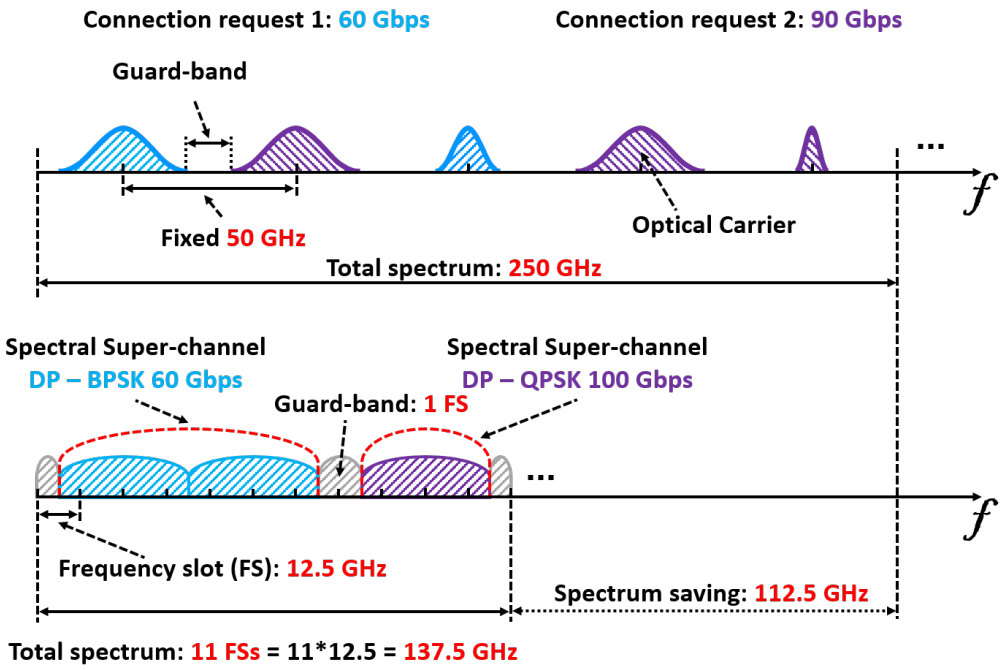

Figure 1.13: Illustration of WDM-based transmission V.S. spectral super-channel transmission.

= 2 optical carriers occupying 6 FSs. In addition, for the 90 Gbps connection request, we require $\lceil 90/100 \rceil$ = 1 optical carrier occupying 3 FSs. Moreover, note that the switching guard-bands between the optical carriers that belong to a single Spe SpCh are unnecessary, but they are necessary between two Spe SpCh to guarantee the effect of optical switching cascading [51]. Therefore, the total required spectrum to serve these two connection requests are 11 FSs. We can see that compared to the case of flexible single-carrier transmission, the Spe SpCh transmission requires more spectrum because the use of fixed symbol-rate transceivers inevitably leads to certain waste of spectrum. Nevertheless, the Spe SpCh transmission also achieves 112.5 GHz (9 FSs) spectrum saving compared to the traditional WDM-based transmission, and, as we have discussed above, it is more suitable for larger traffic volume compared to the flexible single-carrier transmission.

1.2.6 Bandwidth variable optical cross-connect

In Section 1.2.4 and Section 1.2.5 above, we have introduced two transmission technologies (i.e., flexible single-carrier transmission and Spe SpCh transmission) to generate optical-channels that can support flexible bit-rates. These flexible optical-channels occupy different numbers of FSs to meet connection requests with different traffic volumes. However, in traditional WDM-based optical networks, the switching positions of the optical cross-connect (OXC) are spaced in accordance with a fixed 50 GHz as shown in Fig. 1.14.a, which is unable to be applied in EON because the required spectra of flexible optical-channels are varying. Therefore, bandwidth variable optical cross-connect

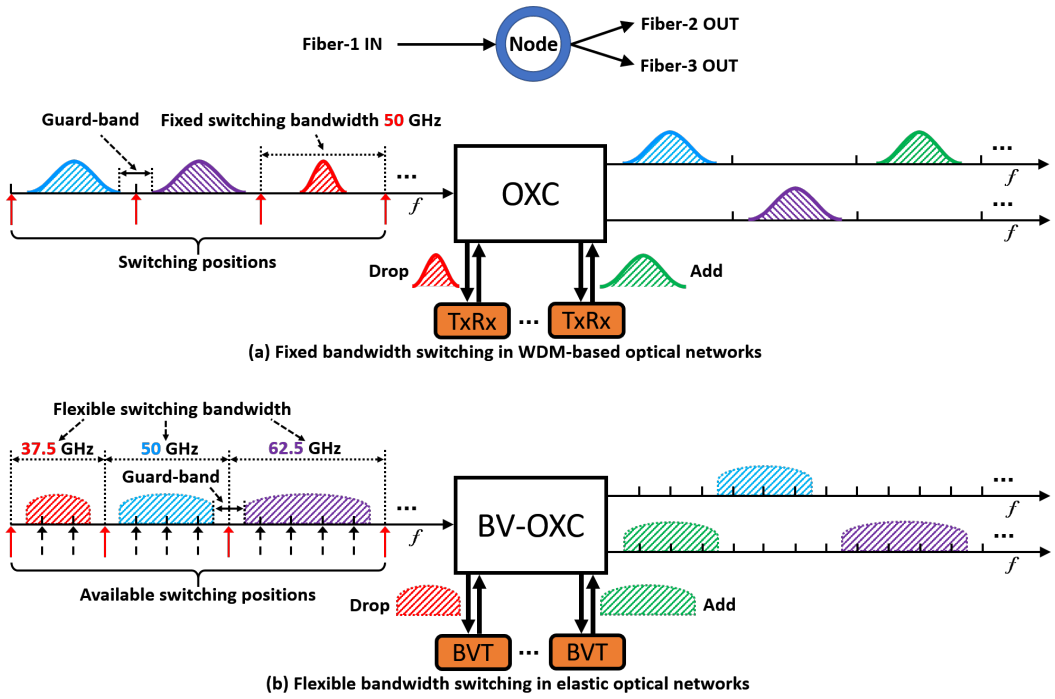

Figure 1.14: Comparing of traditional optical cross-connect and bandwidth variable optical cross-connect.

(BV-OXC) as shown in Fig. 1.14.b has been proposed in order to route/switch these flexible optical-channels.

From Fig. 1.14, we can see that different from the traditional optical cross-connect, the available switching positions are spaced in accordance with a 12.5 GHz grid to support flexible optical switching. As a result, the combination of the flexible optical-channel and BV-OXC enables us to achieve a successful flexible transmission between any source-destination node pair in EONs.

1.2.7 Routing and spectrum assignment

The problem of routing and spectrum assignment (RSA) in EONs is similar to that of RWA problem in WDM-based optical networks. As we discussed above, the 4 THz total spectra are divided into 320 numbers of fine 12.5 GHz FSs in EONs, and the objective of RSA is to minimize the required FSs (i.e., occupied spectrum) in the network while assigning a lightpath and FSs to each connection request. However, in EONs, there is a difference that an additional constraint of the so-called spectrum contiguity should be considered when assigning the FSs, that is, the FSs assigned to each connection request should be contiguous considering the feature of flexible single-carrier transmission and/or Spe SpCh transmission (see Section 1.2.4 and Section 1.2.5). Fig. 1.15 illustrates the spectrum continuity, contiguity, and no-overlapping constraints in EONs by a simple example. Moreover, as we have stated before, compared to the traditional WDM-based optical networks, in

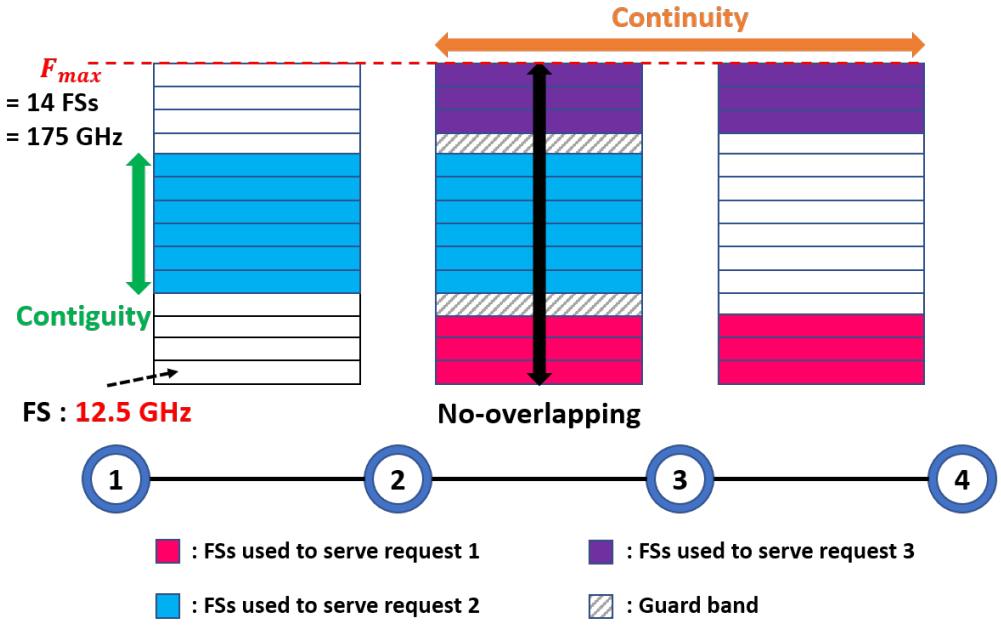

Figure 1.15: Illustration of spectrum continuity, contiguity and no-overlapping constraints in RSA problem.

EONs, the adaptive modulation allows us to select an appropriate modulation format for each connection request depending on its path-length, leading to higher spectral efficiency. Therefore, if the adaptive modulation is taken into account, the RSA problem will be extended to a more complicated routing, modulation, and spectrum assignment (RMSA) problem. Finally, as the evolutionary problems of RWA, the RSA and RMSA problems have also been proved to be NP-hard [52]. Many works concerning RSA and RMSA problems already exist, such as Refs. [37–42, 52], and please refers to the surveys [53, 54] for more details.

1.2.8 Routing, modulation, spectrum, and tranceiver assignment

In the RSA and RMSA problems, optical signal regeneration will be applied at an intermedia node by a pair of back-to-back placed transceivers, only when the length of the lightpath exceeds the transmission reach of the selected modulation format. However, even if the length of the lightpath does not exceed the transmission reach, we can actually use additional transceivers to partition a lightpath into several consecutive lightpaths to further reduce the required spectrum resources. This problem is called routing, modulation, spectrum, and transceiver assignment (RMSTA) problem [26, 27, 55–57].

We present a simple example involving a chain network to help readers understand the differences between the RSA, RMSA and RMSTA problems shown in Fig. 1.16, where different modulation formats with varying transmission reach and modulation levels listed in Table 1.1 are

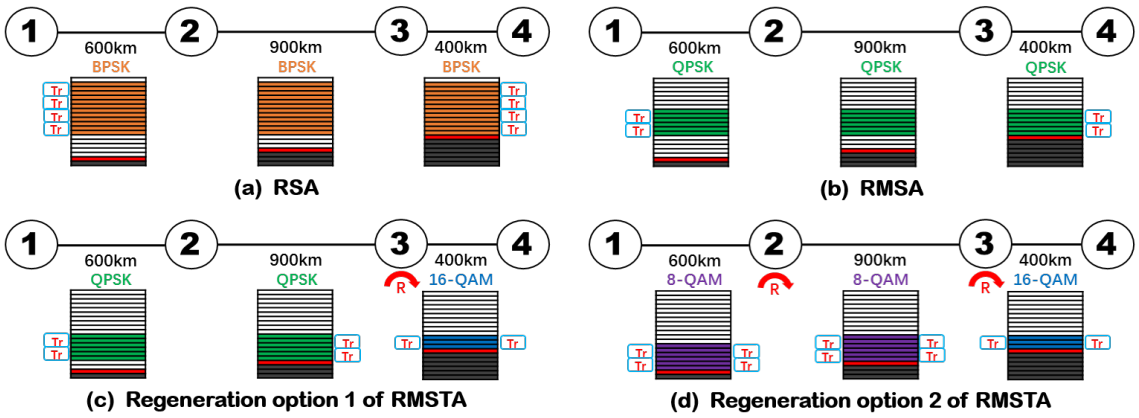

Approach	Regeneration	Modulation	Max slice index	Total slice usage	Transceiver usage
a	-	BPSK	19	57	8
b	-	QPSK	13	39	4
c	3	QPSK + 16-QAM	10	30	6
d	2, 3	8-QAM + 8-QAM + 16-QAM	10	28	10

Figure 1.16: Illustration of routing, modulation, spectrum, and tranceiver assignment problem.

considered. We assume that the CO-OFDM-based Spe SpCh transmission technology is applied, and each transceiver operates at a fixed symbol-rate of 28 Gbaud with 50 Gbps supportable traffic volume under DP-BPSK (i.e., 3 Gbaud for ECC). Each optical carrier and switching guard-band occupies 3 FSs and 1 FS of 12.5 GHz, respectively.

The example shown in Fig.1.16 assumes that some FSs are already allocated (in gray), while the switching guard-bands are shown in red. We consider a connection request with 200 Gbps traffic volume to be carried on a physical path with an overall length of 1900 km. As shown in Fig.1.16.a, in the case of RSA, we do not consider the adaptive modulation and use the basic DP-BPSK modulation format, leading to a requirement of 19 FSs and 8 transceivers. Since 1900 km is shorter than the transmission reach of DP-QPSK, in the case of considering the adaptive modulation, 13 FSs and 4 transceivers are required as shown in Fig.1.16.b. Moreover, compared to spectrum assignment in the RSA and RMSA problems, dividing the lightpath into two lightpaths (i.e., regenerate the optical signals) at node 3 yields a better spectrum utilization, leading to a less spectrum occupation of 10 FSs. However, it simultaneously requires 2 additional transceivers for signal regeneration compared to the case of RMSA.

Moreover, Fig. 1.16 shows only two regeneration options. There are actually exist $2^{hop(p)-1}$ numbers of valid regeneration options depending on the hop length of the lightpath $hop(p)$, and the different options will result in different usages of FSs and transceivers as shown in Fig.1.16.c and Fig.1.16.d. Consequently, the RMSTA problem is considerably more complex than the RSA and RMSA problems and it is a problem worth considering and conforms to the real-world case. The objective of RMSTA is, in addition to the assignment of lightpath and FSs to each connection request, to find the best regeneration option among the valid options for each connection request that

minimize the cost of network operations considering both the spectrum resource and transceivers.

1.2.9 Our contribution to routing, modulation, spectrum, and tranceiver assignment

The main difference between the RMSTA problem and the RSA/RMSA problem is the transceiver placement (TP), that is, whether and where the optical signal should be regenerated at a node for each connection request. To the best of our knowledge, there are only a few works that focus on the RMSTA problem [26, 27, 55–58].

In Ref. [55], integer linear programming (ILP) optimization models and heuristic algorithms were proposed to solve the RMSTA problem. However, the authors did not consider all the regeneration options for each lightpath; therefore, their solution could not guarantee the best spectrum allocation. Moreover, when the optical signal is regenerated, modulation conversion is not allowed, that is, the same modulation format must be used on each partitioned lightpath along the routing path, resulting in a loss of one of the advantages of optical signal regeneration.

In Ref. [56], the authors focused on the RMSA and TP problems separately. They proposed an ILP optimization model and a heuristic algorithm to solve the problems. However, the optimization objective of this work is similar to the basic RSA, that is, to minimize the spectrum usage only but not consider the cost owing to the use of the transceivers.

In Ref. [57], multiple ILP models to solve the RMSTA problem are proposed. The objective is either related to the usage of the spectrum or takes a balance on the cost of the optical signal regeneration and spectrum resources. However, in the proposed model of the regeneration cost, only the number of regeneration nodes are considered, which excludes the detailed number of the required transceivers. Moreover, the authors did not propose any scalable algorithm (e.g., greedy), and indeed the proposed ILP models have been evaluated considering only 50 numbers of loaded connection requests.

In Ref. [58], the RMSTA problem has been addressed considering a metro ring network. An ILP model and a heuristic algorithm have been proposed. However, these proposed algorithms correspond to metro ring networks only; they are not able to solve the problem in arbitrary networks.

In summary, since the TP problem is challenging by itself, the problems considered in the mentioned works above are fundamentally different from the original RMSTA problem because they have simplified the original problem by different considerations to make it easier to solve.

The first work on the original RMSTA problem is [26] (an extension of the authors' previous works [27]), in which the authors proposed a path-based ILP model and presented a heuristic algorithm called *Minimum Cost Lightpaths assignment for Ordered Demands* (MCLOD) that integrates the KSP algorithm to solve it. In their proposed heuristic algorithm, they first pre-calculated k candidate paths for each connection request by the k-shortest path (KSP) algorithm. Then, they assigned the connection requests one-by-one conforming to an ordered sequence. For each connec-

tion request, they considered all the valid regeneration options for all k candidate paths and select the one that leads to the lowest value of the objective function. However, as we stated above, each routing path in the k candidate path set has $2^{hop(p)-1}$-th valid regeneration options (the regeneration or non-regeneration choice is applied to every node on the path except the source and destination nodes). Therefore, the proposed algorithm has an extremely high computational complexity. As the network size increases, the computational time of their algorithm will increase significantly.

In our work [59], we addressed the original RMSTA problem. Our objective is to minimize the total cost, which includes both the spectrum usage and transceiver usage, of network construction. The key contributions of this work are listed as follows:

- Since the RMSTA problem is NP-hard, it is quite difficult to be solved in a large-scale network using the ILP models. In our work, we proposed a novel virtual network-based heuristic algorithm. According to our simulation experiments, the results show that it not only achieves a better performance than those of previous algorithms but it also greatly reduces the computational time in large-scale networks.

- To evaluate the performance of the proposed virtual network-based heuristic algorithm, we proposed two approaches to analyze the lower-bound of the RMSTA problem in large-scale networks, and the simulation results show that the proposed approaches can obtain a tight lower-bound. To the best of our knowledge, all the lower-bound analysis approaches proposed in the previous works are based on the ILP models, which can be applied only in the small-scale networks, and this is the first work that discussed the lower-bound of the RMSTA problem in large-scale networks.

The proposed algorithms and simulation results of our work [59] entitled "Routing, Modulation, Spectrum, and Transceiver Assignment in Elastic Optical Networks" will be detailed in Chapter 2.

1.3 Space-division multiplexing-based elastic optical network

As we have discussed, the EON is a promising technology that leads to more efficient utilization of spectrum resources than does traditional WDM-based optical networks. However, the growth in the transmission capacity of standard single-mode fiber (SMF) has dramatically slowed because the transmission capacity per fiber is close to the nonlinear Shannon limit of the existing SMF [60–63], while the strongly continuous increasing future Internet traffic will inexorably reach this capacity limit. In this context, space-division multiplexing (SDM) has emerged as a viable solution for overcoming this limitation [60, 61, 63–67]. The basic concept of SDM is expanding the available optical transmission dimension of the space domain from the current one (SMF) to multiple parallel dimensions. These transmission dimensions may be the cores/modes in a single SDM fiber, or

current SMFs, which are called spatial dimension or space. The expansion of the space domain will increase network capacity to higher orders of magnitude compared with what can be achieved with the SMF-based network infrastructure, enabling transport networks to keep pace with traffic growth beyond the petabit-per-second level [65, 68, 69].

1.3.1 SDM fibers

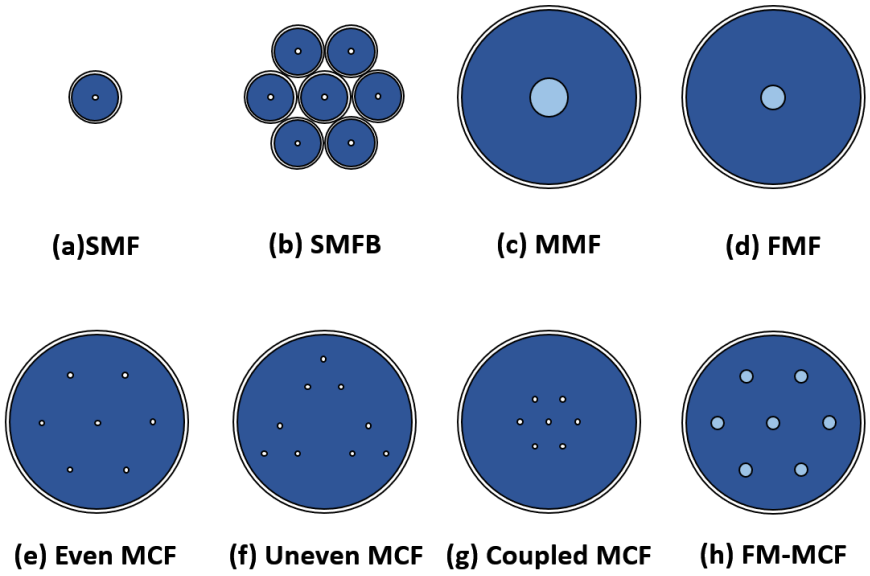

Figure 1.17: Illustration of different types of the SDM fiber.

As shown in Fig. 1.17, the expansion of spatial dimensions can be achieved by different types of SDM fiber. The first one is to upgrades the current network link (SMF) to a bundle of parallel SMFs (SMFB, as shown in Fig. 1.17.b) straightforwardly. A new design of SDM fiber is the multi-core fiber (MCF, as shown in Fig. 1.17.e ∼ g) [70–72], which is implemented by increasing the core-count within the same fiber cladding. These cores belonging to an MCF are weakly-coupled or strongly-coupled with each other. The strongly-coupled MCF is called as coupled-MCF (as shown in Fig. 1.17.g) [73–75]. Another new design of SDM fiber is the multi-mode fiber (MMF, as shown in Fig. 1.17.c) [76, 77], which allows multiple strongly-coupled modes transmitted over a single core. If only a few modes are allowed in an MMF, this MMF is called as few-mode fiber (FMF, as shown in Fig. 1.17.d) [78, 79]. Finally, if an SDM fiber contains multiple cores and a few modes are allowed to transmit over each core, it is referred to as few-mode multi-core fiber (FM-MCF, as shown in Fig. 1.17.h) [80, 81].

In Table 1.2 we list the previous works on resource allocation that considered different SDM fiber types. As shown in Table 1.2, the SDM fibers whose physical entities are parallel single-mode cores (i.e., SMFB or MCF) are the most frequently considered SDM fiber in the previous works,

Table 1.2: SDM fiber types of previous works on resource allocation.

SDM fiber type	References
SMFB	[28, 46–50, 82–89]
MCF	[83, 88–115]
MMF or FMF	[46, 89, 116–118]
FM-MCF	[114, 119, 120]

because they are more compatible with the existing SMF technologies. Of course, there exist other SDM fibers such as FMFs, coupled MCFs, MMFs, and FM-MCFs that we described above, they are less preferred currently due to the following reasons: i) they require a complicated multi-input-multi-output (MIMO) DSP to undo the optical signal, whose complexity increases nonlinearly with the increase of the number of the strongly-coupled modes/cores [121, 122]; ii) they provide less routing flexibility because the strongly-coupled modes/cores belong to such an SDM fiber should be generated, routed and received jointly [29]; iii) they may need a long time to be widely deployed [122]. Therefore, the same with the majority of the previous works, we only consider the SMFB or MCF in this thesis.

1.3.2 Basic solution to achieve the SDM-EON

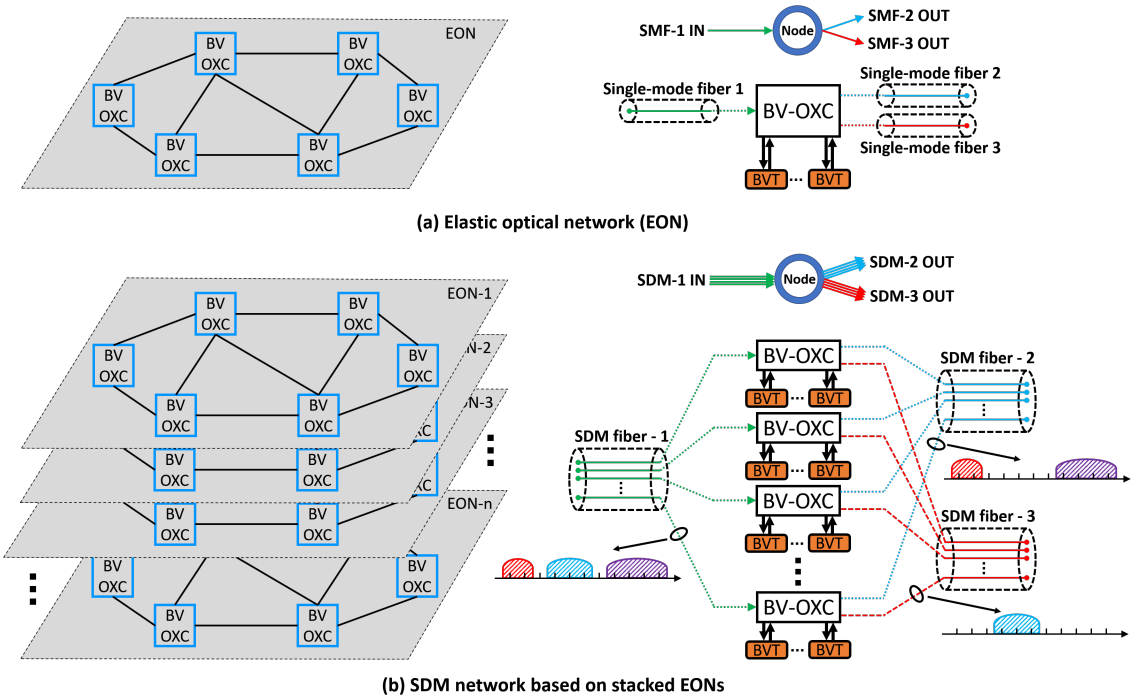

Figure 1.18: Illustration of the overlay of multiple EONs to achieve an SDM optical network.

The most straightforward solution to achieve an SDM-EON is shown in Fig. 1.18, which can

be treated as an overlay of multiple independent SMF-based EONs [122, 123]. Of course, as shown in Fig. 1.19, it enables us to transmit data by either flexible single-carrier transmission or Spe SpCh transmission over each spatial dimension (e.g., each core of 4-core MCFs or 4-SMFBs in the example), such like what we can do in the EON.

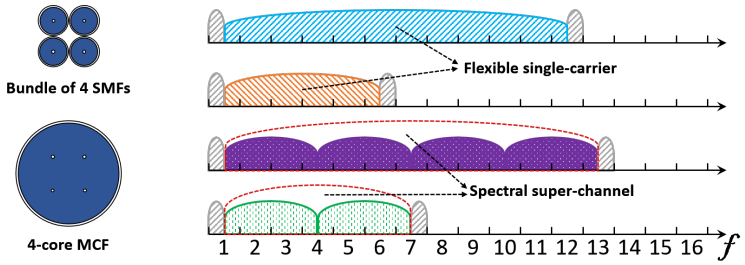

Figure 1.19: Illustration of flexible single-carrier transmission and spectral super-channel transmission in SDM-EONs.

However, such a straightforward solution has some disadvantages. The first disadvantage is that the less utilization of the physical devices. Let us consider a scenario that the transceivers installed at EON-1 are almost deactivated because few connection requests only are loaded to EON-1, and some connection requests loaded to EON-2 are blocked because of the lack of transceivers. As shown in Fig. 1.18.b, in such a straightforward solution implemented by the stacked EONs, the deactivated transceivers in EON-1 is unable to be used by other EON layers, leading to less utilization of the physical devices. Therefore, the reconfigurable optical add/drop multiplexer (ROADM) has been proposed to overcome this disadvantage. As shown in Fig. 1.20.a, the ROADM integrates the function of multiple independent BV-OXCs and all of the transceivers are connected to it, which enables that these transceivers can be shared by different EONs, leading to better utilization of physical devices.

Another disadvantage of the overlay solution is that there is no interaction between different EONs while the data are transmitted. As shown in Fig. 1.18.b, if we assume that the logical indices of spatial dimensions (cores in MCF, or SMFs in SMFB) belonging to each SDM fiber (i.e., link) in the network are the same, the indices of the spatial dimensions assigned to a connection request on the ingress link and egress link at a node should be identical. In other words, the indices of the assigned spatial dimensions on the links along the lightpath cannot be changed for each connection request. That is, the spatial dimension assignment for each connection request should conform to the space continuity constraint. Therefore, the space lane change (SLC) technology has been proposed to relax this constraint. As shown in Fig. 1.20.b, a ROADM with SLC support can switch a spatial dimension on the ingress link to any spatial dimension on the egress links (shown as the gray dotted lines), leading to much higher routing flexibility compared to the one without SLC support (shown in Fig. 1.20.a). However, as we will discuss in the later Section 1.3.7, the architecture of a ROADM

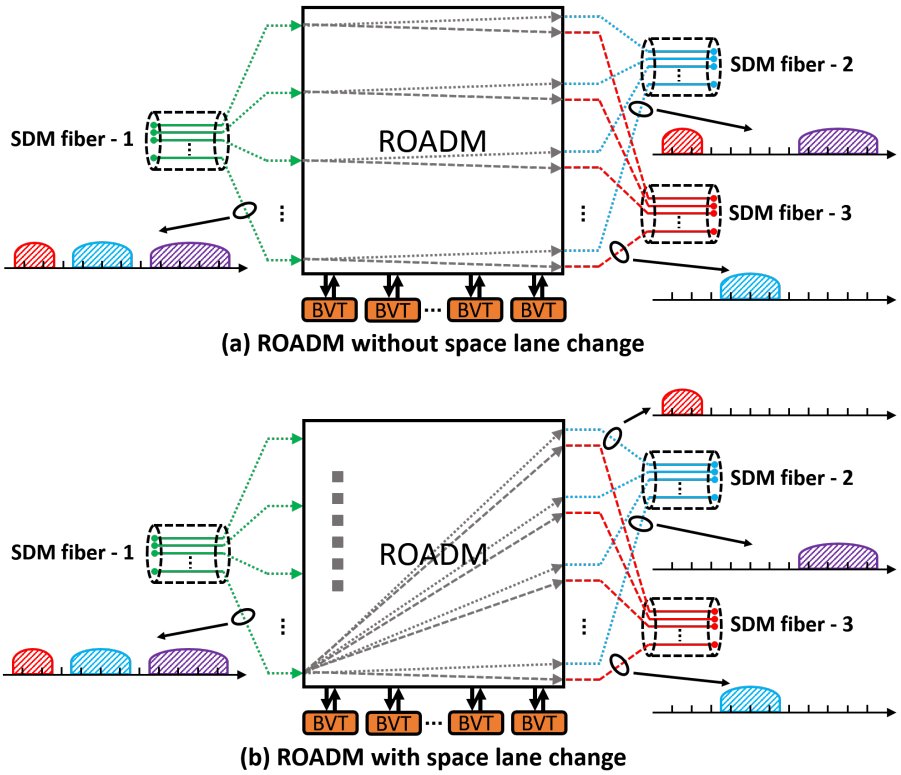

Figure 1.20: Illustration of reconfigurable optical add/drop multiplexer (ROADM) with/without space lane change (SLC).

with SLC support is more complex. Finally, we list the previous works that considered the SLC and did not consider the SLC in Table 1.3.

Table 1.3: Previous works on resource allocation regarding the space lane change technology.

Space lane change	References
With	[28, 83, 84, 87, 90, 93–100, 103–106, 108, 114, 115]
Without	[50, 82, 83, 86, 89, 91, 101, 102, 105, 110, 114, 116–118]

1.3.3 Routing, spectrum, and space assignment

The introduction of the parallel spatial dimensions in the SDM-EON enables us to allocate the optical carriers using not only continuous FSs on the spectrum domain but also to distribute them over different spatial dimensions. Therefore, the RSA problem in EONs converts into the problem of Routing, spectrum, and space (i.e., spatial dimension) assignment (RSSA) problem in SDM-EONs. Compared to the RSA problem, in RSSA problem, for each connection request, additional variables related to the selection of spatial dimensions on each link along the lightpath should be decided, which makes the RSSA problem more complex than the RSA problem. Similar to the RSA

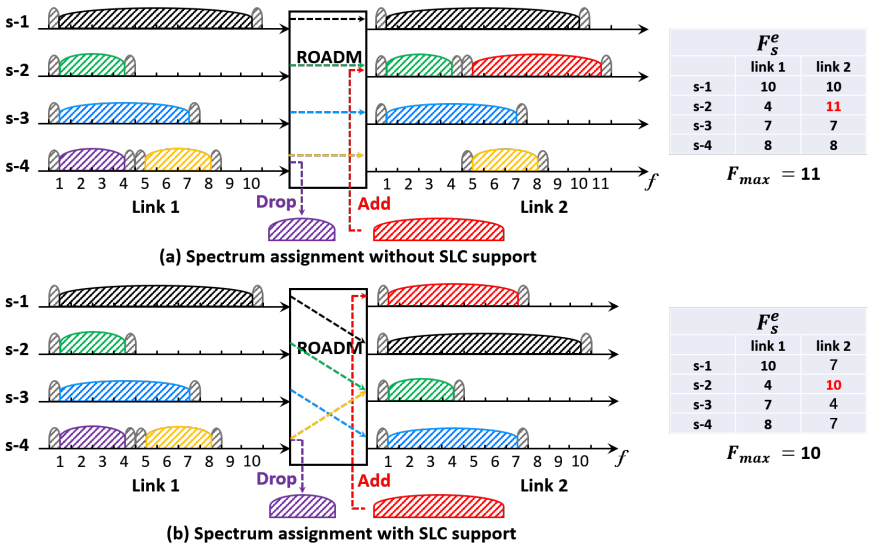

Figure 1.21: Illustration of spetrum assignment in the SDM-EON.

problem, the objective of the RSSA problem is to minimize the required FSs in the network (F_{max}) as shown in Fig. 1.21. For example, if we assume that the F_s^e indicate the maximum index of the occupied FS on the spatial dimension s in link e, the F_{max} can be calculated by Eq. (1.1), where the E and S represents the set of links in the network and the set of spatial dimensions of the SDM fibers, respectively.

$$F_{max} = max\{ F_s^e \mid e \in E, s \in S \} \tag{1.1}$$

Moreover, note that in the case of applying the ROADMs without SLC, the space continuity constraint should be satisfied when assigning the spatial dimensions to each connection request as shown in Fig. 1.21.a, while relaxing this constraint by applying the ROADMs with SLC can achieve higher routing flexibility, and may lead to lower F_{max}, as shown in Fig. 1.21.b.

1.3.4 Routing, spectrum, and core assignment

In SDM-EONs, the spatial dimensions could be either SMFs, cores or modes. If the SDM-EON is connected by MCFs, the inter-core interference of MCF, called the inter-core crosstalk (XT), will become a crucial constraint that may severely affect the propagation quality. The XT will occur when the same FSs are assigned to adjacent cores in a common fiber link to serve different connection requests [91, 105, 113, 114].

A simple example of XT in the 7-core MCF is shown in Fig. 1.22. For simplicity, we assume that the connection requests are assigned to only three cores (i.e., cores 1, 2 and 3) and that core 1 (or core 3) and core 2 are adjacent. The strength of the XT on the f-th FS of core c is related to the number of active adjacent cores of core c (i.e., the same f-th FS has been assigned to other connection requests). For example, since the FSs with the same index of that of $R.1$ have not been

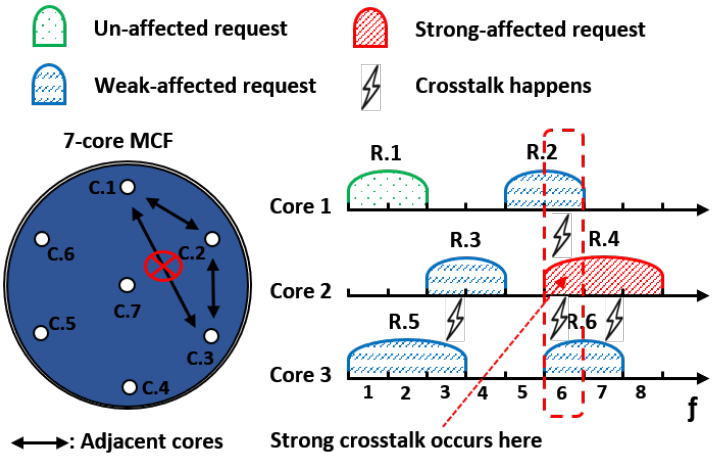

Figure 1.22: Illustration of inter-core crosstalk (XT) in the 7-core MCF.

assigned to any connection request on the adjacent cores, there is no occurrence of XT for $R.1$. In contrast, there is an occurrence of weak XT for $R.2$ and $R.6$ on the 6-th FS because the same 6-th FS has been assigned to $R.4$ in the adjacent core 2. Moreover, note that the XTs are affecting each other on the adjacent cores, there is an occurrence of strong XT for $R.4$ on the 6-th FS because it is affected by $R.2$ and $R.6$ simultaneously.

For a connection request, only when the XT on each assigned FS for the connection request is less than an acceptable XT threshold (XT_{max}), the signals can be successfully transmitted on these assigned FSs.

To minimize the XT and achieve a dense core arrangement to enable high-capacity and long-distance transmissions, how to suppress the XT has become a primary challenge in the development of MCFs [124–129]. K.Takenaga et al. developed a trench-assisted multi-core fiber (TA-MCF) in [129]. In TA-MCF, XT is directly related to the mode-coupling coefficient, which can be estimated without the need for numerical simulations.

According to the equations proposed in [130], if the f-th FSs of two adjacent cores c and c' in a common link e are assigned to different connection requests, the XT between them can be obtained by the following equation:

$$XT_{cc'}^{ef} = \frac{1 - exp(-2hL_e)}{1 + exp(-2hL_e)} \tag{1.2}$$

where $h = \frac{2k^2 r}{\beta \omega_{tr}}$ represents the mean XT increase per unit length of the fiber and is also regarded as the power coupling coefficient in coupled-power theory [130], which is fixed for a given type of MCF. The parameters k, r, β and ω_{tr} represent the coupling coefficient, bend radius, propagation constant and core pitch, respectively [95, 100, 128]. L_e represents the length of link e.

In addition, Hayashi et al. [128] claimed that "The mean XT from multiple cores to one core can be represented as a sum of the mean crosstalk from each of the multiple cores to the single core."

Therefore, on a given f-th FS, if a core c is affected by multiple adjacent cores where the same f-th FSs are assigned to other connection requests, the XT on the f-th FS of core c can be calculated as follows:

$$XT_c^{ef} = \sum_{c' \in A_c^e} XT_{cc'}^{ef} \tag{1.3}$$

In Eq. (1.3), the XT on the f-th FS between two adjacent cores $XT_{cc'}^{f}$ is calculated using Eq. (1.2), where A_c^e represents the set of active adjacent cores of core c in link e; in other words, for each core $c' \in A_c^e$, the same f-th FS of core c' has been assigned to other connection requests. Moreover, for a connection request r, the lightpath of it may pass through multiple cores on different links and occupy a number of continuous FSs on each of these cores. The XT of the connection request r on each occupied f-th FS can be calculated by Eq .(1.4) as follows:

$$XT_r^f = \sum_{\langle c,e \rangle \in p_r} \sum_{c' \in A_c^e} XT_{cc'}^{ef} \tag{1.4}$$

The p_r in Eq. (1.4) represents the routing path of the connection request r, which contains the selected core c in each link (i.e., $\langle c, e \rangle$) along the lightpath. Finally, it is worth noting that the XT on each assigned f-th FS of the connection request should less than an acceptable XT threshold to ensure successful transmission, which depends on A_c^e and L_e along the selected lightpath. Therefore, in addition to the development of MCF with low XT on the physical layer, from the perspective of networking, we can also avoid spectrum overlaps between adjacent cores in a common link (i.e., reduce the number of elements in A_c^e) or select a lightpath with short length (i.e., smaller L_e for each link) to ensure that the XT on each assigned f-th FS less than the XT threshold. Consequently, in the case of SDM-EONs with MCF, considering the additional complexity owing to the XT management, the RSSA problem becomes the routing, spectrum, and core assignment (RSCA) problem.

1.3.5 Our contribution to routing, spectrum, and core assignment

As we listed in Table 1.2, many works have concentrated on the RSCA problem in recent years. Among those works, some of them did not consider the influence of XT [84, 97, 101, 103, 104, 111, 115]. In the works who considered the influence of XT, the proposed algorithms for XT management can be mainly divided into three cases:

- The XT-avoid case: the XT-avoid approach is to avoid spectrum overlaps between adjacent cores in the fiber links while allocating FSs and cores to different connection requests. As shown in Fig. 1.23.a, the same FSs cannot be assigned to different connection requests that traverse through adjacent cores in the common links. The XT-avoid approach can simplify

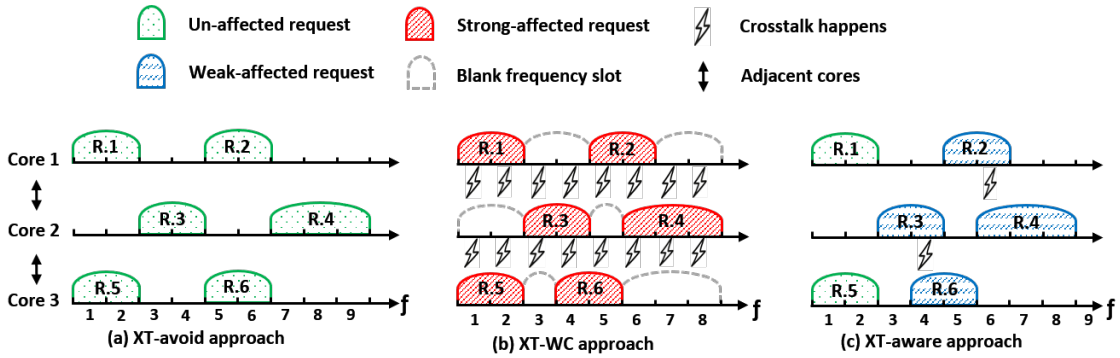

Figure 1.23: Illustration of three XT management approaches in the 7-core MCF.

the RSCA problem and significantly reduce the complexity of the problem. However, it prevents the use of the same FSs on the adjacent cores of a fiber. Thus, even though the XT-avoid approach can completely prevent the XT from occurring, the efficiency of the spectrum multiplexing of MCF will be decreased.

- The XT-worst case: the XT-worst approach is to consider the XT in the worst interference scenario. As shown in Fig. 1.23.b, the blank FSs are the empty FSs (i.e., have not been assigned to any connection request), but for the XT-worst approach, they are considered to be occupied to evaluate the XT. In other words, if we assume that the N_c^e represents the set of the adjacent cores of core c in link e, for the XT-worst approach, A_c^e is always identical with N_c^e, that is, all the adjacent cores are treated as active cores even though they are may actually inactive. Since all adjacent cores of a target core c are contained in A_c^e, for a strict XT threshold, to ensure that the XT on each assigned FS less than the threshold, the L_e for the links along the lightpath should be shorter. Therefore, the transmission reach will be bounded significantly in this case, which is shorter than what the optical signal can actually reach. This makes the XT-worst approach over-conservative since the set of the feasible lightpaths — the length of each feasible lightpath is shorter than the bounded transmission reach — may become significantly small. In an extreme case, the XT-worst approach may become unworkable, because no any feasible lightpath can be found between a node pair (i.e., the bounded transmission reach is shorter than the length of the shortest path), even though some feasible lightpaths actually exist (if $A_c^e \neq N_c^e$).

- The XT-aware case: the XT-aware approach is to compute the XT strictly depending on the interference of a core with other active adjacent cores that share the same FS and link, as shown in Fig. 1.23.c. The XT-aware approach can always perform better than both the XT-avoid and the XT-worst approaches and leads to an optimal solution. It strictly calculates the XT depending on the active adjacent cores that share the same FS on a common link

along the lightpath. Therefore, for a strict XT threshold, the XT-aware approach can prevent the same FSs from being assigned to adjacent cores to ensure that the XT of the lightpath (for a given connection request) is less than the XT threshold. For a relaxed XT threshold, the same FSs on adjacent cores are allowed to be multiplexed more times to achieve higher spectral efficiency. However, in the XT-aware approach, how to calculate the XT is a key and challenging task, which results in the problem becoming more complicated.

Table 1.4: XT management approaches of previous works on static/dynamic RSCA problem.

XT management approach	References	
	Static problem	Dynamic problem
XT-avoid	[109]	[90]
XT-worst	[95, 98, 99, 102, 106, 110]	[107, 113]
XT-aware	-	[83, 91, 93, 94, 96, 100, 105, 108, 112, 114]

In Table 1.4, we list the previous works that considered the different XT management approaches above for RSCA problem. We can see that many previous works have addressed the static or dynamic RSCA problem considering XT management. In our work Ref. [131], we address the static RSCA problem. Compared to the previous works, the key contributions of our work are summarized as follows:

- We introduce a node-arc-based ILP model considering the XT based on the XT-worst approach. In contrast to previous path-based ILP models [95, 102] that need to pre-compute several candidate paths for each connection request during the pre-processing stage, the proposed ILP model can simultaneously find an optimal combination of routing paths and assign corresponding FSs and cores for each connection request in a node-arc manner [38, 39]. The numbers of both variables and constraints of the proposed node-arc-based ILP model are less than the ones of the previous models, leading to much higher convergence efficiency. Our simulation experiments show that it achieves a significantly shorter computational time compared with the previous path-based ILP models.

- We introduce a mixed integer linear programming (MILP) optimization model considering the XT strictly based on the XT-aware approach. In contrast to the XT-worst approach-based ILP models, XT is calculated depending on the actual interference between cores on a common link and therefore ensures a complete feasible routing path space for each connection request; consequently, a strictly optimal solution can be obtained by the proposed MILP model.

- The static RSCA problem is an extension of the static RSA problem, which is known to be NP-hard. The problem is difficult to solve in a reasonable time by the ILP/MILP models for large-scale problem instances. For this reason, we propose an XT-aware-based heuristic

algorithm for achieving scalability. In the proposed heuristic algorithm, a strict XT-aware FS check mechanism is proposed to achieve the XT-aware approach. The simulation experiments show that compared to the previous heuristic algorithms, the proposed heuristic algorithm can obtain solutions that are closer to the optimal solutions or lower-bound.

Finally, to the best of our knowledge, our work is the first work that considers the XT-aware for the static RSCA problem. The proposed (M)ILP models, heuristic algorithm, and simulation results of our work Ref. [131] entitled "Routing, Spectrum and Core Assignment in SDM-EONs with MCF: Node-arc ILP/MILP Methods and an Efficient XT-aware Heuristic Algorithm" will be detailed in Chapter 3.

1.3.6 Spectrally & spatially flexible super-channel transmission

In Section 1.3.2, we introduced the basic solution to achieve SDM-EONs. However, it is not yet the economically sustainable solution [132], because it can not provide any potential reduction of the network cost per unit capacity. For instance, in the case of achieving the SDM by a simple overlay of the SMF-based EONs, the S parallel EONs can provide S times the capacity, but meanwhile brings S times the network CAPEX (e.g., cost and power consumption). That is, network CAPEX per bit-rate would not be changed compared to the SMF-based EON systems. In addition, although the application of ROADM can achieve a certain degree of cost savings by improving the transceiver utilization, such a cost reduction is not remarkable compared to the solution of stacked EONs, especially in the case of heavy load (i.e., all the transceivers are activated).

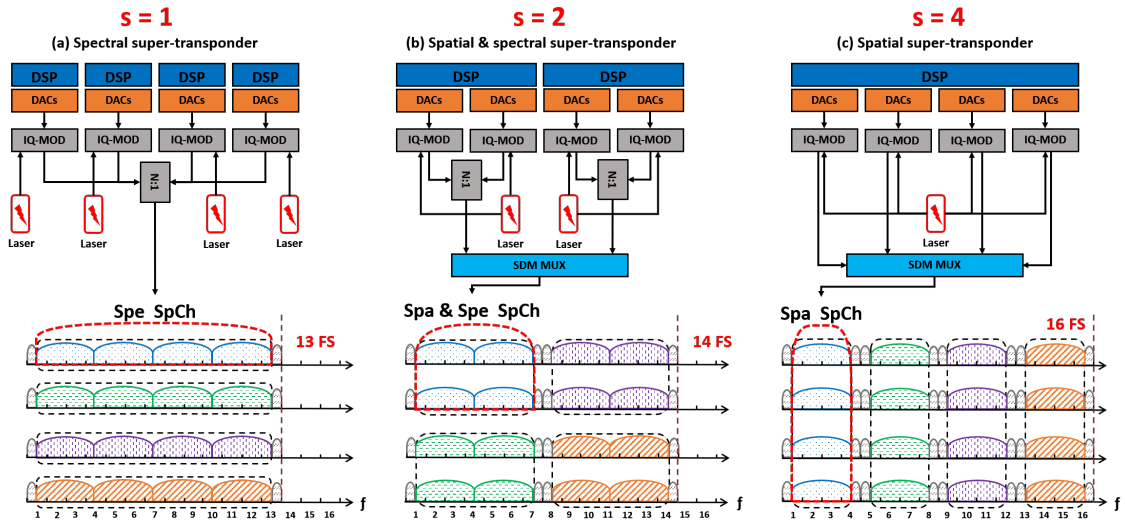

Figure 1.24: Illustration of spectrally & spatially flexible super-channels.

Therefore, to further make full use of the expanded spatial dimensions and achieve more cost-efficient transmission [123, 132, 133], the spectrally & spatially flexible SpCh transmission has been

recently proposed. The spectrally & spatially flexible SpChs can be mainly divided into three types. A simple illustration of these three types of SpChs is shown in Fig. 1.24 (only transponders are shown).

For simplicity, we consider four 200 Gbps connection requests to be transmitted in the DP-BPSK modulation format over 4 spatial dimensions. In addition, each optical carrier is generated by a transceiver supporting 50 Gbps under DP-BPSK with 28 Gbaud symbol-rate (3 GBaud for ECC is assumed), and occupies 37.5 GHz spectrum. As in Fig. 1.24, the spectrum granularity is set to 12.5 GHz, and a 12.5 GHz switching guard-band (6.25 GHz at both sides) is applied to separate adjacent SpChs.

A spectral super-channel (Spe SpCh), which is composed of several continuous optical carriers as shown in Fig. 1.24.a, can offer high spectral efficiency for serving connection requests with flexible traffic volumes. The optical carriers are placed near the Nyquist condition, that is, without switching guard-bands between them; switching guard-bands are necessary only between neighboring Spe SpChs. Note that an Spe SpCh can be generated by an array of independent transceivers as we have shown in Fig.1.13, or by a spectral super-transceiver which integrated these independent transceivers together as shown in Fig. 1.24.a. According to Refs. [133, 134], such an integrated SpCh transceiver can achieve a 40% reduction in the device cost of all components (except lasers and DSP) compared to multiple independent transceivers.

A spatial super-channel (Spa SpCh) is an extension of the Spe SpCh concept to the spatial domain as shown in Fig. 1.24.c. The optical carriers are arranged across numbers of or all of the spatial dimensions over the same spectral range. The key feature of an Spa SpCh is that the optical carriers at the same frequency but distributed over different spatial dimensions can share a common laser at the transponder (and one laser at the receiver used as local oscillator), but meanwhile switching guard-bands are necessary for each of the spatial dimensions occupied by an Spa SpCh.

A spatial and spectral super-channel (Spa & Spe SpCh) is a hybrid of an Spe SpCh and an Spa SpCh as shown in Fig. 1.24.b. In other words, an Spa & Spe SpCh can be created by combining multiple Spe SpChs in the same spectral range extending over multiple spatial dimensions. Thus, the allocation of an Spa & Spe SpCh can span both the spectral and spatial domains.

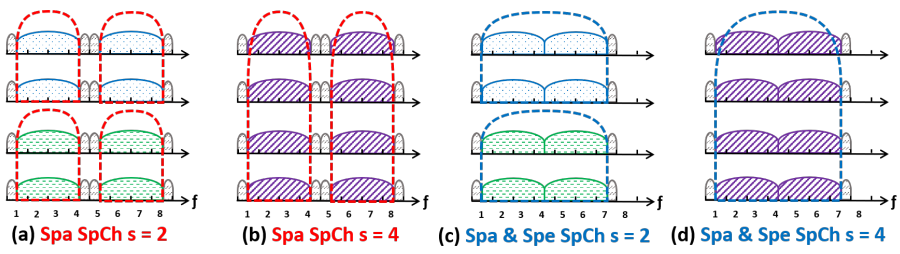

Figure 1.25: Comparison of Spa SpCh and Spa & Spe SpCh.

Indeed, both an Spe SpCh and an Spa SpCh can be treated as special cases of an Spa & Spe SpCh. If we consider that an $s \times o$ SpCh represents an Spa & Spe SpCh in which one Spe SpCh consisting of o contiguous optical carrier(s) (i.e., o is the spectral span) is allocated to each of s spatial dimensions (i.e., s is the spatial span) in the same spectral range, an Spa SpCh is actually an $s \times 1$ SpCh whose spectral span o equals 1, and an Spe SpCh is an $1 \times o$ SpCh whose spatial span s equals 1. It is worth noting that the concepts of the Spa SpCh and the Spa & Spe SpCh have not been clearly distinguished in many previous works. In order to avoid the possibility of confusion, we use an additional example shown in Fig. 1.25 to further explain the difference between them.

As shown in Fig. 1.25, an SpCh belongs to an Spa SpCh only when its spectral span o equals 1. Therefore, for a connection request with large traffic volume, leading to more than s optical carriers are required, we should use multiple $s \times 1$ Spa SpChs to transmit this connection request and s numbers of guard-bands should be placed between them. On the other hand, even though an SpCh occupies all spatial dimensions of an SDM fiber as shown in Fig. 1.25.d, if it is composed of more than 1 optical carriers on the spectral domain without switching guard-bands (i.e., $o > 1$), it does not belong to an Spa SpCh, but to an Spa & Spe SpCh. Overall, it is obvious that the Spa & Spe SpCh inherits the advantages of both the Spa SpCh and Spe SpCh. On the spectral domain, it can achieve spectrum savings by avoiding the placement of additional switching guard-bands. On the spatial domain, it can achieve cost savings by sharing the components (e.g., lasers). Since both an Spe SpCh and an Spa SpCh can be treated as special cases of an Spa & Spe SpCh, we use the $s \times o$ SpCh to refer to all types of the SpChs in the rest of the thesis.

In the case that a connection request with T Gbps traffic volume is to be transmitted by such a $s \times o$ SpCh with a given spatial span of s, the spectral span o of this SpCh can be calculated using Eq. (1.5). In Eq. (1.5), ml represents the modulation level (see Table 1.1) of the selected modulation format, and B represents the symbol-rate (excluding the ECC) of each inter-integrated transceiver.

$$o = min\{x \in \mathbb{Z}^+ \mid T \leq B \cdot ml \cdot s \cdot x\} \tag{1.5}$$

Based on Eq. (1.5), the number of required FSs in each of the s patial dimensions (including the switching guard-bands) can be calculated using Eq. (1.6) [135], where the W_{OC}, W_{GB}, and W_{FS} represents the spectrum occuppied by an optical carrier, guard-band, and FS, respecetively.

$$n_{FS} = min\{x \in \mathbb{Z}^+ \mid (o \cdot W_{OC} + W_{GB}) \leq W_{FS} \cdot x\} \tag{1.6}$$

In the example shown in Fig. 1.24, T, B, ml equals 200 Gbps, 25 Gbaud (i.e., 28 Gbaud - 3 Gbaud for ECC), 2 bits/symbol (for DP-BPSK), respectively. According to Eq. (1.5), we require a 1×4 Spe SpCh, a 2×2 Spa & Spe SpCh, and a 4×1 Spa SpCh for each connection request in the case of spatial span s equaling 1, 2, and 4, respectively. Futhermore, according to Eq. (1.6), these SpChs requires $1 \cdot 13$, $2 \cdot 7$ and $4 \cdot 4$ FSs, respectively. Therefore, it is obvious that the SpCh with

smallest spatial span s (i.e., 1×4 Spe SpCh) clearly achieves the highest spectral efficiency (13 FSs) but has the largest requirement of lasers per connection request. Meanwhile, the SpCh with largest spatial span s (i.e., 4×1 Spa SpCh) requires 16 FSs since guard-bands are necessary in each spatial dimension, while a single laser can be shared over the 4 spatial dimensions. The 2×2 Spa & Spe SpCh strikes a balance between them.

In summary, if an SpCh with a larger spatial span s is applied, considerable savings in terms of device cost can be achieved due to the components sharing (e.g., lasers). However, it is less spectrally efficient than one with a smaller s that can support an equivalent capacity because switching guard-bands need to be placed on each spatial dimension to separate neighboring SpChs. Finally, we list the previous works on resource allocation that applied different SpChs in Table 1.5.

Table 1.5: Spuer-channel policies of previous works on resource allocation.

Spuer-channel policy	References
Spe SpCh	[28, 47, 83, 84, 87, 89, 92–98, 100, 102–105, 108, 109, 112–115]
Spa SpCh	[28, 46–50, 82, 85–89]
Spa & Spe SpCh	[105, 107, 111, 114]

1.3.7 All-optical switching/routing for Spe & Spa SpChs

Similar to why the BV-OXC is required when the optical networks evolve from WDM-based optical networks to EONs, ROADMs with different architectures are also needed to offer different routing/switching strategies corresponding to different Spe & Spa SpChs in SDM-EONs. There are two key factors that have a considerable influence on the ROADM architecture: i) the spatial switching granularity (denoted by g), and ii) the SLC technology as we have shown in Fig. 1.20, leading to different switching strategies.

The first category of switching strategies is called independent switching (Ind-Sw) and represents the case in which g is equal to 1. Indeed, Fig. 1.20 in Section 1.3.2 illustrate the case of Ind-Sw. In the absence of SLC support, each spatial dimension can be switched independently to any output port with the same spatial dimension index (i.e., conforming to the spatial continuity constraint mentioned before). In contrast, the spatial continuity constraint is relaxed in the situation with SLC support, as shown in Fig. 1.20.b. Ind-Sw can offer the highest routing flexibility, especially in the case with SLC support. Ind-Sw is used to switch the $s\times o$ SpChs whose spatial span s equals 1 (i.e., Spe SpChs) or support the flexible single-carrier transmission (refers to Section 1.2.4).

The second category of switching strategies is called joint switching (J-Sw) and represents the case in which g is equal to S. As shown in Fig. 1.26, all the spatial dimensions are switched jointly as a single entity, resulting in the lowest routing flexibility. Besides, it is obvious that the case with

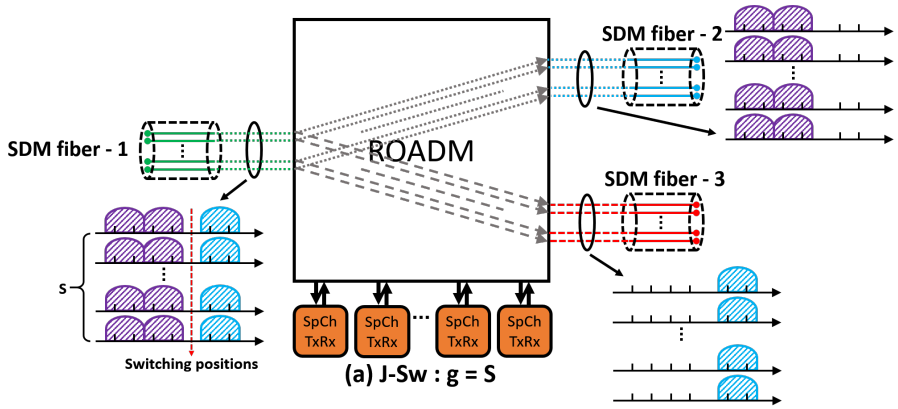

Figure 1.26: Illustration of joint switching.

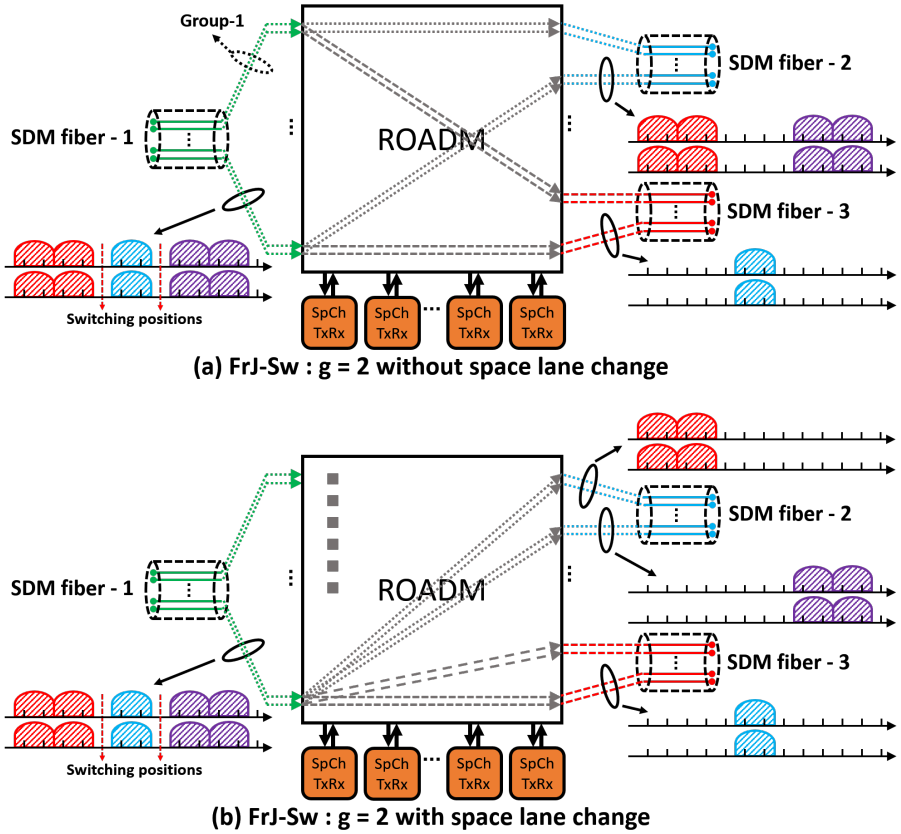

Figure 1.27: Illustration of fractional joint switching.

SLC support does not exist in this case. J-Sw is used to switch the $s \times o$ SpChs whose spatial span s equals S (i.e., $S \times 1$ Spa SpChs or $S \times o$ Spa & Spe SpChs).

The last category of switching strategies is called fractional joint switching (FrJ-Sw), which is a hybrid approach combining the Ind-Sw and the J-Sw. As shown in Fig. 1.27, the spatial dimensions are divided into several (i.e., S/g) groups such that g numbers of spatial dimensions are contained

in each group, and the spatial dimensions belong to a single group should be switched jointly. In the case without SLC support, the indices of the spatial dimension groups on each link along a lightpath should maintain the same as shown in Fig. 1.27.a, while the changing of group indices is allowed to achieve relatively higher routing flexibility in the case with SLC support as shown in Fig. 1.27.b. FrJ-Sw is used to switch the SpChs whose spatial span s equals g (i.e., $g \times 1$ Spa SpChs or $g \times o$ Spa & Spe SpChs).

Indeed, both Ind-Sw and J-Sw can be treated as special cases of FrJ-Sw. When spatial switching granularity g is equal to 1, it corresponds to the case of Ind-Sw. When g is equal to S, all spatial dimensions are considered as one group which corresponds to the case of J-Sw. Therefore, it is obvious that the switching strategies are different for different applied spatial granularities g, as well as whether the SLC is supported, and of course, leading to different architectures of the corresponding ROADM.

The bottom of Fig. 1.28 illustrates the ROADM architecture at an intermediate node with nodal degree D equaling 3, in the case of g equaling 2 without SLC support for 4-SMFBs/MCFs. The segment in the dotted green frame is actually identical to the case (c) - FrJ-Sw: $g = 2$ without SLC support - shown in the top of Fig. 1.28. This segment can be replaced with the corresponding architectures to achieve other switching strategies. Therefore, according to Fig. 1.28, we can summarize the number of required WSSs and the port-count per WSS for different switching strategies in Table 1.6.

Table 1.6: The number of required WSSs and port-count per WSS for different switching strategies.

	Num. of WSSs	Port-count per WSS
With SLC	$2 \cdot D \cdot \frac{S}{g}$	$g \times \{1 \times [\frac{S}{g} \cdot (D-1)+1]\}$
Without SLC		$g \times (1 \times D)$

According to Table 1.6, for a given network topology (i.e., the nodal degree D for each node and the number of spital dimensions S for each link are given), J-Sw is a promising approach for achieving economical SDM optical networks [136] since it requires the smallest number of wavelength selective switches (WSSs), while the Ind-Sw who offers the highest routing flexibility requires the largest number of WSSs, and FrJ-Sw strikes a balance between Ind-Sw and J-Sw. In addition, it is obvious that for the switching strategies with the same switching granularity, they require the same number of WSSs, but the one with SLC support requires the larger port-counts per WSS. In summary, the switching strategy with smaller switching granularity g and/or SLC support can provide higher routing flexibility, but meanwhile requires more WSSs and/or larger port-counts per WSS, leading to more device cost of networks.

Finally, in Table 1.7 we listed the previous works on the resource allocation that considered different switching strategies.

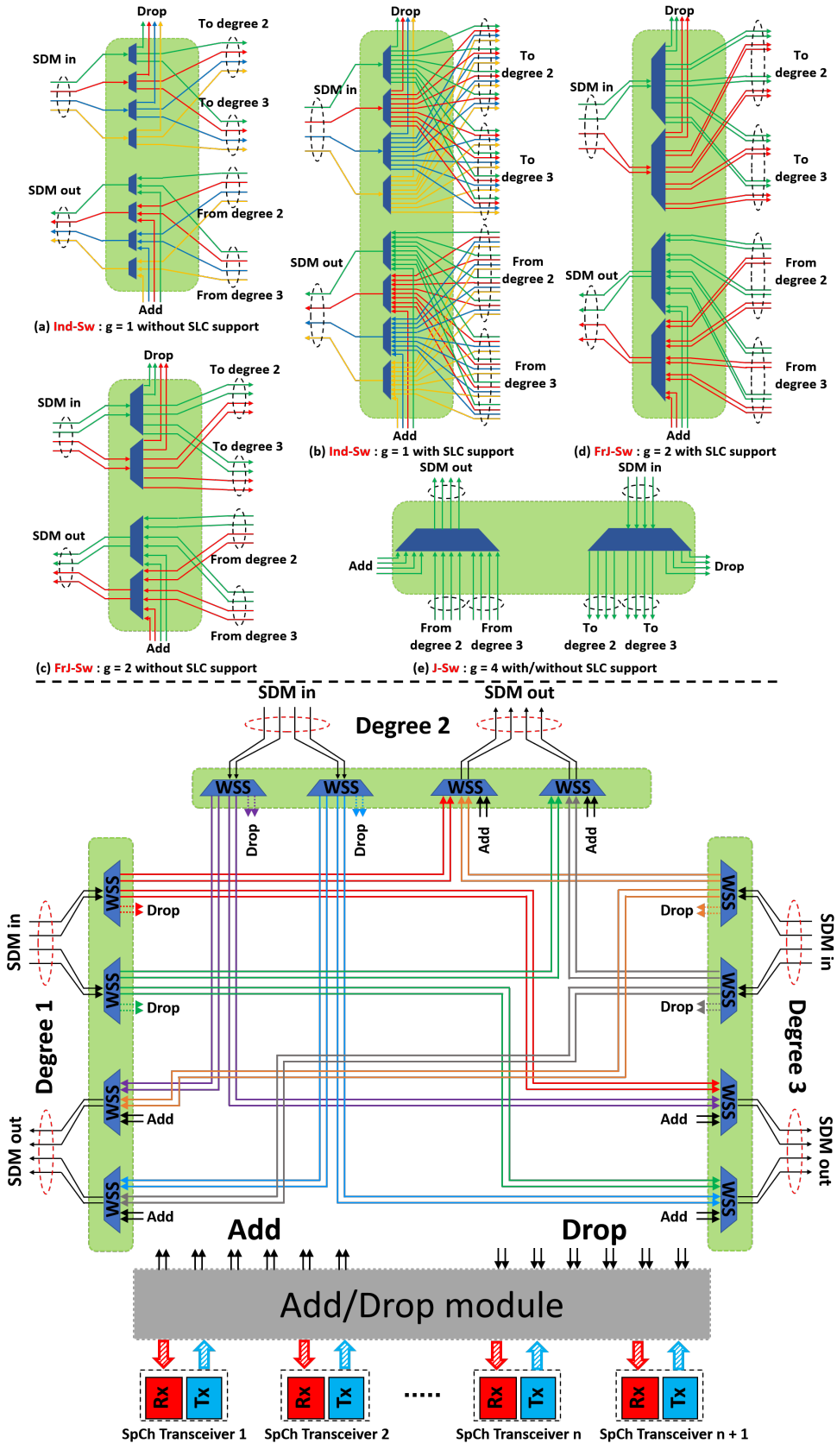

Figure 1.28: Illustration of ROADM with spatial switching granularity g equaling 2 at an intermediate node with 3 degree.

Table 1.7: Switching strategies of previous works on resource allocation.

Switching strategy	References
Ind-Sw	[28, 47–50, 82–87, 89–106, 108, 110–115]
J-Sw	[28, 46–50, 82, 85–89, 107]
FrJ-Sw	[28, 46–50, 82, 85–87]

1.3.8 Routing, modulation, spectrum, space, and spatial granularity assignment

From Section 1.3.6 and Section 1.3.7, we can see that there is a one-to-one relationship exists between the spatial switching granularity g of the switching strategies and the spatial span s of the SpChs, that is, g must be always identical to s, because all of the s spatial dimensions belonging to an SpCh should be switched jointly and an SpCh should be routed as a single entity. In other words, once we decide the spatial switching granularity g of the switching strategy, the corresponding SpChs with spatial span s equaling g should also be applied for transmission. Therefore, in the rest of the thesis, we use spatial granularity i to refer to both spatial switching granularity g and spatial span s.

As shown in Fig. 1.24 and Fig. 1.28, it is obvious that the spatial granularity i has a great impact on the number of WSSs in ROADMs, port-count per WSS, the number of laser pairs in SpCh transceivers, and the number of required FSs in the network. In this thesis, we assume that a WSS type is selected beforehand for all ROADMs with different spatial granularity i, regardless of whether all the ports of the selected WSS are fully utilized. In this case, the cost related to ROADMs only depends on the number of required WSSs. If we consider the situation shown in Fig. 1.24 and Fig. 1.28, the usages of network resources (i.e., FSs, WSSs, and lasers) can be summarized in Table 1.8.

Table 1.8: The usages of network resources (i.e., FSs, WSSs, and lasers) for different spatial granularities i.

Spatial granularity	Num. of FSs	Num. of WSSs	Num. of laser pairs
$i = 1$	13	24	16
$i = 2$	14	12	8
$i = 4$	16	6	4

As shown in Table 1.8, a trade-off relationship exists between these network resources, a smaller spatial granularity i will result in more cost on the devices (i.e., more WSSs and lasers), but better utilization on the spectrum (i.e., fewer FSs are required to transmit the same traffic volumes). By comparison, a larger spatial granularity i can achieve significant cost savings, but meanwhile requires more numbers of FSs. Such results are in accordance with what we have discussed in Section 1.3.6 and Section 1.3.7. Consequently, the spatial granularity i is a key factor that has a great

impact on the spectrally & spatially flexible SDM optical networks, and it is worth considering in network design.

In Refs. [28, 49], the authors compared the performances (e.g., spectral efficiency and the usage of WSSs) for varying spatial and spectral granularities in SDM networks and noted that a smaller spatial and spectral granularity can lead to significant performance improvement for small connection requests, while J-Sw is a suitable option for networks with large connection requests. In Refs. [48, 82, 85], the authors investigated the performances of several SDM switching options (spatial granularity) and the corresponding SpCh policies. They noted that J-Sw/FrJ-Sw offers similar performance to that of Ind-Sw for particular network load profiles while also significantly reducing the number of WSSs.

However, in all the works mentioned above, the authors focused on a comparative performance analysis of transmission strategies applying different spatial granularities in dynamic scenarios, while the spatial granularities are assumed to be given beforehand. In our work Ref. [137] entitled "Joint Assignment of Spatial Granularity, Routing, Modulation and Spectrum in SDM-EONs: Minimizing the Network CAPEX Considering Spectrum, WSS and Laser Resources", we propose a problem called routing, modulation, spectrum, space, and spatial granularity assignment (RMSSGA), which further consider the assignment of spatial granularity i and adaptive modulation compared to the basic RSSA problem. Our objective is to minimize network CAPEX by considering varying network resources containing the FSs, WSSs, and lasers in SDM network design. Different from previous works, we try to find the best spatial granularity and the assignment of each connection request simultaneously. That is, the best spatial granularity is one of the variables that should be decided in our work, which is not given beforehand. To the best of our knowledge, this is the first work to consider the spatial granularity assignment in SDM network design.

To address the proposed RMSSGA problem, we first jointly optimize the problem by an ILP model. Next, we present a decomposition method that divides the RMSSGA problem into two substituent subproblems, namely, (i) routing, modulation, space, and spatial granularity and (ii) spectrum assignment (RMSG + SA), and then solve them sequentially. Furthermore, since the RMSSGA problem is an extension of the basic RSSA problem which is known to be NP-hard, we propose a re-routing (RR)-based heuristic algorithm combining with a simulated annealing metaheuristic to achieve scalability. The proposed algorithm and simulation results of our work Ref. [137] will be detailed in Chapter 4.

Chapter 2

Routing, Modulation, Spectrum and Transceiver Assignment in Elastic Optical Networks

As we discussed in Section 1.2, the EON is a promising new optical technology that uses spectrum resources much more efficiently than does traditional WDM-based optical network. This chapter focuses on the RMSTA problem in EON. In contrast to previous works that consider only the basic RSA or RMSA problem, we additionally consider the transceiver allocation problem.

As we have shown in Fig. 1.16, transceivers can be used to regenerate signals (by connecting two transceivers back-to-back) along the routing path, and different regeneration sites on a routing path result in the different spectrum and transceiver usage. Therefore, the RMSTA problem is both more complex and more challenging than are the basic RSA and RMSA problems. To address this problem, we first propose an ILP model whose objective is to optimize the balance between spectrum usage and transceiver usage by tuning a weighting coefficient to minimize the cost of network operations. Then, we propose a novel virtual network-based heuristic algorithm to solve the problem and present the results of experiments on representative network topologies. The results verify that, compared to previous works, the proposed algorithm can significantly reduce both resource consumption and time complexity.

This chapter is organized as follows. In Section 2.1, we propose the ILP model of the RMSTA problem. In Section 2.2, we analyze the lower-bound of the RMSTA problem. In Section 2.3, we propose an efficient heuristic algorithm to suboptimally solve the RMSTA problem. In Section 2.4, we present numerical results and evaluate the performance of the proposed algorithm.

2.1 Integer liner programming model for the RMSTA problem

This subsection presents our integer linear programming (ILP) model for the static RMSTA problem. We assume that the optical signals are transmitted by CO-OFDM transmission technology.

The objective is to minimize the network CAPEX considering (the maximal index of) the required FSs and the number of required transceivers in the whole network, that is, make a trade-off between these two network resources.

Parameters

V : The set of network nodes.
E : The set of network links.
NP : The set of node pairs in the network. Generally, node pair $\langle i, j\rangle$ is different from node pair $\langle j, i\rangle$.
λ_{sd} : The traffic volume (Gbps) of the connection request between a source-destination pair $\langle s, d\rangle$.
M : The set of available modulation formats. As shown in Table 1.1, a modulation format with higher modulation level can support a higher bit-rate but holds a shorter transmission reach.
P_{ij} : The set of all the possible routing paths from node i to node j, while each of which can be established by a lightpath using DP-BPSK.
m_p : The modulation format with the highest modulation level that can be used over path p, which depends on the length of path p.
L_p : The set of physical links traversing path p.
N_p : The set of nodes along path p.
S : The maximum usable FSs for each link in the network.
G : The bandwidth of the switching guard-band used to separate two adjacent lightpaths, denoted by the number of FSs.
$\triangle_{OC}$: The number of FSs occupied by each optical carrier.
C_m : The bit-rate that an optical carrier can support using modulation format m, which in accordance with what is shown in Table 1.1
α : The weighting coefficient ($0 \leq \alpha \leq 1$).

Variables

$x_{ijp}^{sd} \in \{0, 1\}$: Indicates whether path $p \in P_{ij}$ has been established for the node pair $\langle i, j\rangle$ to serve the connection request between node pair $\langle s, d\rangle$. This value equals 1 if the path has been established.
$f_{ij}^{sd} \in \mathbb{Z}_0^+$: Denotes the starting index of an FS of a lightpath between the node pair $\langle i, j\rangle$, used to serve the connection request between node pair $\langle s, d\rangle$.
$\varphi_{iji'j'}^{sds'd'} \in \{0, 1\}$: Equals 0 when the starting index of the assigned FSs of a lightpath between the node pair $\langle i', j'\rangle$ used to serve the connection request between node pair $\langle s', d'\rangle$ is smaller than the starting index of the FS of a lightpath between the node pair $\langle i, j\rangle$ used to serve the connection request between node pair $\langle s, d\rangle$ (i.e., $f_{i'j'}^{s'd'} < f_{ij}^{sd}$); otherwise, it equals 1.
$F_{max} \in \mathbb{Z}^+$: The maximal index of FSs used in the entire network.

$T \in \mathbb{Z}^+$: The total number of transceivers used in the entire network.

Objective function

$$\text{Minimize} \quad Cost = \alpha \cdot F_{max} + (1-\alpha) \cdot T \tag{2.1}$$

Constraints

Cost constraints:

$$f_{ij}^{sd} + \triangle_{OC} \cdot \lceil \frac{\lambda_{sd}}{C_{m_p}} \rceil \cdot x_{ijp}^{sd} + G \leq F_{max} \quad \forall \langle s,d \rangle, \langle i,j \rangle \in NP, p \in P_{ij} \tag{2.2}$$

$$\sum_{\langle s,d \rangle, \langle i,j \rangle \in NP} \sum_{p \in P_{ij}} 2\lceil \frac{\lambda_{sd}}{C_{m_p}} \rceil \cdot x_{ijp}^{sd} \leq T \tag{2.3}$$

Constraint (2.2) ensures that the maximum index of utilized FSs is no smaller than the ending FS index of any established lightpath p. Constraint (2.3) computes the number of transceivers required by all lightpaths over all the connection requests.

Route selection constraints:

$$\sum_{p \in P_{ij}} x_{ijp}^{sd} \leq 1 \quad \forall \langle s,d \rangle, \langle i,j \rangle \in NP \tag{2.4}$$

$$\sum_{j \in V: j \neq i} \sum_{p \in P_{ij}} x_{ijp}^{sd} - \sum_{j \in V: j \neq i} \sum_{p' \in P_{ji}} x_{jip'}^{sd} = \begin{cases} 1, \text{ if } s = i \\ -1, \text{ if } d = i \\ 0, \text{ otherwise} \end{cases} \quad \forall \langle s,d \rangle \in NP, i \in V \tag{2.5}$$

Constraint (2.4) ensures that no bifurcation of a traffic flow occurs; each traffic request between node pair $\langle s,d \rangle$ is routed along a single lightpath p between a node pair $\langle i,j \rangle$. Flow conservation on a lightpath is imposed by the Constraint (2.5). Constraints (2.4)~(2.5) ensure a unique path consisting of several partitioned lightpaths established between a node pair.

Spectrum assignment constraints:

$$\varphi_{iji'j'}^{sds'd'} + \varphi_{i'j'ij}^{s'd'sd} = 1 \quad \forall \langle s,d \rangle, \langle s',d' \rangle, \langle i,j \rangle, \langle i',j' \rangle \in NP : \langle s,d \rangle \neq \langle s',d' \rangle \tag{2.6}$$

$$f_{i'j'}^{s'd'} - f_{ij}^{sd} \leq S \cdot \varphi_{iji'j'}^{sds'd'} \quad \forall \langle s,d \rangle, \langle s',d' \rangle, \langle i,j \rangle, \langle i',j' \rangle \in NP : \langle s,d \rangle \neq \langle s',d' \rangle \tag{2.7}$$

$$f_{ij}^{sd} + \triangle_{OC} \cdot \lceil \frac{\lambda_{sd}}{C_{m_p}} \rceil + G - f_{i'j'}^{s'd'} \leq (S+G) \cdot (1 - \varphi_{iji'j'}^{sds'd'} + 2 - x_{ijp}^{sd} - x_{i'j'p'}^{s'd'})$$
$$\forall \langle s,d \rangle, \langle s',d' \rangle, \langle i,j \rangle, \langle i',j' \rangle \in NP, p \in P_{ij}, p' \in P_{i'j'} : \langle s,d \rangle \neq \langle s',d' \rangle, L_p \cap L_{p'} \neq \oslash \tag{2.8}$$

Constraints (2.6)~(2.8) ensure that the spectrum used by the two partitioned lightpaths p and p', which share common link(s) to serve the requests between node pairs $\langle s,d \rangle$ and $\langle s',d' \rangle$, do not overlap. That is, when p and p' share common link(s), the assigned FSs of a lightpath p must either be before the starting FS index of lightpath p' or after the ending FS index of lightpath p'. In other words, constraints (2.6)~(2.8) ensure spectrum continuity, spectrum contiguity, and non-overlap between the different lightpaths that share common link(s).

2.1.1 Discussion of the proposed ILP model

In the proposed ILP model, a path from a source node s to a destination node d may be composed of multiple partitioned lightpaths, which makes the RMSTA problem more complex than the RSA and $RMSA$ problems. We can see that the computational complexity required to solve the problem is dominated by the number of variables, that is, the larger of $O(|NP|^2 \cdot |P|)$ and $O(|NP|^4)$, where $|P|$ denotes the number of paths per node pair. Here, the number of constraints is bound by $O(|NP|^4 \cdot |P|^2)$ from Constraint (2.8). In the worst case, when all the nodes are fully connected, $|P|$ is equal to $(|V|-2)!$. We can see that it is difficult to solve the RMSTA problem by the ILP-RMSTA method for a large-scale network and/or under heavy traffic volumes. In fact, we tried to solve the RMSTA problem in a simple 7-node DT network, but this problem could not be solved to optimality in a 12-hour period. Therefore, in this paper, we propose an efficient heuristic algorithm to solve the problem. To examine the performance of the proposed heuristic algorithm, we use the two lower-bounds obtained as described in the next section.

2.2 lower-bound analysis of the RMSTA problem

In this section, we discuss the lower-bound of the RMSTA problem. We propose two approaches to find the lower-bound of the RMSTA problem. The main idea behind the first approach is to obtain the lower-bounds of the decision variables of the objective function Eq. (2.1), that is, the F_{max} and T, separately. Then, the lower-bound of the problem can be obtained. The main idea behind the second approach is to relax some of the constraints in the proposed ILP model above and then solve the relaxed model using an appropriate approach (e.g., using an ILP solver such as Gurobi [138]).

2.2.1 The lower-bound of F_{max}

Here, we assume that the cost of using a transceiver is zero—that is, a node can use a transceiver without incurring any cost for regeneration. For each link e, the modulation format with the highest modulation level that can be applied on this link is denoted by m_e. For a given traffic volume λ_{sd} between source-destination pair $\langle s, d\rangle$, we can calculate the required FSs for each link e by Eq. (2.9) as follows:

$$W_e = \triangle_{OC} \lceil \frac{\lambda_{sd}}{C_{m_e}} \rceil + G \tag{2.9}$$

Then, we set W_e to be the weight of the link e. Therefore, the routing path that uses the fewest FSs to serve the connection request between node pair $\langle s, d\rangle$ can be obtained using Dijkstra's algorithm and the weight of the shortest path is the one that has the fewest FSs required by the connection request $\langle s, d\rangle$ (denoted as F^{sd}_{min}).

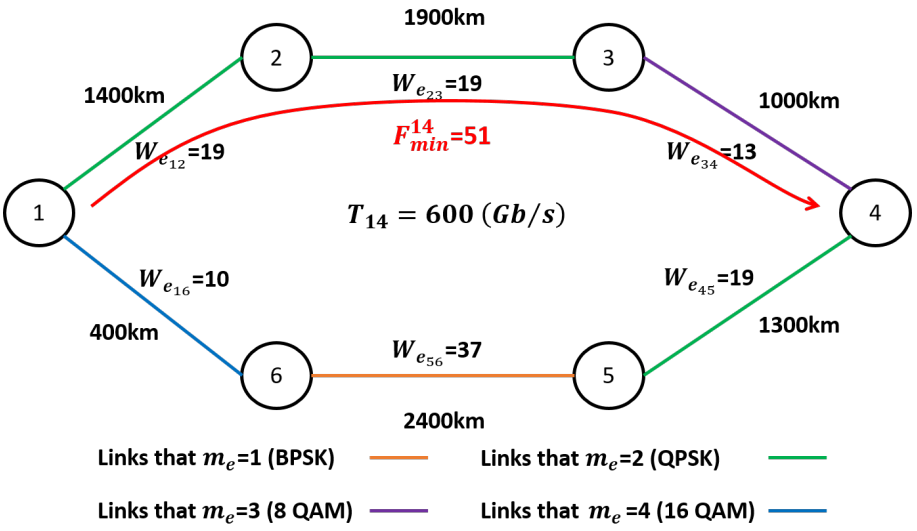

Figure 2.1: Illustration of the required FSs.

A simple example is shown in Fig. 2.1. The traffic volumes of the connection request between node pair $\langle 1, 4\rangle$ and the guard-band G are assumed to be 600 Gbps and 1 FS, respectively. Moreover, the number of FSs occupied by an optical carrier is assumed to be 3. We can see that for link e_{12} with 1400 km length, the DP-QPSK modulation format can be used on this link. Therefore, the weight of link e_{12} is equal to 19 which is obtained by $3\lceil 600/100\rceil + 1$ according to Eq. (2.9) and the supported bit-rate per optical carrier has been shown in Table 1.1. The other connection requests can be determined using the same process. Therefore, the smallest number of FSs required by the connection request $\langle 1, 4\rangle$ (F_{min}^{14}) can be obtained using Dijkstra's algorithm. Here, it equals 51.

Consequently, the total FSs required by all the requests (F_{min}^{total}) on all the links is, at minimum, equal to $\sum_{\langle s,d\rangle \in NP} F_{min}^{sd}$. Therefore, the lower-bound of F_{max} is the ratio of F_{min}^{total} to the number of links in the network (i.e., when the required FSs are evenly assigned to the links in the whole network.). Thus, the processes above eventually yield the lower-bound of F_{max}, as shown in Eq. (2.10).

$$F_{max} \geq \frac{\sum_{\langle s,d\rangle \in NP} F_{min}^{sd}}{|E|} \tag{2.10}$$

2.2.2 The lower-bound of T

In this subsection, we assume that all the requests are routed by the shortest path and that optical signals can be regenerated at any site without considering whether a node actually exists at that site on the routing path. Under the assumptions above, we then try to calculate the minimum number of required transceivers for each connection request. Therefore, following similar processes as those used to obtain the lower-bound of F_{max}, we can obtain the smallest required number of transceivers

for each connection request and then sum them to obtain the lower-bound of T.

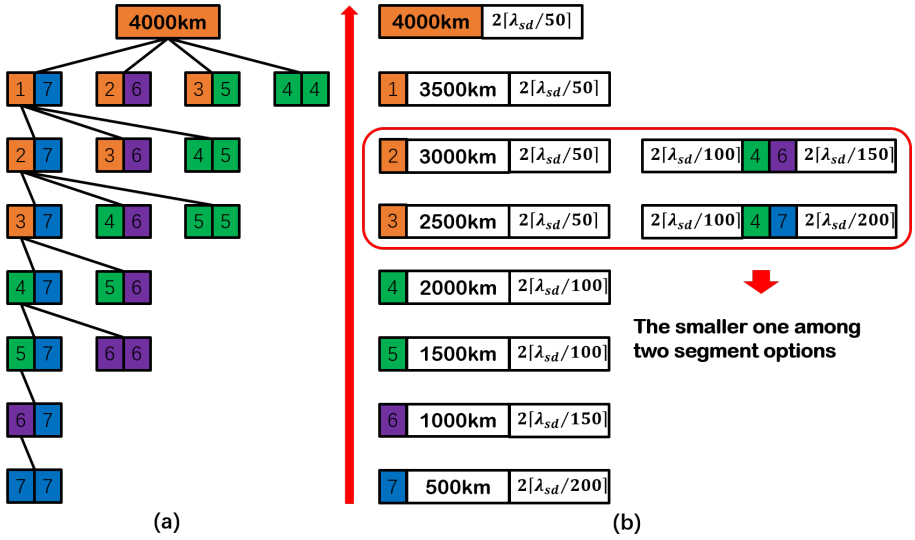

Figure 2.2: Illustration of (a) the recursive invocation tree of a routing path with 4000 km length, (b) the minimum transceiver usage.

For a given request within λ_{sd} Gbps traffic volume, the number of required transceivers depends on how the routing path is segmented. To find the best partitions for a routing path, we use an iterative approach. For any lightpath, we first determine whether to split it into two shorter lightpaths. Then, for each partitioned lightpath we further determine whether to partition it further. This process continues until the path length is within the reachable distance of the modulation format with the fastest bit-rate. In the following example, a path length below 500 km will not be partitioned further. Therefore, the problem for determining the number of transceivers becomes a typical *Rod Cutting* problem [139], which can be solved using a dynamic programming algorithm. To help readers understand this approach, we show the recursive invocation tree of a lightpath with 4000 km length in Fig. 2.2.a. Moreover, in the case of without regeneration, the number of the required transceivers for a routing path with different path lengths can be obtained — according to the transmission reaches and supportable bit-rates per optical carrier for different modulation formats listed in Table 1.1 — as shown in Table 2.1.

Therefore, according to Fig. 2.2.a and Table 2.1, we can determine the best segment options which lead to the smallest value of T^{sd}_{min} by using a bottom-up method. For instance, a path with an index of 6 (500 km $\sim$ 1000 km) can be divided into two paths with indices of 7 (0 km $\sim$ 500 km), each of which uses a higher-level modulation format. Therefore, for this path, non-regeneration requires $2\lceil\lambda_{sd}/150\rceil$ transceivers and the segmented option requires $4\lceil\lambda_{sd}/200\rceil$ transceivers. We select the option that uses the fewest transceivers, save the results of this strategy, and do not recalculate the segment again each time.

Table 2.1: Usable modulation levels and required transceivers of different path lengths.

Reachable range	Index	Modulation	Transceivers
3,500km	1	DP-BPSK	$2\lceil\lambda_{sd}/50\rceil$
3,000km	2	DP-BPSK	$2\lceil\lambda_{sd}/50\rceil$
2,500km	3	DP-BPSK	$2\lceil\lambda_{sd}/50\rceil$
2,000km	4	DP-QPSK	$2\lceil\lambda_{sd}/100\rceil$
1,500km	5	DP-QPSK	$2\lceil\lambda_{sd}/100\rceil$
1,000km	6	DP-8-QAM	$2\lceil\lambda_{sd}/150\rceil$
500km	7	DP-16-QAM	$2\lceil\lambda_{sd}/200\rceil$

Additionally, to simplify the recursive invocation tree (Fig. 2.2.a), we introduce two equations that are always true as follows:

$$\lceil\frac{\lambda_{sd}}{X}\rceil \leq 2\lceil\frac{\lambda_{sd}}{2X}\rceil \quad \forall X \in \mathbb{Z}^+ \tag{2.11}$$

$$\lceil\frac{\lambda_{sd}}{X}\rceil \leq \lceil\frac{\lambda_{sd}}{Y}\rceil \quad \forall X, Y \in \mathbb{Z}^+ : Y \leq X \tag{2.12}$$

According to Eq. (2.11) and Eq. (2.12), we can remove the segment options that require more transceivers, and thus simplify the recursive invocation tree. For example, the 6-index path has two segment options,a non-regeneration option and one that is a combination of two 7-index paths, respectively. The transceiver usages are equal to $2\lceil\lambda_{sd}/150\rceil$ and $4\lceil\lambda_{sd}/200\rceil$, respectively. However, according to Eq. (2.12), we have $2\lceil\lambda_{sd}/150\rceil \leq 2\lceil\lambda_{sd}/100\rceil$, and according to Eq. (2.11), we have $2\lceil\lambda_{sd}/100\rceil \leq 4\lceil\lambda_{sd}/200\rceil$. Thus, non-regeneration is the best option for the 6-index path because it requires less transceivers. The segment option that is the combination of the two 7-index paths can be removed from the recursive invocation tree (Fig. 2.2.a). Then, the recursive invocation tree goes from bottom to top. The 5-index path also has two segment options, non-regenerative and the one that is a combination of a 6- and 7-index path, respectively. According to Eq. (2.11) and Eq. (2.12), the $2\lceil\lambda_{sd}/100\rceil$ (non-regeneration) is smaller than $4\lceil\lambda_{sd}/200\rceil$, and $4\lceil\lambda_{sd}/200\rceil$ is smaller than $2\lceil\lambda_{sd}/150\rceil$ (the 6-index path) + $2\lceil\lambda_{sd}/200\rceil$ (the 7-index path). Therefore, the segment option that is the combination of the 6- and 7-index path can be removed, because non-regeneration is also the best option for the 5-index path. As shown in Fig. 2.2.a, beginning from the 4-index path, more segment options should be considered when making comparisons. According to Eq. (2.11) and Eq. (2.12), we can remove the segment options that require more transceivers to simplify the recursive invocation tree. For some paths, we may not able to obtain a best or unique segment option (e.g., 2-index and 3-index paths), but if the traffic volume λ_{sd} is given, a best segment option can be obtained. This process eventually yields the results shown in Fig 2.2.b, which represents the smallest values of T^{sd}_{min} for different path lengths.

From Fig.2.2.b, for a given request with λ_{sd} Gbps traffic volume and the shortest routing path, we calculate the minimum transceiver usage for this request as T^{sd}_{min}. Thus, we can see that the lower-bound of total transceiver usage, T, will be the sum of T^{sd}_{min} for all node pairs as shown in Eq.

(2.13).

$$T \geq \sum_{\langle s,d\rangle \in NP} T^{sd}_{min}. \tag{2.13}$$

As a result, the lower-bound of the RMSTA problem is the sum of the lower-bounds of F_{max} and T by tuning the weighting coefficient α. However, because we obtained the two variables that affect the objective function separately but did not consider the relationship between the two variables, the lower-bound is not a tight lower-bound for the problem. Therefore, in the following subsection, we also show a different approach that can obtain a relatively tighter lower-bound by relaxing some of the constraints of the ILP model proposed in Section 2.1.

2.2.3 lower-bound obtained by relaxing the problem constraints

Another way to obtain the lower-bound of the problem is to relax the original problem constraints and then use the solution of the relaxed problem as the lower-bound. In the definition of the original RMSTA problem, each connection request is allocated to a set of contiguous FSs over each partitioned lightpath. Here, we assume that we can completely separate a connection request into multiple connection requests, each of which requires only 1 FS and can be individually routed without the need of guard-band G. In other words, there is no need to satisfy the constraints of spectrum continuity for each connection request. Therefore, we can significantly reduce the complexity of the problem, which leads to the lower-bound can be found using a commercial optimization solver in a reasonable time, even for quite large networks with heavy traffic volumes. The ILP model which relaxed the constraints of spectrum continuity is shown in the following, where the $P(e)$ represents the set of routing paths going through link e.

The relaxed ILP model

$$Minimize \quad Cost = \alpha \cdot F_{max} + (1-\alpha) \cdot T \tag{2.14}$$

Constraints

$$\sum_{\langle s,d\rangle,\langle i,j\rangle \in NP} \sum_{p \in P_{ij} \cap P(e)} (\triangle_{OC} \cdot \lceil \frac{\lambda_{sd}}{C_{m_p}} \rceil + G) \cdot x^{sd}_{ijp} \quad \leq F_{max} \quad \forall e \in E \tag{2.15}$$

$$\sum_{\langle s,d\rangle \in NP} \sum_{\langle i,j\rangle \in NP} \sum_{p \in P_{ij}} 2\lceil \frac{\lambda_{sd}}{C_{m_p}} \rceil \cdot x^{sd}_{ijp} \leq T \tag{2.16}$$

$$\sum_{p \in P_{ij}} x^{sd}_{ijp} \leq 1 \quad \forall \langle s,d\rangle, \langle i,j\rangle \in NP \tag{2.17}$$

$$\sum_{j \in V: j \neq i} \sum_{p \in P_{ij}} x^{sd}_{ijp} - \sum_{j \in V: j \neq i} \sum_{p' \in P_{ji}} x^{sd}_{jip'} = \begin{cases} 1, \text{ if } s = i \\ -1, \text{ if } d = i \\ 0, \text{ Otherwise} \end{cases} \quad \forall \langle s,d\rangle \in NP, i \in V \tag{2.18}$$

Constraint (2.15) ensures that the maximum index of the utilized FSs is no smaller than the number of FSs used to serve the requests on any link e. The constraints of spectrum continuity are relaxed. Constraints (2.17) and (2.18) are the same as the routing constraints proposed in the *RMSTA* ILP model. Thus, this approach significantly reduces the dominant numbers of variables and constraints, to $O(|NP|^2 \cdot |P|)$ and $O(|NP|^2)$, respectively, and the model can be solved in an acceptable time using the commercial optimization solvers.

2.3 Heuristic algorithm for RMSTA

In this section, we propose a heuristic algorithm called graph and virtual network-based assignment (GVNA), which consists of two components: *the virtual network construction* and *the routing, modulation, spectrum, and transceiver assignment*.

2.3.1 Virtual network construction

Algorithm 1 Virtual network construction.

Input: Physical network topology $G(V, E)$ and a connection request with $\{\lambda_{sd}\}$ traffic volume between node pair $\langle s, d \rangle$

Output: A virtual network $G_{vn}(V_{vn}, E_{vn})$

```
1: Generate a new network topology, denoted by G_vn(V_vn = V_vn, E_vn = ∅)
2: for each node pair ⟨i, j⟩ ∈ NP do
3:    sp_ij ← calculate the shortest physical path (in weight) between the node pair ⟨i, j⟩ by Dijkstra's algorithm
4:    len(sp_ij) ← calculate the length of sp_ij
5:    for each available modulation format m (from high-level one to the low-level one) do
6:       if len(sp_ij) is smaller than the transmission reach of modulation format m then
7:          Build a virtual link ve_ij between node pair ⟨i, j⟩ — append ve_ij into E_vn
8:          ve_ij.sp ← sp_ij
9:          ve_ij.m ← m
10:         vl_ij.weight ← calculate the the weight of virtual link ve_ij by Eq. (2.19) according to ve_ij.sp and ve_ij.m
11:         break for
12:      end if
13:   end for
14: end for
15: return G_vn
```

The virtual network denoted by $G_{vn}(V_{vn}, E_{vn})$ is constructed based on the physical network topologies, where the V_{vn} and E_{vn} represents the set of virtual nodes and links, respectively. The V_{vn} is always identical with the set of nodes V in the physical network $G(V, E)$. Here, we assume that: i) the function $len(p)$ returns the length (in km) of physical path p, ii) the $SE(p)$ represents the set of physical links along the physical path p, and iii) the ω_e represents the weight of physical link

e. The shortest path (in weight, i.e., the sum of ω_e for each link e along the path) between node pair $\langle i, j \rangle$ can be obtained by the Dijkstra's algorithm, which is denoted by sp_{ij}. If the length of this path $len(sp_{ij})$ is shorter than the transmission reach of a certain modulation format (see Table 1.1), we will build a virtual link ve_{ij} between node pair $\langle i, j \rangle$ and record the modulation format with the highest modulation level which can be applied on this path, depending on the path length $len(sp_{ij})$. Such a virtual link has several attributes as listed Table 2.2.

Table 2.2: Attributes of a virtual link ve_{ij}.

Attribute	Definition
$ve_{ij}.sp$	The shortest physical path sp_{ij} between node pair $\langle i, j \rangle$
$ve_{ij}.m$	The highest-level modulation format can be applied on sp_{ij}
$ve_{ij}.weight$	The weight of the virtual link ve_{ij}

For a given connection request with λ_{sd} traffic volume between node pair $\langle s, d \rangle$, the weight of the virtual link $ve_{ij}.weight$ is computed by Eq. (2.19) as follows:

$$ve_{ij}.weight = \alpha \cdot \frac{F_{ij}}{|E|} + (1 - \alpha) \cdot T_{ve} \tag{2.19}$$

where

$$F_{ij} = |SE(ve_{ij}.sp)| \cdot (\triangle_{OC} \cdot \frac{\lambda_{sd}}{C_{ve_{ij}.m}} + G) \tag{2.20}$$

$$T_{ve} = 2\frac{\lambda_{sd}}{C_{ve_{ij}.m}} \tag{2.21}$$

In Eq. (2.20), $|SE(ve_{ij}.sp)|$ represents the number of the physical links along the shortest physical path $ve_{ij}.sp$; thus, F_{ij} represents the total number of required FSs along the path. T_{ve} in Eq. (2.21) represents the total number of required transceivers, and $|E|$ represents the number of all physical links in the network. Thus, if the virtual link ve_{ij} is selected to serve the connection request, the weight of the virtual link $ve_{ij}.weight$ indicates the weighted sum of the required FSs and transceivers that will be used. Briefly, from Eq. (2.20), we can see that the virtual links (ve_{ij}) whose shortest physical paths $ve_{ij}.sp$ require fewer FSs and transceivers will result in a smaller value of $ve_{ij}.weight$. Finally, for each node pair in the network, we will try to build a virtual link to create a virtual network.

Fig. 2.3 provides an example of virtual network construction using the simple 6-node network shown in Fig. 2.1. We assume that there is a 600 Gbps traffic volume between node pair $\langle 1, 4 \rangle$ and that α and $\triangle_{OC}$ are equal to 0.5 and 3, respectively. For a node pair $\langle 2, 4 \rangle$, for example, the shortest physical path is $[2, 3, 4]$, whose length is 2,900 km; therefore, a virtual link, (ve_{24}) can be established between the node pair $\langle 2, 4 \rangle$. The values of $ve_{24}.sp$, $ve_{24}.m$, and $ve_{24}.weight$ are determined to be $[2, 3, 4]$, 1, and 18.2, respectively. Moreover, we can see that no virtual link can be established

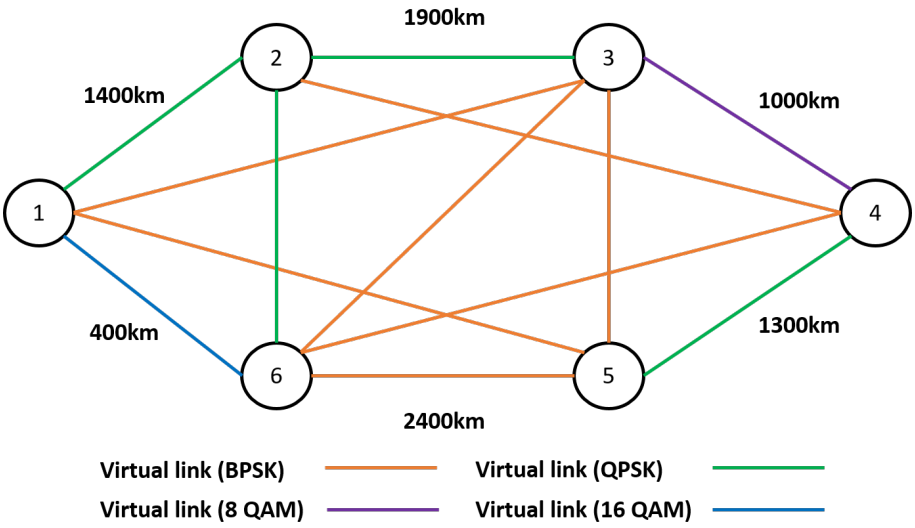

Figure 2.3: Example of virtual network construction.

between the node pairs $\langle 1, 4\rangle$ and $\langle 2, 5\rangle$, because the lengths of the shortest physical paths between these node pairs are beyond the reachable distance of the DP-BPSK modulation format (i.e., 4,000 km as shown in Table 1.1).

The pseudocode for the virtual network construction algorithm is shown in Algorithm 1.

2.3.2 Routing, modulation, spectrum and transceiver assignment

As shown in Algorithm 1, we illustrate how to create a virtual network for a given connection request. In a virtual network, each virtual link has been weighted and the value reflects the FS and transceiver usage required by the physical paths corresponding to this virtual link. Therefore, based on the virtual network, we can find the shortest virtual path using Dijkstra's algorithm for a connection request between node pair $\langle s, d\rangle$. This virtual path denoted as vp_{sd}, has made a trade-off between FS and transceiver usage. Such a virtual path may consist of one or multiple virtual links, and each virtual link corresponds to a physical path. In other words, each virtual link corresponds to a partitioned lightpath on the routing path between node pair $\langle s, d\rangle$. Therefore, each virtual path can be converted to a (physical) routing path consisting of either one or multiple partitioned lightpaths. This is a candidate routing path for the connection request between node pair $\langle s, d\rangle$.

However, we should find multiple candidate routing paths for each connection request. Therefore, at this stage, for a given connection request between node pair $\langle s, d\rangle$, we find candidate paths one-by-one individually: whenever a candidate path is found, we increase the weight of the physical links that correspond to this physical path. In other words, for each physical link e along the currently found candidate routing path, we will double its weight (i.e., ω_e). Then, we generate another new virtual network using Algorithm. 1. Note that the virtual network is constructed based on

Algorithm 2 Routing, modulation, spectrum and transceiver assignment algorithm.

Input: Physical network topology $G(V, E)$
Output: Value of the objective function Eq. (2.1)

Set F_{max} to be 0
Set T to be 0
for connection request with λ_{sd} traffic volume between each node pair $\langle s, d \rangle \in NP$ **do**
  for each link e in E **do**
    $\omega \leftarrow$ length of link e
  end for
  $x \leftarrow 0$
  Generate a new path candidate set $CP_{sd} = \oslash$
  while $x < k$ **do**
    Generate a virtual network $G_{vn}(V_{vn}, E_{vn})$ using Algorithm. 1
    $vp_{sd} \leftarrow$ calculate the shortest virtual path on G_{vn} by Dijkstra's algorithm
    $lp_{sd} \leftarrow$ convert the virtual path vp_{sd} into a physical routing path
    Append lp_{sd} into LP_{sd}
    $x \leftarrow x + 1$
    if $x < k$ **then**
      for each physical link e along lp_{sd} **do**
        Double the ω_e
      end for
    end if
  end while
  $lp_{sd}^{best} \leftarrow$ Select the best routing path in LP_{sd} that yields the smallest value of Eq. (2.22).
  Perform the FF-SA policy to assign the FSs on each partitioned lightpath of lp_{sd}^{best}
  Assign transceivers to the source, destination, and intersection nodes of two partitioned lightpaths
  Update F_{max}, T
end for
Compute $Cost$ using the objective function Eq. (2.1)

the original physical network; thus, when the weights of some of the physical links in the original physical network increase, the shortest path between $\langle i, j \rangle$ pair ($ve_{ij}.sp$) may also change, leading to the change of attributes of some virtual links. Therefore, based on the new virtual network, we can find another candidate routing path by employing Dijkstra's algorithm. This process repeats until we have found k candidate paths.

Thus far, we have obtained k candidate paths using G_{vn}. However, we still need to select the most suitable routing path among the candidate paths. We assume that function $FS\_MAX(lp)$ returns the highest index of the required FSs, if the connection request is transmitted along the candidate routing path lp, where the FSs assigned to each partitioned lightpath (each of which corresponding to a virtual link) on lp are assumed to be allocated using the first-fit spectrum allocation (FF-SA) policy. We will select the one among the k candidate routing paths which can lead to the

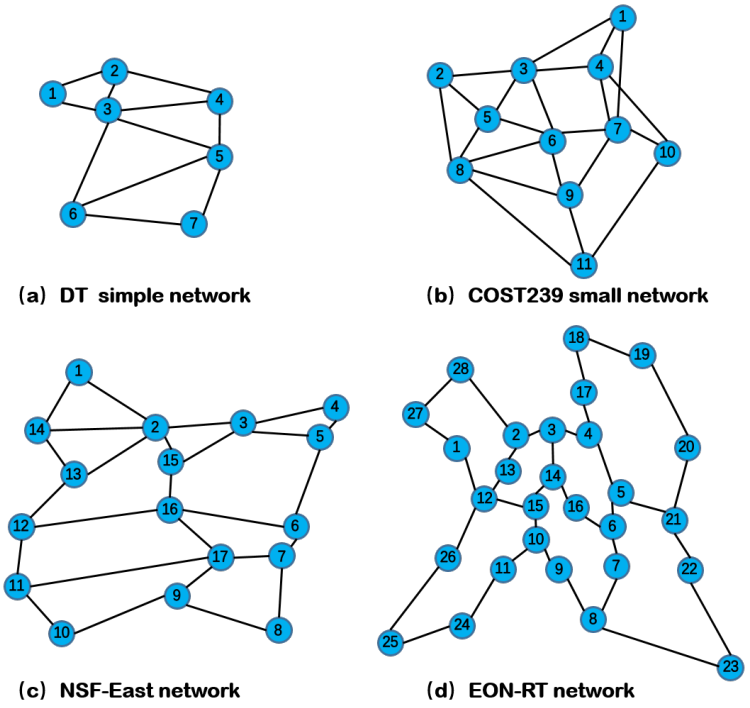

Figure 2.4: Illustration of network topologies: (a) 7-node DT, (b) 11-node COST239, (c) 17-node NSF-East, and (d) 28-node EON-RT.

lowest value of Eq. (2.22) shown as follows:

$$C(lp) = \alpha F' + (1-\alpha) \cdot T_{lp} : F' = max\{F\_MAX(lp), F_{max}\} \tag{2.22}$$

where F_{max} is the current maximal index of the FSs used in the entire network and T_{lp} represents the total number of transceivers required by lp.

The above processes will be repeated for each connection request until all the connection requests have been satisfied. We will serve connection requests one-by-one in accordance with a serving sequence in the following:

- Product of the Hops and Bit-rate First (PHBF) sequence: connection requests are sorted in descending order by the product of the hops in the shortest physical path of the connection request and its requested bit-rate. Then, we serve the connection request that has the largest product value first.

Finally, the pseudocode for *Routing, modulation, spectrum and transceiver assignment algorithm* is shown in Algorithm 2.

2.4 Simulation experiments and performance results

In this section, we evaluate the performance of the proposed heuristic algorithm using four network models of various sizes and scales as shown in Fig. 2.4. Table 2.4 lists the key parameters for the four tested networks.

Table 2.3: Key parameters of networks used in the simulation experiments.

Information	DT [140]	COST239 [141]	NSF-East [142]	EON-RT [143]
Number of nodes	7	11	17	28
Number of links	11	22	26	34
Average node degree	3.1	4.0	3.1	2.4
Average link length	236 km	421 km	630 km	733 km

The simulation experiments were performed on a computer running the Microsoft Windows 10 operating system with 16 GB memory and an AMD Ryzen 3.6 GHz CPU. The tight lower-bound obtained by the relaxed ILP-RMSTA model was obtained using the commercial optimization software AMPL/Gurobi (v8.0.1) [138]. We compared the performance of the proposed algorithm with that of three previously proposed algorithms implemented as listed below.

- *Maximum Reuse Spectrum Allocation* (MRSA) algorithm for the RSA problem as proposed in [38], where the modulation format used in the RSA problem is assumed to be BPSK.
- Longest Path First (LPF) ordering + Heuristic Allocation algorithm for the RMSA problem as proposed in [52]. This algorithm was included because LPF ordering achieves the best results (without considering the iteration).
- The MCLOD algorithm for the RMSTA problem as proposed in [27]. This algorithm was included because it is the only previous work that considers both the spectrum usage and the detailed transceiver usage, which is the same optimization objective as our work. Moreover, for a fair comparison, in the simulation experiments with the MCLOD algorithm, we adopt the same ordering (for a given traffic matrix) used by our algorithm.

For all the algorithms, the spectral super-channel transmission is assumed, where each optical carrier supports 25 Gbaud symbol-rate and occupies $\triangle_{OC} = 3$ FSs (37.5 GHz). A guard-band of 1 FSs (12.5 GHz) is assumed to separate two spectral super-channels. The number of candidate routing paths k is assumed to be 5 (per connection request). We evaluated 10 different connection request matrices and the results are averaged For each connection request matrix, we assume that there is a connection request between each node pair. That is, the number of connection requests equals $V(V-1)$, which equates to 42, 110, 272, 756 for the DT7, COST239, NSF-East and EON-RT networks, respectively. The traffic volume for each connection request is randomly generated with bit-rates ranging from 50 Gbps to 1 Tbps.

2.4.1 Performance of the proposed algorithm

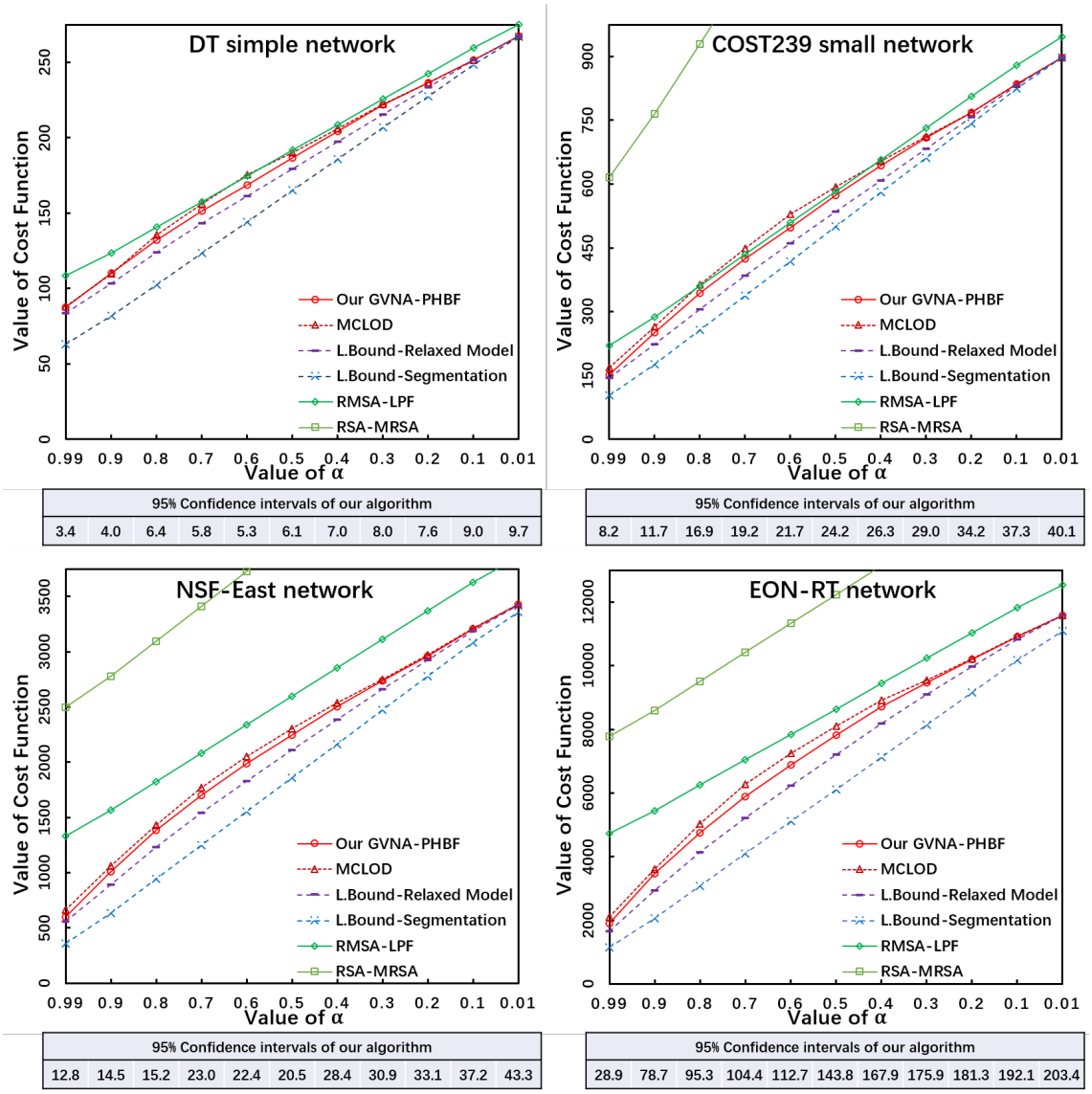

Figure 2.5: Cost comparison of various algorithms.

Fig. 2.5 shows the values of the cost function (see Eq. (2.1) in Section 2.1) of different algorithms as the coefficient α changes from 0.99 (i.e., aiming to minimize the FSs) to 0.01 (i.e., aiming to minimize the transceivers). The tables under the figures show the 95% confidence intervals of the proposed GVNA-PHBF algorithm. In Fig. 2.5 — compared to the algorithm that does not consider signal regeneration and modulation (the RSA problem) — we can see that the proposed algorithm achieves far better results. Moreover, compared to the algorithm that does not consider regeneration (the RMSA problem), the proposed algorithm performs somewhat better on small networks, and considerably better on large networks. Moreover, compared to the MCLOD algorithm, GVNA per-

forms better for all values of the coefficient α. Finally, we can observe that the proposed algorithm is very close to the lower-bound of the RMSTA problem.

To further compare the different algorithms, we use the metric *gain* (denoted by G_i), which is the ratio of the cost achieved by the proposed algorithm to another algorithm i and defined as follows.

$$G_i = \frac{\text{The cost of algorithm } i}{\text{The cost of the proposed algorithm}} - 1. \tag{2.23}$$

Here, we show the cost gains achieved by the proposed algorithm and by the RMSA-LPF algorithm on each network in Fig. 2.6.

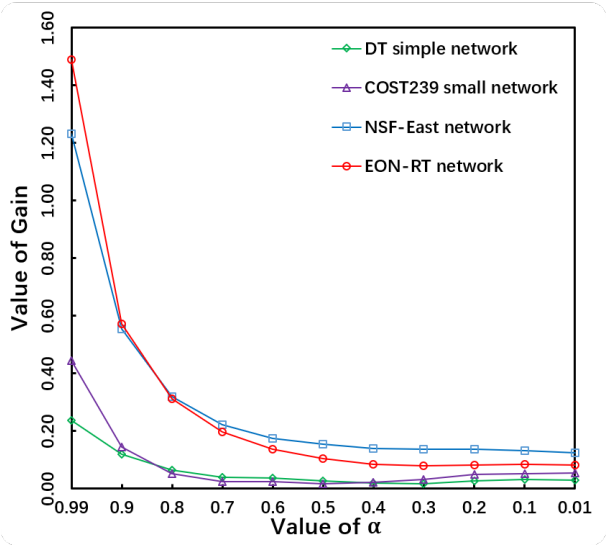

Figure 2.6: The cost gain between GVNA-PHBF and RMSA-LPF.

As Fig. 2.6 shows, cost gains are significantly high as the network size increased. On the NSF-East and EON-RT networks, the proposed algorithm achieved significant improvements (8% $\sim$ 149% and 8% $\sim$ 123% for NSF-East and EON-RT networks, respectively) over the RMSA-LPF algorithm, especially when α is large.

2.4.2 Computational time comparison

Table 2.4 shows the average computational time required by each algorithm on each network (over different α and traffic matrices). The 95% confidence intervals of the computational time of the proposed GVNA-PHBF are shown in line 4 of the table.

From Table 2.4, as the network size increases, we can see that the computational time increases substantially for all the algorithms. The RSA-MRSA and RMSA-LPF algorithms require less computational time because they do not consider the modulation adaptively and/or flexible regeneration; thus, they also lead to the worst results (see Fig. 2.5). Moreover, as we have discussed in

Table 2.4: Computational time (in seconds) of different algorithms on each network.

Algorithm	DT7	COST239	NSF-East	EON-RT
RSA-MRSA	0.005	0.016	0.158	1.897
RMSA-LPF	0.008	0.038	0.461	4.161
GVNA-PHBF	0.061	0.390	2.543	21.550
(95% confidence intervals)	0.001	0.002	0.007	0.112
MCLOD	0.029	0.219	9.230	776.265

Section 1.2.9, for a given connection request, the time complexity of the MCLOD algorithm is $O(2^{n-1})$ per request, where n is equal to the hop-length of the path with the largest hop-length in the allowable paths generated using a KSP algorithm. Therefore, as the network size increase, the compute time of the MCLOD algorithm will increase exponentially. Thus, we can see that while the MCLOD algorithm requires less computational time than the proposed GVNA-PHBF algorithm on small networks, as the network size increases, the computational time difference between the proposed GVNA-PHBF algorithm and the MCLOD algorithm becomes smaller and smaller. Finally, on the 28-node EON-RT network, the MCLOD algorithm requires more than 700 seconds, while the proposed GVNA-PHBF algorithm only requires approximately 20 seconds. This computational time difference can be expected to enlarge further when even larger networks are considered.

From the above results, compared to algorithms that do not consider regeneration (transceiver allocation), the proposed algorithm achieves far better results and is close to the lower-bound. Moreover, compared to algorithms that do consider regeneration, we achieve better results in less time on large networks. Overall, the proposed algorithm is more suitable for large networks than are the previous algorithms.

Chapter 3

Routing, Spectrum and Core Assignment in SDM-EONs with MCF: Node-arc ILP/MILP Methods and an Efficient XT-aware Heuristic Algorithm

In this chapter, we focus on the static RSCA problem in SDM-EONs with MCFs. As we have discussed in Section 1.3.4, for RSCA problems, it is a challenging task to control the inter-core interference, called inter-core crosstalk (i.e., XT), within an acceptable level and simultaneously maximize the spectrum utilization. We first consider XT in a worst interference scenario (i.e., XT-worst approach), which can simplify the RSCA problem. In this scenario, we formulate the RSCA problem using a node-arc-based ILP model in which the numbers of both variables and constraints are greatly reduced compared with previous ILP models, thereby leading to a significant improvement in convergence efficiency. Then, we consider the XT strictly (i.e., XT-aware approach) and formulate the problem using a MILP model, which is an extension of the node-arc-based ILP method mentioned above, and it is more suitable for strict XT thresholds and/or geographically large networks, that is, it has a higher degree of generalizability. Finally, we propose an XT-aware-based heuristic algorithm. The simulation results demonstrate that the proposed heuristic algorithm achieves higher spectral efficiency, the higher degree of generalizability and higher computational efficiency than the existing heuristic algorithms.

This chapter is organized as follows. In Section 3.1, we present our node-arc-based ILP/MILP optimization models for the static RSCA problem based on the XT-WC and XT-aware approaches. In Section 3.2, we propose a novel heuristic algorithm based on the XT-aware approach. In Section 3.3, we present the results and evaluate the performance.

3.1 Problem formulation

In this section, we first present a node-arc-based ILP optimization model based on the XT-WC approach. Then, we present an extended (node-arc-based) MILP optimization model based on the XT-aware approach. Finally, we compare our optimization models with the existing path-based ILP optimization models. The flexible single-carrier transmission shown in Section 1.2.4 and the basic SDM network architecture shown in Section 1.3.2 are considered. Additionally, we assume that the modulation format m used for transmission is given beforehand.

3.1.1 Node-arc-based ILP optimization model based on XT-WC approach

Parameters

V : The set of network nodes.

E : The set of network links.

C : The set of cores on each MCF.

N_c : The set of adjacent cores of core c.

R : The connection request matrix, $r = \{s(r), d(r), \lambda_r\} \in R$, where $s(r)$ and $d(r)$ are the starting and ending nodes of r, respectively, and λ_r is the required FSs of r.

L_i : The set of links that start or end at node i.

$xt^e_{cc'}$: The XT between core c and core c' on link e based on Eq. (1.2) by setting L equal to the length of link e.

Θ_m : The inter-core crosstalk threshold of the given modulation format m.

F : The set of the required FSs in the network. In the worst case (i.e., all connection request pass through the same core in a common link), $|F| = \sum_{r \in R} \lambda_r$.

M : A large number

Variables

$l^{ec}_r \in \{0,1\}$: A binary variable that is equal to 1 if core c on link e is selected to serve connection request r and equal to 0 otherwise.

$n^i_r \in \{0,1\}$: A binary variable that is equal to 1 if the lightpath that is used to serve connection request r passes through node i and equal to 0 otherwise.

$\alpha_r \in \mathbb{Z}^+$: An integer variable that denotes the starting FS index of the lightpath that is used to serve connection request r.

$\beta_r \in \mathbb{Z}^+$: An integer variable that denotes the ending FS index of the lightpath that is used to serve connection request r.

$\varphi^{r'}_r \in \{0,1\}$: A binary variable that takes a value of 0 if the ending FS index $\beta_{r'}$ of the lightpath that is used to serve connection request r' is smaller than the starting FS index α_r of the lightpath that is

used to serve connection request r.

$F_{max} \in \mathbb{Z}^+$: An integer variable that indicates the number of maximum required FSs for the network.

Objective Function

$$\text{Minimize} \quad F_{max} \tag{3.1}$$

Constraints

Cost constraint:

$$\beta_r \leq F_{max} \quad \forall r \in R \tag{3.2}$$

Constraint (3.2) ensures that the maximum FS index F_{max} is not smaller than the ending FS index of the lightpath for any connection request r.

Route selection constraints

$$\sum_{c \in C} l_r^{ec} \leq 1 \quad \forall r \in R, e \in E \tag{3.3}$$

$$\sum_{c \in C} \sum_{e \in L_{s(r)}} l_r^{ec} = 1 \quad \forall r \in R \tag{3.4}$$

$$\sum_{c \in C} \sum_{e \in L_{d(r)}} l_r^{ec} = 1 \quad \forall r \in R \tag{3.5}$$

$$\sum_{c \in C} \sum_{e \in L_i} l_r^{ec} - 2n_r^i = 0 \quad \forall r \in R, i \in V : i \neq s(r), d(r) \tag{3.6}$$

$$2 \sum_{c \in C} l_r^{ec} \leq n_r^i + n_r^j \quad \forall r \in R, e : (i,j) \in E \tag{3.7}$$

Constraint (3.3) ensures that there is at most one core that can be selected on a link e for any connection request r. Constraint (3.4) ensures that for a connection request r, the first link of a lightpath starts from node $s(r)$. Thus, the sum must be equal to one. Constraint (3.5) ensures that for a connection request r, the last link of a lightpath ends at node $d(r)$. Thus, the sum must be equal to one. Constraint (3.6) ensures that for any intermediate node traversed by a lightpath, there are one link that should end at the node and one link that should start from the node. Constraint (3.7) ensures that if the lightpath for a connection request r traverses a link e:(i,j), it must also traverse nodes i and j.

Spectrum assignment constraints:

$$\varphi_r^{r'} + \varphi_{r'}^r = 1 \quad \forall r, r' \in R \tag{3.8}$$

$$\beta_{r'} - \alpha_r \leq |F|(\varphi_{r'}^r + 2 - l_r^{ec} - l_{r'}^{ec}) - 1 \quad \forall r, r' \in R : r \neq r', e \in E, c \in C \tag{3.9}$$

$$\beta_r = \alpha_r + \lambda_r - 1 \quad \forall r \in R \tag{3.10}$$

Constraints (3.8) and (3.9) ensure that the FSs of two lightpaths that share a common core on a link do not overlap. In other words, when two lightpaths share a core on a common link, the assigned FSs of one connection request can be either before or after the FSs of the other connection request. Thus, the spectrum non-overlapping constraint is satisfied. Constraint (3.10) ensures that the ending FS index β_r is equal to the starting FS index α_r plus the number of required FSs minus one for each connection request r, which ensures the constraint of spectrum contiguity. In addition, α_r and β_r are assigned as belonging to each connection request r, which potentially ensures the spectrum continuity.

Crosstalk constraints:

$$\sum_{c' \in N_c} \sum_{e \in E} xt^e_{cc'} \cdot l^{ec}_r \leq \Theta_m \quad \forall r \in R, c \in C \tag{3.11}$$

Constraint (3.11) ensures that for each connection request r, the XT of the lightpath that is selected by the route selection constraints (3.3)~(3.7) should be less than the XT threshold, where, based on the XT-WC approach, the worst interference scenario is considered, that is, we set A^e_c (see Eq. (1.3)) equal to N_c for all links.

3.1.2 Extended MILP optimization model based on XT-aware approach

The strict XT-aware MILP model is an extension of the node-arc-based ILP model in Section 3.1.1. The point is that we should calculate the XT on each assigned FS f for each connection request r strictly. Here, we introduce some additional variables and constraints, as follows.

Variables

$o^{ecf}_r \in \{0, 1\}$: A binary variable that is equal to 1 if the f-th FS of core c on link e is assigned to serve connection request r and equal to 0 otherwise.
t^{ef}_r: A continuous variable that indicates the XT on link e at the f-th FS for connection request r.

Constraints

$$\sum_{f \in F} o^{ecf}_r - \lambda_r \cdot l^{ec}_r = 0 \quad \forall r \in R, e \in E, c \in C \tag{3.12}$$

$$|F| \cdot (\sum_{c \in C} o^{ecf}_r - 1) \leq f - \alpha_r \quad \forall r \in R, e \in E, f \in F \tag{3.13}$$

$$|F| \cdot (\sum_{c \in C} o^{ecf}_r - 1) \leq \beta_r - f \quad \forall r \in R, e \in E, f \in F \tag{3.14}$$

Constraints (3.12)~(3.14) ensure the relationship between l^{ec}_r, α_r, β_r and the additional variable o^{ecf}_r. In other words, when core c on link e is selected to serve connection request r ($l^{ec}_r = 1$), the FSs between the starting FS index α_r and ending FS index β_r should be assigned to serve connection request r on core c of link e ($o^{ecf}_r = 1$, $f \in [\alpha_r, \beta_r]$).

Crosstalk constraints

For strict XT-aware, the XT Constraint (3.11) for the above node-arc-based ILP method is not available here, and two new constraints are introduced.

$$\sum_{c' \in N_c} \sum_{r' \in R} xt^{e}_{cc'} \cdot o^{ec'f}_{r'} - t^{ef}_{r} \leq M \cdot (1 - o^{ecf}_{r}) \quad \forall r \in R, e \in E, c \in C, f \in F \tag{3.15}$$

$$\sum_{e \in E} t^{ef}_{r} - \Theta_m \leq 0 \quad \forall r \in R, f \in F \tag{3.16}$$

Constraint (3.15) ensures that if the f-th FS of core c on link e is assigned to serve connection request r ($o^{ecf}_{r} = 1$), then the XT of connection request r on link e at the f-th FS (t^{ef}_{r}) should be greater than the sum of the XT due to the active adjacent cores on the common link e that share the same f (see Eq. (1.3)). For example, when $o^{ecf}_{r} = 1$, Constraint (3.15) becomes $\sum_{c' \in N_c} \sum_{r' \in R} xt^{e}_{cc'} \cdot o^{ec'f}_{r'} \leq t^{ef}_{r}$. If an active adjacent core c' of core c (in N_c) on the common link e is excited to serve another connection request r' ($o^{ec'f}_{r'} = 1$), then the XT between these two cores ($xt^{e}_{cc'}$) should be summed. Then, t^{ef}_{r} should be greater than the sum. In another case, when $o^{ecf}_{r} = 0$, Constraint (3.15) is deactivated due to the larger value $|F|$ on the right-hand side of the constraint. In other words, t^{ef}_{r} can be 0 in this case. Constraint (3.16) ensures that for each connection request r, the XT of the selected lightpath should be less than the XT threshold on each assigned FS. Overall, according to the constraints above, we have incorporated the XT-limit constraint into the MILP model based on the strict XT-aware approach.

3.1.3 Analysis of the proposed ILP/MILP models

In this subsection, we summarize the proposed node-arc-based ILP/MILP optimization models and compare them with the previous path-based ILP optimization models [95, 102]. The major differences are stated as follows.

First, the proposed ILP/MILP methods, which belong to the node-arc category, decide the optimal routes and allocate FSs and cores for all the connection requests simultaneously, whereas the ILP methods in [102] and [95], which belong to the path category, only allocate FSs for the lightpath services but do not find routes for the lightpath services. That is, several candidate paths between each source-destination pair should be pre-calculated as the input parameters of the ILP optimization models. If we assume that the XT-threshold is large enough, the optimal solutions can be obtained using the proposed node-arc-based ILP method. In contrast, only when all the routing paths for each connection request are considered, it is guaranteed that the optimal solutions can be obtained using the existing path-based ILP methods in [102] and [95]. If only a few (e.g., the KSP) pre-calculated candidate paths are considered for each connection request, a very efficient or even optimal solution may also be found, but we cannot claim that the current solutions are the optimal solutions if all the routing paths for each connection request are not considered in the optimization

process.

Second, the previous ILP methods [95, 102] consider the XT in the worst interference scenario (XT-WC), and the feasible lightpath space may become smaller (see Section 1.3.5) for a strict XT threshold, particularly in geographically large networks. In an extreme case, some connection requests may not be satisfied since in the worst interference scenario, the XT may be greater than the XT threshold, even for the shortest path of these connection requests. In contrast, the proposed MILP method considers the XT strictly (i.e., XT-aware). Therefore, the optimal solution can be obtained.

Next, we examine the convergence efficiency of the optimization models by counting the numbers of variables and constraints of the optimization models. Note that in some cases, adding constraints in an optimization model will not reduce but rather improve the convergence speed of the model. However, the numbers of variables and constraints are still a metric that is worth considering [39]. For all the optimization models, we assume that the number of cores of a multi-core fiber, denoted by $|C|$, is equal to an invariant constant.

For the proposed ILP optimization model (Section 3.1.1), the dominant numbers of variables and constraints are $O(|R|^2)$ (according to $\varphi_r^{r'}$) and $O(|R|^2 \cdot |E|)$ (according to Constraint (3.9)), respectively, where $|R|$ and $|E|$ represent the total numbers of connection requests and links in the network, respectively.

For the ILP optimization model in [95], the number of variables is bounded by $O(|R|^2 \cdot |E|)$, while the number of constraints is bounded by the larger of $O(|R|^2 \cdot |E|)$ and $O(|R| \cdot |P|)$, where $|P|$ represents the number of pre-calculated candidate routing paths per connection request. When all the possible routing paths are considered, the ILP method in [95] can safely ensure finding the optimal solution, but an upper bound for $|P|$ can be up to $O(2^{|N|})$ [144]. Meanwhile, when only k-shortest paths are considered, an optimal solution may not be found, but the $|P|$ can be significantly reduced to k. For the ILP optimization model in [102], the numbers of both variables and constraints are bounded by $O(|R|^2 \cdot |P|^2)$.

Finally, for the proposed MILP optimization model (Section 3.1.2), the dominant number of variables is the larger one between $O(|R|^2)$ (according to $\varphi_r^{r'}$) and $O(|R| \cdot |E| \cdot |F|)$ (according to o_r^{ecf}), and the dominant number of constraints is the larger one between $O(|R|^2 \cdot |E|)$ (according to Constraint (3.9)) and $O(|R| \cdot |E| \cdot |F|)$ (according to Constraint (3.15)), where $|F|$ is the total number of required FSs, which is the objective of the optimization model. Because it is difficult to find an exact number for $|F|$ before the optimization model is solved, we set it as its upper bound, which is equal to $\sum_{r \in R} \lambda_r$, where λ_r is the traffic volume units in FS for connection request r. Here, we set λ as the average number of traffic volume units in FS for each connection request; thus, we can derive the upper bound for the dominant numbers of both variables and constraints as $O(|R|^2 \cdot |E| \cdot \lambda)$.

Overall, we can observe that the proposed ILP optimization model has considerably smaller

numbers of variables and constraints. However, for the proposed MILP optimization model, to achieve the XT-aware, we need to mark the status of each FS on each core and link, which inevitably introduces more variables and constraints. We summarize the convergence efficiencies of the four optimization models in Table 3.1.

Table 3.1: Comparison among four optimization models.

Model	#Variables	#Constraints
The proposed ILP model	$O(\|R\|^2)$	$O(\|R\|^2 \cdot \|E\|)$
The proposed MILP model	$O(\|R\|^2 \cdot \|E\| \cdot \lambda)$	$O(\|R\|^2 \cdot \|E\| \cdot \lambda)$
ILP model in [95]	$O(\|R\|^2 \cdot \|E\|)$	$O(\|R\|^2 \cdot \|E\|)$ or $O(\|R\| \cdot \|P\|)$
ILP model in [102]	$O(\|R\|^2 \cdot \|P\|^2)$	$O(\|R\|^2 \cdot \|P\|^2)$

We also present the total numbers of columns (variables) and rows (constraints) given by the Gurobi ILP solver [138] when solving the optimization models for a 6-node 9-link simple network [95] (Fig. 3.2.a in Section. 3.3) in Table 3.2, where $|R|$ is set to be 15 (a connection request between each node pair) and λ_r is set as a random number from 1-3 (FSs). The number of cores of a multi-core fiber $|C|$ is set to be 3. Three different cases of pre-calculated candidate paths per node pair P are considered, which represent all the routing paths (for each connection request) in the n6s9 network topology, 5-shortest paths, and 3-shortest paths.

Table 3.2: Comparison among four optimization models in the n6s9 network (by GUROBI v.7.0.1 solver).

Model	Columns	Rows	Non-zeros
Our ILP model (Sec. 3.1.1)	736	6,285	31,185
Our MILP model (Sec. 3.1.2)	35,836	33,823	449,578
ILP Model in [95] (All-paths)	15,623	23,239	95,490
ILP Model in [95] ($\|P\| = 5$)	14,671	23,205	94,026
ILP Model in [95] ($\|P\| = 3$)	13,831	23,175	92,796
ILP Model in [102] (All-paths)	44,674	99,560	375,536
ILP Model in [102] ($\|P\| = 5$)	21,586	47,850	180,240
ILP Model in [102] ($\|P\| = 3$)	8,026	17,550	65,820

As shown in Table 3.2, the proposed ILP optimization model (Section 3.1.1) has significantly fewer rows and columns than previous ILP optimization models even though we have bound the number of the pre-calculated candidate paths $|P|$ equal to 3. These results are consistent with the analytical results shown in Table 3.1.

3.2 Heuristic algorithm for the RSCA problem with XT management

In this section, we present our XT-aware heuristic algorithm, which contains two components: a strict XT-aware FS check mechanism and a routing, spectrum and core assignment component.

3.2.1 Strict XT-aware frequency slice check mechanism

Algorithm 3 Strict XT-aware frequency slice check mechanism.

Input: $p = \cup(e, c)$, f_s, f_e
Output: 1 or 0
for frequency slice f in range $[f_s, f_e]$ **do**
  Set XT_f^{self} equal to 0 as the XT of the new connection request itself on f
  for (link e,core c) in routing path p **do**
    for each adjacent core c' of core c **do**
      Set ar equals to $U[e, c', f]$, that is, the previously assigned connection request that occupies the f on core c' of link e
      if $ar \neq$None **then**
        The current XT of previously assigned connection request $XT[ar, f] += \Delta xt(c, c', e)$
        $XT_f^{self} += \Delta xt(c, c', e)$
        if $XT[ar, f] >$ XT threshold **then**
          return 0
        end if
      end if
    end for
  end for
  if $XT_f^{self} >$ XT threshold **then**
    return 0
  end if
end for
return 1

Our strict XT-aware FS check mechanism works as follows. When a new connection request arrives, we should check the increased XTs of the previously assigned connection requests to ensure that they are still less than the XT threshold, because the XTs of previously assigned connection requests will increase if the same FS(s) in an adjacent core are assigned to the new connection request. Moreover, since XT between two adjacent cores is mutual affected, we should also ensure that the XTs on each assigned FS of the new connection request itself are less than the XT threshold, which are related to the number of active adjacent cores on the same FS (used to serve the previously assigned connection requests).

We use the following two tables in the strict XT check mechanism.

- A usage table represents the FS usage per core and link, which is denoted as follows:

$$U[e, c, f] = \begin{cases} ar & \text{If FS } f \text{ on core } c \text{ of link } e \text{ has been assigned to request } ar \\ \text{None} & \text{Otherwise} \end{cases}$$

- A table of the current XT of previously assigned connection requests ar on their assigned FSs, which is denoted as follows:

$$XT[ar, f] = \begin{cases} \text{The current XT of } ar \text{ on FS } f\text{: If } f \text{ is assigned to } ar \\ \text{None} \quad \text{Otherwise} \end{cases}$$

The pseudocode for our strict XT-aware FS check mechanism is shown in Algorithm 3. The inputs of the algorithm are the pre-assigned routing path $p = \cup(e, c)$ containing links and cores

along the path and the pre-assigned FSs, that is, the starting FS f_s and the ending FS f_e. The output of the algorithm is a Boolean number, where 1 represents that the connection request can be transmitted successfully on these pre-assigned FSs and 0 otherwise.

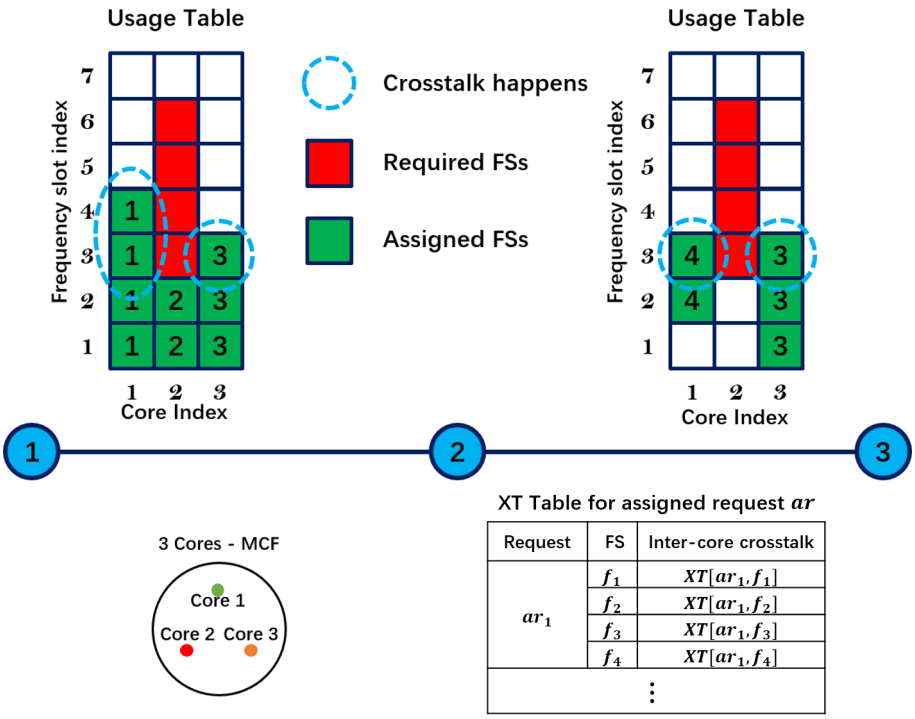

Figure 3.1: Example of our strict XT check mechanism.

We present a simple example in Fig. 3.1 to show how our XT-aware mechanism works. We consider a simple chain network, where each link has a 3-core MCF. We assume that there are some FSs already successfully assigned to other connection requests ar (shown in green). The XTs on each of their assigned FSs (i.e., $XT[ar, f]$) are less than the XT threshold. For instance, we can observe that ar_2 shares the same FSs (i.e., f_1 and f_2) with ar_1 and ar_3 on a common link e_{12}; therefore, the XT of ar_2 on f_1 (i.e., $XT[ar_2, f_1]$) can be calculated by Eq. (1.3), which equals the sum of $\Delta xt(c_1, c_2, e_{12})$ (see Eq. (1.2), where L equals the length of link e_{12}) and $\Delta xt(c_2, c_3, e_{12})$. In the same way, $XT[ar_2, f_2]$ can also be calculated as $\Delta xt(c_1, c_2, e_{12}) + \Delta xt(c_2, c_3, e_{12})$. Since the ar_2 is already successfully assigned, the $XT[ar_2, f_1]$ and $XT[ar_2, f_2]$ are less than the XT threshold.

Here, a new connection request arrives with a requirement of 4 FSs from source node 1 to destination node 3. We assume that the connection request is pre-assigned to core 2 starting from the f_3 FS on each link. We need to check, for example, whether we can successfully assign the FSs, shown in red, to the new connection request.

First, we should check the increased XTs of the previously assigned connection requests due to the new connection request to ensure that they are still less than the XT threshold (line 4 $\sim$ line 10

in Algorithm 3). For example, since the previously assigned connection request ar_1 shares the same f_3 on adjacent cores of the common link e_{12} with the new connection request, the XT of ar_1 on the f_3 FS will increase by $\Delta xt(c_1, c_2, e_{12})$ according to Eq. 1.2 and Eq. 1.3. We should ensure that the sum of $XT[ar_1, f_3]$ (the current XT stored in the XT table) and $\Delta xt(c_1, c_2, e_{12})$ is less than the XT threshold. Similarly, for $ar3$, because it shares the same f_3 FS with the new connection request on two common links (i.e., e_{12} and e_{23}), the XT of ar_3 on f_3 will increase twice (i.e., $\Delta xt(c_2, c_3, e_{12})$ and $\Delta xt(c_2, c_3, e_{23})$), and it should also be less than the XT threshold. We should repeat this process for each pre-assigned FS of the new connection request. If the increased XTs of the previously assigned connection requests on their occupied FSs — due to sharing the same FSs with the new connection request — are greater than the XT threshold, the pre-assigned FSs and cores cannot be successfully assigned to the new connection request.

Then, we should check the XT of the new connection request itself on each pre-assigned FS to ensure that it can be successfully transmitted (line 15 in Algorithm 3). As can be seen in Fig. 3.1, the XT of the new connection request itself on the f_3 ($XT_{f_3}^{self}$) is the sum of $\Delta xt(c_1, c_2, e_{12})$, $\Delta xt(c_2, c_3, e_{12})$, $\Delta xt(c_1, c_2, e_{23})$ and $\Delta xt(c_2, c_3, e_{23})$. Using the same approach, the XTs on the f_4, f_5, and f_6 can be calculated to be $\Delta xt(c_1, c_2, e_{12})$, 0, and 0, respectively. Then, we should check these XTs, and if any of them is greater than the XT threshold, the new connection request cannot be successfully transmitted.

3.2.2 Routing, spectrum and core assignment

Algorithm 4 Routing, spectrum and core assignment.

Input: Connection request matrix R ($r = \{s(r), d(r), \lambda_r\} \in R$)

1: Sort R in descending order by the required FSs λ_r
2: Calculate the k shortest routing paths for each pair of nodes based on the *KSP* algorithm [52]
3: **for** each r in R **do**
4: Set the starting FS of r equal to 1 as f_s
5: **for** each ksp in KSP_r **do**
6: **if** FSs between $[f_s, f_s + \lambda_r - 1]$ are available on at least one core (the core is selected according to the predefined reducing XT algorithm in [96]) of each link along the ksp **then**
7: Check XTs based on Algorithm 3
8: **if** Algorithm 3 returns 1 **then**
9: Assign the FSs between $[f_s, f_s + \lambda_r - 1]$, lightpath ksp and the selected cores to serve connection request r
10: Update usage table $U[e, c, f]$ and XT table $XT[r, f]$
11: **break for** — Move to the next r
12: **end if**
13: **end if**
14: **end for**
15: f_s+ = 1
16: return to line 5
17: **end for**

For a given connection request matrix R, we first sort the connection requests in descending order according to the traffic volume and then determine the routing, the spectrum and the core

assignment for the connection requests $r \in R$ one by one, starting from the one with the largest traffic volume. For two connection requests with the same traffic volume, we first serve the one whose shortest path has more hops because it is difficult to assign available consecutive FSs for a connection request with more hops due to the spectrum contiguity and continuity constraints.

The algorithm works as follows. First, we pre-calculate the k shortest routing paths for each connection request r as a set of KSP_r in a pre-processing phase based on the *KSP* algorithm [52]. Then, for each r in sorted R, the starting FS f_s will start from the 1-st FS. For each ksp in KSP_r, if the FSs between $[f_s, f_s + \lambda_r - 1]$ are available on at least one core (the core is selected according to the predefined reducing XT algorithm in [96]) of each link along the ksp (i.e., satisfying the contiguity and continuity constraints), check the XT-limit constraint based on Algorithm 3. If the XT-limit constraint is also satisfied (Algorithm 3 returns 1), assign the FSs between $[f_s, f_s + \lambda_r - 1]$, the routing path ksp and the cores to the connection request r. However, if all the ksp in KSP_r are not feasible on the current f_s, we increase the starting FS f_s by one and repeat the above processes until there is at least one ksp in KSP_r that is feasible. Finally, we update the usage table $U[e, c, f]$ and XT table $XT[ar, f]$ and move to the next connection request. The pseudocode of our *routing, spectrum, and core assignment algorithm* is shown in Algorithm 4.

3.3 Simulations and performance evaluations

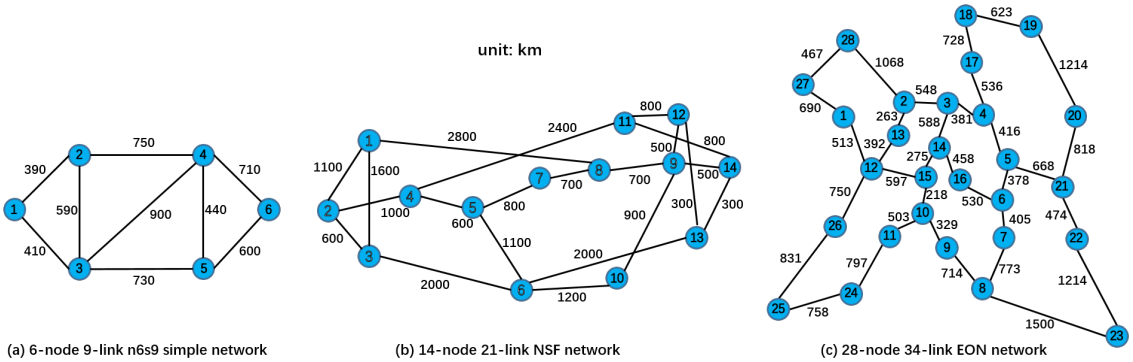

Figure 3.2: Illustration of network topologies: (a)6-node n6s9 simple network, (b)14-node NSF network, and (c)28-node EON network.

In this section, we evaluate the performance of the proposed ILP/MILP methods and heuristic algorithm. Two types of MCFs are considered in the simulation experiments, which are a 3-core MCF (for small-scale problem instances) and a 7-core MCF [91, 100] (for large-scale problem instances). The parameters r, β, k, ω_{tr} of the MCFs are set as 50 mm, 4×10^{6} m^{-1}, 4×10^{-4}, 4.5×10^{-5} m, respectively [91, 95, 100]. The simulation experiments were performed on Microsoft Windows 10 using a computer with an Intel Xeon 8-core 3.5 GHz CPU and 64 GB of memory. We used the

Gurobi Optimizer 7.0.1 [138] to solve the optimization models, and for all the heuristic algorithms, we used the same KSP algorithm proposed in [52], where k is set to be 3. Moreover, in the simulation experiments, a unit FS (i.e., the grid granularity) is assumed to be 12.5 GHz bandwidth [13,52], and two neighboring optical carriers are separated by a guard-band that occupies 1 FS.

3.3.1 Simulation experiments in small-scale problem instances

We first evaluate the performance of the proposed ILP/MILP methods and heuristic algorithm in small-scale instances (simple network topology, 3-core MCF, the small set of offered connection requests, and so forth).

Convergence efficiency of the proposed ILP/MILP optimization models

We employ the existing ILP optimization models proposed in [102] and [95] as benchmarks to evaluate the convergence efficiency of the proposed ILP/MILP optimization models. For the existing two path-based ILP optimization models, we consider three different cases of pre-calculated candidate paths, which are all the possible routing paths (AP), 5-shortest paths (5SP) and 3-shortest paths (3SP). Moreover, the two existing ILP methods in [95, 102] and the proposed ILP method consider the XT in the worst interference scenario. To ensure that the candidate path space will not be bounded by the XT threshold (see Section 3.1.3), we consider a simple and geographically small six-node nine-link (n6s9) network [95], as shown in Fig. 3.2.a. In the n6s9 network, the XTs (worst case) of all the paths are less than the XT threshold (set as -30 dB in this part of the simulation experiments [95, 102]).

According to the statements above, the solutions obtained by the proposed node-arc-based ILP/MILP methods and the existing path-based ILP methods (AP) can guarantee the optimality. A fair comparison should be considered among these four methods, but for reference, we also evaluate the performance of the existing ILP methods in the cases of 3SP and 5SP.

The number of connection requests $|R|$ is set to be 15 (a connection request between each node pair). The traffic volumes ranges considered are from 1-3, 2-4, and to a maximum of 5-7 units of FSs. For each of the traffic volume ranges, we generate 10 different connection request matrices R. The criterion for the convergence efficiency measurement is the 'runtimes' that are given by AMPL/Gurobi [138].

Fig. 3.3 shows the convergence efficiencies of the four optimization models in the n6s9 network. The x-axis shows different ranges of traffic volumes. The y-axis shows the computational time. The results are averaged by 10 different connection request matrices R.

As shown in Fig. 3.3, the computational time increases with increasing traffic volume range for all the methods because the feasible solution spaces of the optimization models expand with the increase in required FSs, leading to longer computational time. We can observe that the proposed

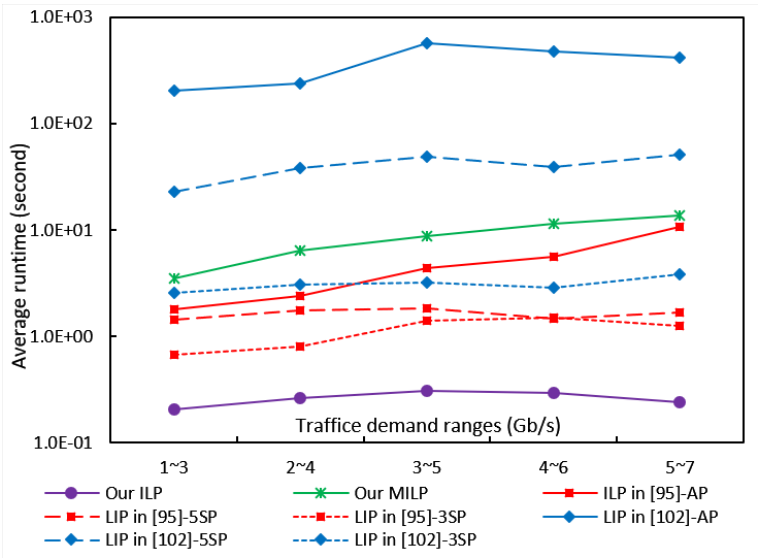

Figure 3.3: Convergence efficiency comparison among the four optimization models for the n6s9 network.

ILP method can solve the problem in less than 1 second, and even compared with the cases of 3SP and 5SP of the existing ILP methods, it requires less computational time. However, because the proposed MILP method consider the XT strictly (i.e., XT-aware), it takes more computational time. The results are consistent with the theoretical analysis in Table 3.1 and Table 3.2.

Generalizability of the proposed MILP method and heuristic algorithm

To evaluate the generalizability of the proposed MILP method and heuristic algorithm, we consider the previous n6s9 network and let the XT threshold decrease from -30 dB to -40 dB (the different modulation formats [145] and the XT margin [146], which can be set by the network operators, will lead to different XT thresholds). The decrease of the XT threshold can also be viewed as the geographical size of the network becomes larger but the XT threshold remains the same, where the number of connection requests $|R|$ is fixed as 15 (between each node pair) and the required FSs are randomly selected between 1 to 5 FSs. For each XT threshold value, we generated 10 different connection request matrices R, and the results are averaged as shown in Fig. 3.4.

As shown in Fig. 3.4, there are no points for the two existing XT-WC-based heuristic algorithms (i.e., the *SPSA* algorithm proposed in [95] and the *ARSCA-SP* algorithm proposed in [102]) when the XT threshold is reduced to -34 dB, because they become unable to assign the lightpaths to some connection requests. That is, in the worst interference scenario, the XTs of the shortest path for these connection requests become greater than -34 dB (e.g., the connection request between node pair [1,6]); thus, these connection requests will be blocked. In contrast, the proposed XT-aware-based MILP method and heuristic algorithm can assign the FSs adaptively to ensure successful

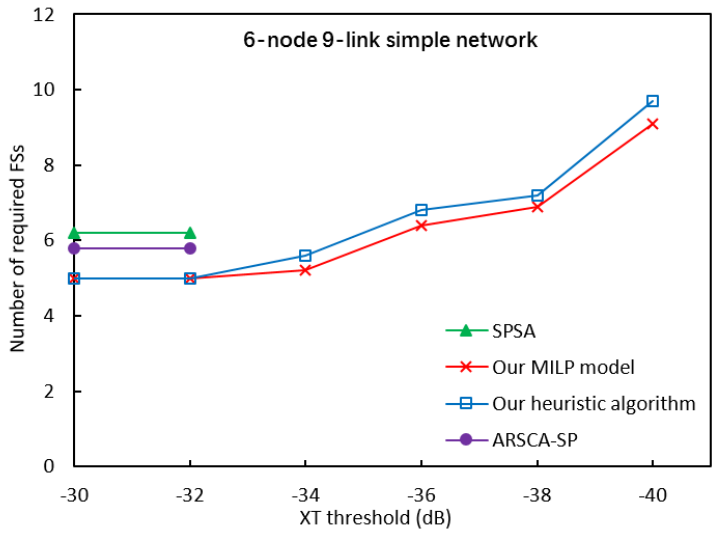

Figure 3.4: Evaluation of generalizability for the n6s9 simple network.

transmissions by avoiding assigning the same FSs to adjacent cores on some common links along the lightpaths. Thus, as shown in Fig. 3.4, the required FSs become large as the XT threshold decreases. We list the number of blocked connection requests by the existing XT-WC-based heuristic algorithms for each XT threshold in Table 3.3 as follows.

Table 3.3: The number of blocked connection requests by the XT-WC-based heuristic algorithms in the n6s9 network.

Θ (dB)	-30	-32	-34	-36	-38	-40
Num. of Blocked r	0	0	1	3	7	12

Spectrum efficiency of the proposed heuristic algorithm

In this paragraph, we evaluate the spectral efficiency achieved by the proposed heuristic algorithm in small-scale problem instances compared with the heuristic algorithms proposed in the previous works [95, 102]. The solutions obtained based on the proposed ILP optimization model are set as the benchmarks. Because in geographically small networks, the solutions obtained based on the proposed ILP optimization model are also the most optimal solution (see Section 3.3.1), but the proposed ILP method requires the least computational time. In this part, the XT threshold is fixed to be -30 dB.

Fig. 3.5 presents the results of the spectral efficiency of each approach in the n6s9 network, in which the x-axis shows the numbers of connection requests $|R|$, and the source node and destination node for all connection requests are randomly selected. The required FSs for each connection request are considered as a random number from 1 to 5 (FSs). For each $|R|$, we generate 10 different

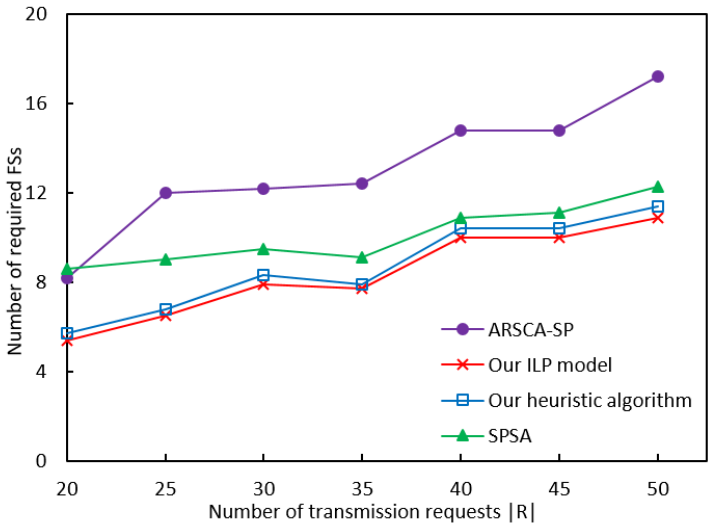

Figure 3.5: Spectrum efficiency comparison among different approaches for the n6s9 simple network.

connection request matrices R, and the results - maximum required bandwidth (FSs) in the entire network - are averaged, as shown on the y-axis.

As shown in Fig. 3.5, in small-scale problem instances, the proposed heuristic algorithm performs better than the two existing heuristic algorithms, and the solutions are closer to the optimal solutions.

3.3.2 Simulation experiments in large-scale problem instances

We evaluate the performance of the proposed heuristic algorithm in large-scale problem instances, i.e., two realistic geographically large network topologies (i.e., the NSF network [147] and the EON network [148] as shown in Fig. 3.2.b and Fig. 3.2.c), a 7-core MCF [91, 100] and a large set of connection requests.

Spectrum efficiency of the proposed heuristic algorithm in large-scale problem instances

First, we evaluate the spectral efficiency achieved by the proposed heuristic algorithm. The numbers of connection requests $|R|$ are considered ranging from 100 to 1000 with 100 granularity (shown on the x-axis), and the source node and destination node for all connection requests are randomly selected. The required FSs for each connection request are considered as a random number from 1 to 10 (FSs). We generate 10 different connection request matrices R, and the results - maximum required FSs - are averaged. Because it is very difficult for the ILP/MILP methods to find the effective solutions for large-scale problem instances in an acceptable time, we use the cut-set approach — a cut separates the network with N nodes into 2 disjoint induced sub-graphs. All the

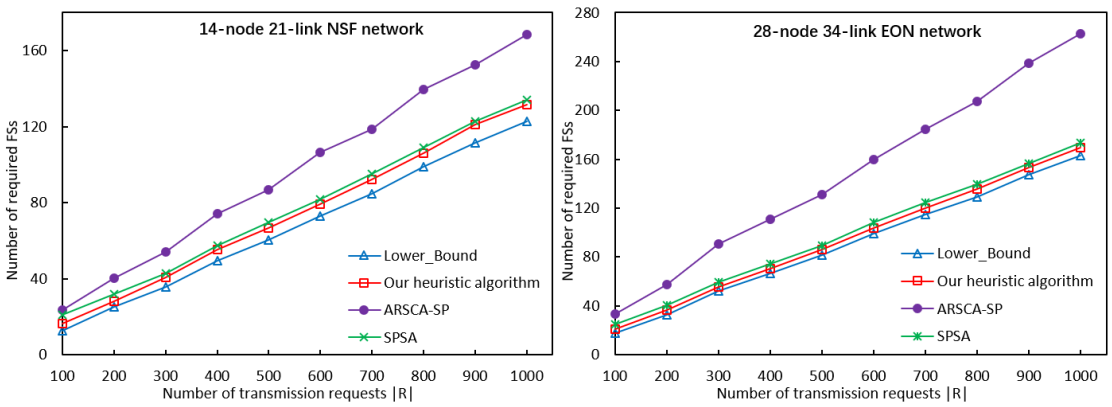

95% Confidence intervals of our algorithm									
1.06	1.25	1.84	1.31	1.54	2.02	2.00	2.68	2.02	3.36

95% Confidence intervals of our algorithm									
1.72	1.81	2.48	2.87	3.47	3.93	2.56	3.26	3.39	4.03

Figure 3.6: Spectrum efficiency comparison among different algorithms for the NSF network and the EON network.

traffic volumes between those 2 disjoint sub-graphs are carried by the links that compose the cut, and the traffic volumes are assigned to the cores and links evenly. — to obtain the lower bounds of the problem. Additionally, for a fair comparison, the XT threshold is set as -20 dB to ensure that the pre-calculated candidate path space of the existing XT-WC-based heuristic algorithms in [95] and [102] will not be bounded by the XT threshold.

Fig. 3.6 presents the results of the spectral efficiency of each heuristic algorithm, while the tables under the figures show the 95% confidence intervals of the proposed GVNA-PHBF algorithm. From Fig. 3.6, we can observe that in large-scale problem instances, the proposed heuristic algorithm also performs better than the two existing heuristic algorithms, and the solutions are closer to the lower bounds.

Computational efficiency of the proposed heuristic algorithm in large-scale problem instances

In this paragraph, we evaluate the computational efficiency achieved by the proposed heuristic algorithm. Fig. 3.7 shows the computational time of the heuristic algorithms in the simulation experiments above (Section 3.3.2).

As shown in Fig. 3.7, as the number of connection requests $|R|$ increases, the computational time of the existing *SPSA* algorithm in [95] increases exponentially. In contrast, the computational time of the proposed XT-aware-based heuristic algorithm increases almost linearly as $|R|$ increases. The *ARSCA-SP* algorithm in [102] achieves the highest computational efficiency, because it only considered one routing path (i.e., the shortest path) for each node pair. However, as shown in Fig. 3.6, the *ARSCA-SP* algorithm has the worst spectral efficiency.

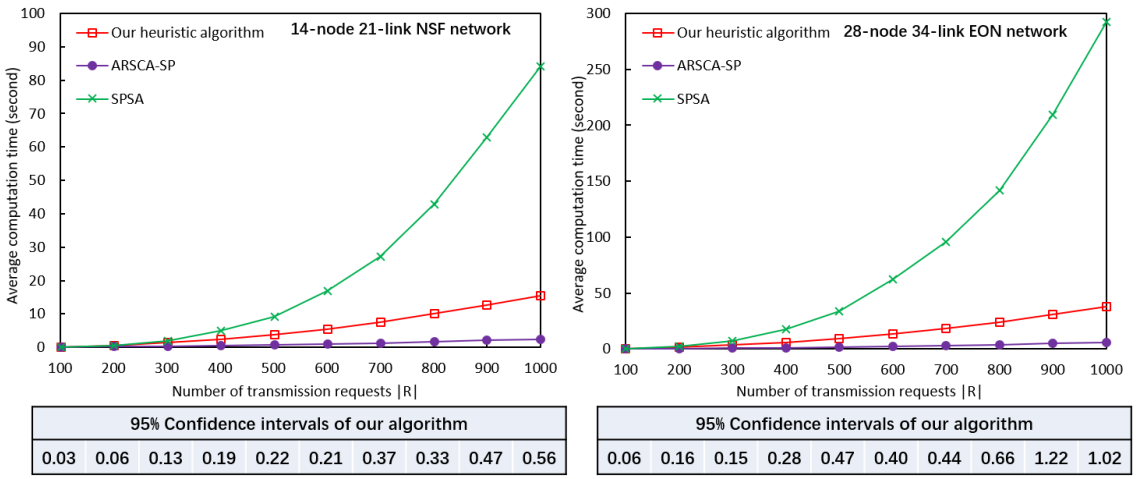

95% Confidence intervals of our algorithm									
0.03	0.06	0.13	0.19	0.22	0.21	0.37	0.33	0.47	0.56

95% Confidence intervals of our algorithm									
0.06	0.16	0.15	0.28	0.47	0.40	0.44	0.66	1.22	1.02

Figure 3.7: Computational efficiency comparison among different heuristic algorithms for the NSF network and the EON network.

Generalizability of the proposed heuristic algorithm in large-scale problem instances

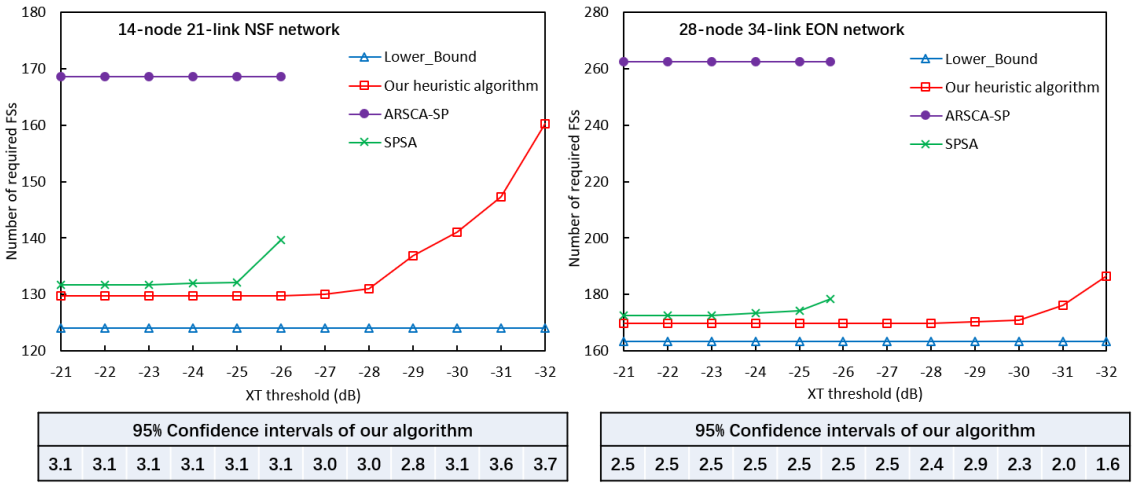

95% Confidence intervals of our algorithm											
3.1	3.1	3.1	3.1	3.1	3.1	3.0	3.0	2.8	3.1	3.6	3.7

95% Confidence intervals of our algorithm											
2.5	2.5	2.5	2.5	2.5	2.5	2.5	2.4	2.9	2.3	2.0	1.6

Figure 3.8: Generalizability of different heuristic algorithms for the NSF network and the EON network.

In this paragraph, we evaluate the generalizability of the proposed heuristic algorithm. The XT thresholds are considered from -21 dB to -32 dB per -1 dB step. The number of connection requests $|R|$ is fixed as 1000, and the required FSs for each connection request are considered as a random number from 1 to 10 (FSs). For each XT threshold value, we generate 10 different connection request matrices R, and the results are averaged, as shown in Fig. 3.8.

As shown in Fig. 3.8, the results of the *ARSCA-SP* remain the same because the *ARSCA-SP* algorithm does not consider multiple candidate paths (i.e., all the connection requests are connected

by the shortest path).

Moreover, for the 14-node 21-link NSF network, we can observe that when the value of the XT threshold is relaxed (-21 dB ~ -25 dB), for the XT-WC-based *SPSA* algorithm, all the pre-calculated candidate paths (e.g., KSPs) are almost feasible. This leads to a relatively small difference between the proposed heuristic algorithm and the *SPSA* algorithm. However, when the value of the XT threshold is reduced to -26 dB, for the *SPSA* algorithm, its feasible candidate path space will be significantly bounded. In contrast, the proposed XT-aware-based heuristic algorithm is not notably affected, which will result in a greater difference in performance between the two heuristic algorithms. Moreover, when the XT threshold is further reduced (-27 dB ~ -32 dB), the XT-WC-based algorithms become unable to find even one feasible candidate path for some connection requests, because the shortest paths of these connection requests become infeasible due to the strict XT threshold in this case. Therefore, these connection requests cannot be satisfied by the XT-WC-based *SPSA* and *ARSCA-SP* algorithms. Meanwhile, we can observe that the required FSs of the proposed heuristic algorithm increase in this case because the proposed heuristic algorithm starts to avoid assigning the same FSs to adjacent cores to ensure successful transmissions. A similar tendency can also be observed for the 28-node 34-link EON network. Furthermore, we list the percentage of blocked connection requests by the XT-WC-based algorithms in Table 3.4.

Table 3.4: The average percentage of blocked connection requests by the XT-WC-based heuristic algorithms in the NSF network and the EON network.

Θ (dB)	-26	-27	-28	-29	-30	-31	-32
NSF-14	1.1	8.7	23.8	40.7	56.6	70.9	81.5
EON-28	0.0	16.5	31.9	44.0	62.6	71.4	80.2

In conclusion, for large-problem instances, the proposed heuristic algorithm can cope well with strict XT thresholds (see Fig. 3.8), and better solutions (see Fig. 3.6) can be obtained based on the proposed heuristic algorithm within acceptable time (see Fig. 3.7).

Chapter 4

Joint Assignment of Spatial Granularity, Routing, Modulation and Spectrum in SDM-EONs: Minimizing the Network CAPEX Considering Spectrum, WSS and Laser Resources

As we have discussed in Section 1.3.6 and Section 1.3.7, in spectrally & spatially flexible super-channel transmission-based SDM-EONs, the spatial dimensions can be divided into one or several group(s). Spatial dimensions in the same group can be jointly switched based on J-Sw / FrJ-Sw, resulting in less WSS usage. Additionally, the optical carriers on the same frequency of these spatial dimensions in the same group can share a single laser source. Therefore, a larger spatial granularity can reduce the usage of both WSS and laser devices. However, compared to the case of a smaller spatial granularity, this scenario leads to more guard-bands, i.e., more spectrum resources, are required. Consequently, spatial granularity i is a key factor of minimizing the CAPEX in SDM-EON design. In this chapter, we address the RMSSGA problem proposed in Section 1.3.8. The objective is to minimize the network CAPEX, i.e., minimize the total cost related to the network resources containing the spectrum, WSS, and laser. We first present a joint ILP-RMSSGA model to solve this problem. Next, we present a decomposition method that divides RMSSGA into two substituent sub-problems, and then solve them sequentially. Because of the limitation of the ILP model in larger-scale problem instances, a rerouting-based heuristic algorithm is proposed. We examine the performances of the proposed algorithms via simulation experiments and find that the best spatial granularity is related to the network resources to which network operators attached more importance. Moreover, we analyze the impact of guard-band width and the traffic volume of the connection requests on the decision regarding the best spatial granularity.

This chapter is organized as follows. In Section 4.1, we present our ILP formulations for the

static RMSSGA problem, from the joint RMSSGA ILP model to the decomposed RMSG + SA ILP models. In Section 4.2, we propose our rerouting-based heuristic algorithm. In Section 4.3, we present the results and evaluate the performances of the proposed algorithms.

4.1 ILP formulations for RMSSGA problem

In this section, we first present a joint optimal ILP-RMSSGA optimization model. We next divide the RMSSGA problem into the RMSG and SA subproblems and formulate each problem separately and sequentially.

4.1.1 Joint ILP-RMSSGA model

Parameters

V: the set of network nodes.
E: the set of network links.
R: the set of connection requests r.
P_r: the candidate paths of r.
ml_p: the availiable highest modulation level of path $p \in P_r$ depends on the path length [km] of p (refer to Table 1.1).
S: the set of all spatial dimensions of the links (fibers).
I: $I = \{1,....,i,...|S|\}$, the set of all available spatial granularities i.
$\mathscr{G}_i$: the set of spatial dimension groups G of spatial granularity i. In the case of uniform grouping, each spatial dimension group G in $\mathscr{G}_i$ contains i spatial dimensions (i.e., $|G| = i$).
$\mathcal{G}$: $\mathcal{G} = \bigcup_{i \in I} \mathscr{G}_i$, the set of all spatial dimension groups G.
l^r_{pG}: the number of required laser pairs — one laser source at transmitting side and one local oscillator at receiving side — for r if spatial dimension group $G \in \mathcal{G}$ and path $p \in P_r$ are selected to serve r. It can be calculated using Eq. (1.5) in Section 1.3.6 with parameter ml_p.
f^r_{pG}: the number of required FSs (containing guard-bands) in each spatial dimension in G if spatial dimension group G and path p are selected to serve r. It can be calculated using Eq. (1.6) in Section 1.3.6.
α, β, γ : parameters represent the cost related to unit spectrum (FS), WSS and laser pair, respectively, which are set depending on how much the network operators attached importance to these resources.
D_{total}: the total number of node degrees in the network.
M_{fs}, M_{laser}, M_{wss}: large positive numbers, which represent the upper bounds of FSs, laser pairs and WSSs, respectively.

Variables

$F_{max} \in \mathbb{Z}^+$: An integer variable that indicates the (maximal index of) required FSs in the network.
$S_{max} \in \mathbb{Z}^+$: An integer variable that indicates the total number of required WSSs in the network.
$L_{max} \in \mathbb{Z}^+$: An integer variable that indicates the total number of required laser pairs in the network.
$a_r \in \mathbb{Z}^+$: An integer variable that denotes the starting FS index of the connection request r.
$b_r \in \mathbb{Z}^+$: An integer variable that indicates the number of required laser pairs to serve r.
$\delta^{rr'} \in \{0,1\}$: A binary variable that takes a value of 0 if the ending FS index of r' is smaller than the starting FS index of r (a_r) and 0 otherwise.
$\theta_i \in \{0,1\}$: A binary variable that is equal to 1 if i is selected to be the best spatial granularity to serve the connection requests and 0 otherwise.
$x^r_{pG} \in \{0,1\}$: A binary variable that is equal to 1 if spatial dimension group G of path p is selected to serve r and 0 otherwise.

Objective function

$$\text{Minimize} \quad \alpha \cdot F_{max} + \beta \cdot S_{max} + \gamma \cdot L_{max} \tag{4.1}$$

As shown in Eq. (4.1), the objective is to minimize the total cost related to the network resources containing spectrum (FS), WSS and laser pair (i.e., network CAPEX).

Constraints

Constraint for spatial granularity decision:

$$\sum_{i \in I} \theta_i = 1 \tag{4.2}$$

Constraint (4.2) ensures that there is only one spatial granularity $i \in I$ that can be selected to serve the connection requests.

Constraint for FS:

$$F_{max} \geq a_r + f^r_{pG} \cdot x^r_{pG} \quad \forall r \in R, p \in P_r, G \in \mathcal{G} \tag{4.3}$$

For a connection request r, we have $x^r_{pG} = 1$ if the spatial dimension group G on path p is selected to serve the connection request. Thus, the ending FS index of r is the sum of the starting FS index a_r and the required FSs f^r_{pG}. Constraint (4.3) ensures that F_{max} is not smaller than the ending FS index of any $r \in R$.

Constraint for WSS:

$$M_{wss} \cdot (1 - \theta_i) + S_{max} \geq 2 \cdot \sum_{v \in V} D_v \cdot |S|/i \quad \forall i \in I \tag{4.4}$$

As shown in Table 1.6 of Section 1.3.7, the usage of WSSs at a node $v \in V$ is related to the selected spatial granularity i and the node degree D_v, which is equal to $2 \cdot D_v \cdot |S|/i$. Therefore, if the spatial granularity i is selected (i.e., $\theta_i = 1$), Constraint (4.4) becomes $S_{max} \geq 2 \cdot \sum_{v \in V} D_v \cdot |S|/i$. In another case (i.e., $\theta_i = 0$), Constraint (4.4) is deactivated due to the larger value M_{wss} on the left-hand side of the constraint.

Constraints for laser pairs:

$$b_r + M_{laser} \cdot (1 - x^r_{pG}) \geq l^r_{pG} \quad \forall r \in R, p \in P_r, G \in \mathcal{G} \tag{4.5}$$

$$L_{max} \geq \sum_{r \in R} b_r \tag{4.6}$$

For each $r \in R$, we have $b_r \geq l^r_{pG}$, according to Constraint (4.5), when $x^r_{pG} = 1$, where the number of laser pairs required by r (i.e., l^r_{pG}) can be calculated by Eq. (1.5) in Section 1.3.6. In another case (o.e., $x^r_{pG} = 0$), Constraint (4.5) is deactivated. Then, the total number of required laser pairs L_{max} should be greater than the sum according to Constraint (4.6).

Constraint for routing:

$$\sum_{p \in P_r} \sum_{G \in \mathcal{G}_i} x^r_{pG} = \theta_i \quad \forall r \in R, i \in I \tag{4.7}$$

If spatial granularity i is selected ($\theta_i = 1$), for each $r \in R$, only one combination of G and p can be selected to serve the connection request r. That is, the sum should be 1. In another case (i.e, $\theta_i = 0$), the sum should be 0. Therefore, Constraint (4.7) ensures a unique lightpath for each connection request $r \in R$.

Constraints for spectrum continuity, contiguity and non-overlapping:

$$\delta^{rr'} + \delta^{r'r} = 1 \quad \forall r, r' \in R : r \neq r' \tag{4.8}$$

$$a_r \geq a_{r'} + f^{r'}_{p'G} - M_{fs} \cdot [3 - (x^r_{pG} + x^{r'}_{p'G} + \delta^{rr'})]$$
$$\forall r, r' \in R, p \in P_r, p' \in P_{r'}, G \in \mathcal{G} : r \neq r', p \cap p' \neq \emptyset \tag{4.9}$$

The following is an example illustrating Constraint (4.9): If $x^r_{pG} = 1$, $x^{r'}_{p'G} = 1$ and $p \cap p' \neq \emptyset$, then the selected two lightpaths p, p' have joint links, and the two connection requests r, r' are transmitted by the same dimension group G. According to Constraint (4.8), either $\delta^{rr'}$ or $\delta^{r'r}$ must be equal to 1. If $\delta^{rr'} = 1$, then Constraint (4.9) indicates that the starting FS index of r (i.e., a_r) should be greater than the ending FS index of r' (i.e., $a_{r'} + f^{r'}_{p'G}$). This is consistent with the definitions of $\delta^{rr'}$. In other cases, Constraint (4.9) is deactivated due to the larger value of M_{fs} on the right-hand side of the constraint. Therefore, Constraint (4.8) and Constraint (4.9) ensure the constraints of spectrum contiguity and non-overlapping. Moreover, since we employ a path-based method to formulate the problem, the spectrum continuity constraint is satisfied automatically.

4.1.2 Decomposed ILP-RMSG + SA formulations

According to the the joint ILP model, we can see that the constraint related to the spectrum continuity is the main reason for limiting the convergence efficiency of the joint ILP-RMSSGA model. In this subsection, we first propose an ILP-RMSG model by relaxing the constraint of spectrum continuity in the joint ILP-RMSSGA model to determine the best spatial granularity in the network, and lightpath (i.e., routing path, modulation format) for each connection request. Then, based on the outputs of the ILP-RMSG model, we assign the spectrum resource (FSs) to each connection request considering the spectrum continuity constraint.

ILP-RMSG model

Parameters

In the ILP-RMSG model, the parameters are the same as those in the joint ILP-RMSSGA model (see Section 4.1.1).

Variables

Most of the variables in Section 4.1.1 can be used in the ILP-RMSG model. However, since we relax the spectrum continuity constraint, the corresponding variables F_{max}, a_r and $\delta^{rr'}$ in Section 4.1.1 are not applied. Moreover, the following additional variable is necessary in the ILP-RMSG model:

$F_{use} \in \mathbb{Z}^+$: An integer variable that indicates the maximal number of used FSs in each spatial dimension of all the links in the network.

Objective function

$$\text{Minimize} \quad \alpha \cdot F_{use} + \beta \cdot S_{max} + \gamma \cdot L_{max} \tag{4.10}$$

Eq. (4.10) is similar to the objective of the joint ILP-RMSSGA model (see Eq. (4.1)). However, in the ILP-RMSG model, we consider only the number of used FSs (see the definition of F_{use}) regardless of how these FSs are assigned. That is, we do not consider the spectrum continuity constraint.

Constraints

Most of the constraints for the joint ILP-RMSSGA model in Section 4.1.1 can be used here, though the original spectrum-related constraints (i.e., Eq. (4.3), Eq. (4.8) and Eq. (4.9)) are not applied. Moreover, the following additional constraint for F_{use} is necessary:

$$F_{use} \geq \sum_{r \in R} \sum_{p \in P_r : e \in p} x^r_{pG} \cdot f^r_{pG} \quad \forall G \in \mathcal{G}, e \in E \tag{4.11}$$

As shown in Constraint (4.11), for each spatial dimension group $G \in \mathcal{G}$ on each link $e \in E$, the value of F_{use} should be greater than the total number of required FSs used to serve the connection requests that pass through spatial dimension group G on link e. This is consistent with the definition of F_{use}.

ILP-SA model

Parameters

The ILP-SA model is applied after the RMSG subproblem is solved. Thus, we have some additional parameters that can be used in the ILP-SA model based on the outputs of the ILP-RMSG model, as shown below:

i_{out}: $i_{out} = \{i \in I | \theta_i = 1\}$, the spatial granularity used to serve the connection requests.

p^r_{out}, G^r_{out}: $p^r_{out}, G^r_{out} = \{p \in P_r, G \in \mathcal{G} | x^r_{pG} = 1\}$, the assigned lightpath p^r_{out} and the spatial dimension group G^r_{out} used to serve the connection request r.

Variables

In the ILP-RMSG model, we can determine the spatial granularity and lightpaths (modulation formats) for connection requests. However, to address the problem, the FSs should be assigned to each connection request while considering the spectrum continuity constraint. Therefore, the spectrum-related variables that are not applied in the ILP-RMSG model (i.e., F_{max}, a_r and $\delta^{rr'}$) are applied in the ILP-SA model.

Objective function

$$\text{Minimize} \quad \alpha \cdot F_{max} + \beta \cdot S_{max} + \gamma \cdot L_{max} \tag{4.1}$$

The objective of the decomposed ILP-SA model is the same as the joint ILP-RMSSGA model. However, according to Table 1.6, we can see that the number of required WSSs per degree is equal to $2 \cdot |S|/i$ which is related to only the spatial granularity i. Note that we have already decided the spatial granularity i_{out} by applying the decomposed ILP-RMSG model, thus the usage of WSSs (S_{max}) in the network is equal to the product of the total degrees of network D_{total} and $2 \cdot |S|/i_{out}$, which is a constant at this time. Moreover, in Eq. (1.5), T represents the bit-rate of a connection request which is fixed. In the case of uniform grouping assumed in our work, $|G|$ is equal to spatial granularity i_{out} actually; the value of BR_m is related to the length of selected lightpath (see Table 1.1). Therefore, similar to the WSS, since we have decided the lightpath for each connection request (i.e., p^r_{out}, G^r_{out}) and spatial granularity i_{out}, N_{OC} (i.e., the number of required optical carriers on each assigned spatial dimension, which is equal to the number of required laser pairs) is a constant for a given

connection request. Consequently, the usage of laser pairs (L_{max}) in the network is equal to the sum of N_{OC} for all connection requests, which is also a constant. Therefore, in this case, Eq. (4.1) can be considered as:

$$\text{Minimize} \quad F_{max} \tag{4.12}$$

Constraints

As shown in Eq. (4.12), the objective of the ILP-SA model is to assign the FSs to each connection request while considering the spectrum continuity constraint to minimize the (maximal index of) required FSs (i.e., F_{max}) in the network. The following spectrum-related constraints which are not considered in the ILP-RMSG model should be considered here to obtain a feasible solution.

$$F_{max} \geq F_{use} \tag{4.13}$$

$$F_{max} \geq a_r + f^r_{p^r_{out} G^r_{out}} \quad \forall r \in R \tag{4.14}$$

$$\delta^{rr'} + \delta^{r'r} = 1 \quad \forall r, r' \in R : r \neq r' \tag{4.15}$$

$$a_r \geq a_{r'} + f^{r'}_{p^{r'}_{out} G^{r'}_{out}} - M_{fs} \cdot (1 - \delta^{rr'})$$
$$\forall r, r' \in R : r \neq r', p^r_{out} \cap p^{r'}_{out} \neq \emptyset, G^r_{out} = G^{r'}_{out} \tag{4.16}$$

Since the the spatial granularity and lightpaths (modulation formats) for the connection requests have been determined by the ILP-RMSG model, the constraints in Eq. (4.14), Eq. (4.15) and Eq. (4.16) are much simpler than the corresponding constraints in Eq. (4.3), Eq. (4.8) and Eq. (4.9) in Section 4.1.1. Moreover, note that F_{use} is one of the outputs of the ILP-RMSG model, which is obtained by relaxing the spectrum continuity constraint; it is a lower bound of F_{max}. Therefore, an additional constraint (Eq. (4.14)) is applied here to improve the convergence efficiency of the ILP-SA model.

4.1.3 Analysis of the proposed ILP formulations

In this subsection, we examine the convergence efficiency of the optimization models by counting the numbers of variables and constraints of them. Note that in some cases, adding constraints to an optimization model will not reduce but rather improve the convergence speed of the model. However, the numbers of variables and constraints are still a metric worth considering [39, 131].

For the joint ILP-RMSSGA model, the dominant number of variables is the larger one of $O(|R|^2)$ (according to $\delta^{r'}_r$) and $O(|R| \cdot |P_r| \cdot |\mathcal{G}|)$ (according to x^r_{pG}), while the dominant number of constraints is bounded by $O(|R|^2 \cdot |P_r|^2 \cdot |\mathcal{G}|)$ according to Constraint (4.9). In this paper, we consider k candidate paths for each connection request r; thus, $|P_r|$ is equal to k. Meanwhile, we can treat $|\mathcal{G}|$ as a constant multiple of the number of spatial dimensions $|S|$ because $\mathcal{G}$ equals $\bigcup_{i \in I} \mathcal{G}_i$. $|R|$ represents the total number of connection requests. Therefore, we can derive the upper bounds for

the dominant numbers of variables and constraints as $\max\{O(|R|^2),\ O(k \cdot |R| \cdot |S|)\}$ and $O(k^2 \cdot |R|^2 \cdot |S|\}$, respectively.

For the decomposed ILP-RMSG model, the dominant numbers of both variables and constraints are bounded by $O(k \cdot |R| \cdot |S|)$ according to x_{pG}^{r} and Constraint (4.3) / Constraint (4.5), respectively.

For the decomposed ILP-SA model, the dominant numbers of both variables and constraints are bounded by $O(|R|^2)$ according to $\delta_r^{r'}$ and Constraint (4.15) / Constraint (4.16), respectively.

Table 4.1: Comparison among the ILP formulations.

Model	# Variables	# Constraints
ILP-RMSSGA	$\max\{O(\|R\|^2),\ O(k \cdot \|R\| \cdot \|S\|)\}$	$O(k^2 \cdot \|R\|^2 \cdot \|S\|\}$
ILP-RMSG	$O(k \cdot \|R\| \cdot \|S\|)$	$O(k \cdot \|R\| \cdot \|S\|)$
ILP-SA	$O(\|R\|^2)$	$O(\|R\|^2)$

Overall, compared to the joint ILP-RMSSGA model, the optimal solutions to the RMSSGA problem might not be found by the decomposed formulations. Nevertheless, as shown in Section 4.3, the decomposed ILP-RMSG + SA formulations achieve very reasonable results that are comparable to the optimal solutions. Moreover, the decomposed ILP-RMSG and ILP-SA formulations have considerably fewer numbers of variables and constraints than does the joint ILP-RMSSGA model. An overview of the dominant numbers of variables and constraints of the proposed ILP formulations is shown in Table 4.1.

Table 4.2: Comparison among the ILP formulations in the simple 6-node-and-18-link network (using the GUROBI solver).

Model	Columns	Rows	Non-Zeros
ILP-RMSSGA	2,017	24,204	115,135
ILP-RMSG	1,117	1,422	5,995
ILP-SA	901	901	1,801

We also present the total numbers of columns (variables) and rows (constraints) yielded by the GUROBI ILP solver [138] when solving the optimization models for a simple network topology (as shown in Fig. 4.2.a) in Table 4.2, comprising 6 nodes and 18 directed links with 6 spatial dimensions for all links ($|S| = 6$), where $|R|$ is set as 30 (one connection request exists between each node pair) and, for each $r \in R$, 3 candidate paths are considered (i.e., k = 3).

As shown in Table 4.2, the decomposed ILP-RMSG and ILP-SA formulations have significantly fewer columns, rows, and nonzeros than the joint ILP-RMSSGA model. These results are consistent with the analytical results shown in Table 4.1.

4.2 Heuristic algorithm

Similar to the decomposed ILP-RMSG + SA formulations, we propose a re-routing(RR)-based heuristic algorithm that divides the RMSSGA problem into RMSG and SA subproblems and solve each subproblem separately and sequentially.

4.2.1 Decomposed RR-RMSG + ILP-SA heuristic algorithm

RR-based RMSG heuristic algorithm

In this subsection, we focus on the RMSG subproblem. The optimization goal is to find the best spatial granularity and the corresponding routing path for each connection request r in the given traffic matrix R that can minimize RMSG cost — the value of the RMSG objective function Eq. (4.10). The proposed heuristic algorithm is executed via the following three steps:

- STEP 1: Preassignment step. For a given spatial granularity i, preassign the routing paths and laser pairs to all the connection requests.
- STEP 2: RR step. According to the assignment above, try to minimize RMSG cost by rerouting some connection requests.
- STEP 3: Spatial granularity decision step. For all the available spatial granularities, repeat STEP 1 and STEP 2. Then, select the best spatial granularity and its corresponding assignment as the final solution.

More detailed descriptions are presented below:

Preassignment algorithm:

For a given spatial granularity i, we serve the connection requests in R one by one. For each new connection request r, the preassignment algorithm selects the path p and the spatial dimension group G – among P_r and $\mathscr{G}_i$ – leading to the minimum value of Eq. (4.17), as shown below.

$$C^r_{pG} = \alpha \cdot \frac{F^r_{pG} \cdot H_p}{|E|} + \beta \cdot S_{max} + \gamma \cdot L^r_{pG} \tag{4.17}$$

In Eq. (4.17), if spatial dimension group G on path p is selected to serve connection request r, F^r_{pG} represents the maximum number of used FSs in spatial dimension group G of the links along path p. H_p represents the hops of path p, and L^r_{pG} represents the number of required laser pairs, which can be calculated by Eq. (1.5). Therefore, $F^r_{pG} \cdot H_p$ can be treated as the approximate total number of the required FSs to serve the connection request r. Minimizing $F^r_{pG} \cdot H_p$ can reserve more available FSs for the subsequent connection requests. Besides, note that F_{use} indicates the maximal number of used FSs in the network. We divide $F^r_{pG} \cdot H_p$ by $|E|$ because, for a given FS

usage $F^r_{pG} \cdot H_p$, the more physical links $|E|$ that exist in the network, the lower the impact on F_{use} it will have. Moreover, since the spatial granularity i is given, the S_{max} in Eq. (4.17) is a constant at this time (see Table 1.6).

RR algorithm:

According to the results of the preassignment algorithm, we can calculate the RMSG cost by Eq. (4.10), which is represented by C_{PA}. The following two tables report the usage/assignment information.

- $F[e,G]$: A usage table representing the required number of FSs in spatial dimension group G of link e.
- $R[e,G]$: An assignment table representing the set of connection requests assigned to spatial dimension group G of link e.

Algorithm 5 Re-routing-based heuristic algorithm for the RMSG sub-problem.

Input: $F[e,G]$, $R[e,G]$, C_{PA}
Output: $F[e,G]$, $R[e,G]$, C_{RR}
1: $C_{current} \leftarrow C_{PA}$.
2: **while** True **do**
3: Find the currently most congested combination of [link e, spatial dimension group G] as $[e_{max}, G_{max}]$ by: $[e_{max}, G_{max}] = \underset{e \in E, G \in \mathscr{G}_i}{\operatorname{argmax}} \{F[e,G]\}$
4: $RR_{info} \leftarrow$ An empty set to store the RR information.
5: **for** each connection request r in $R[e_{max}, G_{max}]$ **do**
6: **for** each candidate path p in P_r **do**
7: **for** each spatial dimension group G in $\mathscr{G}_i$ **do**
8: **if** rerouting connection request r to spatial dimension group G of path p can reduce the current RMSG cost (i.e., $C_{current}$) **then**
9: Add $[r, p, G, X_{cost}]$ to RR_{info}, where X_{cost} is the cost difference before and after rerouting r.
10: **end if**
11: **end for**
12: **end for**
13: **end for**
14: **if** RR_{info} is not an empty set **then**
15: According to RR_{info}, reroute the connection request that has the largest X_{cost} (i.e., the one that can minimize the $C_{current}$)
16: Update $F[e,G]$, $R[e,G]$ and $C_{current}$.
17: **else**
18: **Break while**
19: **end if**
20: **end while**
21: $C_{RR} \leftarrow C_{current}$
22: **return** $F[e,G]$, $R[e,G]$, C_{RR}

The pseudo-code of the RR algorithm is shown in Algorithm 5. The inputs of Algorithm 5 are C_{PA} and the two tables mentioned above. The outputs of the algorithm are the same as the inputs; however, to achieve a lower RMSG cost, the assignment may be updated by the RR algorithm.

As shown in Algorithm 5, our RR algorithm works as follows. According to the assignment of the preassignment algorithm, we first find the currently most congested combination of [link e , spatial dimension group G] and record it as $[e_{max}, G_{max}]$ (line 3). Then, we check each connection request that passes through spatial dimension group G_{max} of link e_{max} according to the assignment table $R[e_{max}, G_{max}]$ (line 5) and reroute the one that can maximally reduce the RMSG cost. Finally, we update the assignment and the current RMSG cost $C_{current}$ (line 16). The above process is repeated (line 2) until we cannot find a connection request that can reduce $C_{current}$ by rerouting it (line 18).

Spatial granularity decision:

According to the preassignment and the RR algorithms above, we can obtain the RMSG cost for each available spatial granularity $i \in I$. Note that the service sequence is very important in the preassignment algorithm. The different sequences will lead to different assignment results of preassignment algorithm, because the preassignment algorithm assigns the connection requests one by one. Moreover, since the RR algorithm is executed based on the assignment results of the preassignment algorithm, the service sequence also has an impact on the results of the RR algorithm. Therefore, we apply the simulated annealing (SimAn) metaheuristic proposed in Ref. [52] to find a good sequence that yields better RR algorithm results. However, to reduce the computational complexity of the algorithm, we do not iterate all the available spatial granularities in I (via SimAn). We employ a filter parameter Θ ($\geq$ 1) to select the spatial granularities that need to be iterated ($I_{iteration}$).

First, we sort the service sequence of the connection requests in R by the longest-path-first (LPF) criterion [52]. We next apply Algorithm 5 once by using the sorted service sequence to obtain the RMSG cost for each available spatial granularity $i \in I$. Then, we can calculate the threshold by multiplying the lowest RMSG costs of the spatial granularities and the filter parameter. The spatial granularities that need to be iterated are those with their RMSG costs are less than the threshold. A simple example is shown in Fig. 4.1.

As shown in Fig. 4.1, we assume that the set of the available spatial granularities I is { 1, 2, 3, 4, 6, 12 }, and the corresponding RMSG costs of them are equal to 1650, 1420, 1000, 1250, 1530 and 1880, respectively. We assume that the filter parameter Θ is set as 1.5. We can see that the lowest RMSG cost of spatial granularities is equal to 1000. Thus, we can calculate the threshold by 1000×1.5 which equals 1500. Therefore, the spatial granularities that need to be iterated are $i = 2$, $i = 3$, $i = 4$ because their RMSG costs are less than 1500. That is, $I_{iteration}$ is equal to $\{2, 3, 4\}$, which is a sub-set of I.

Finally, the best spatial granularity is the one resulting in the lowest RMSG cost after iterating the spatial granularities in $I_{iteration}$. The outputs of the spatial granularity decision algorithm are

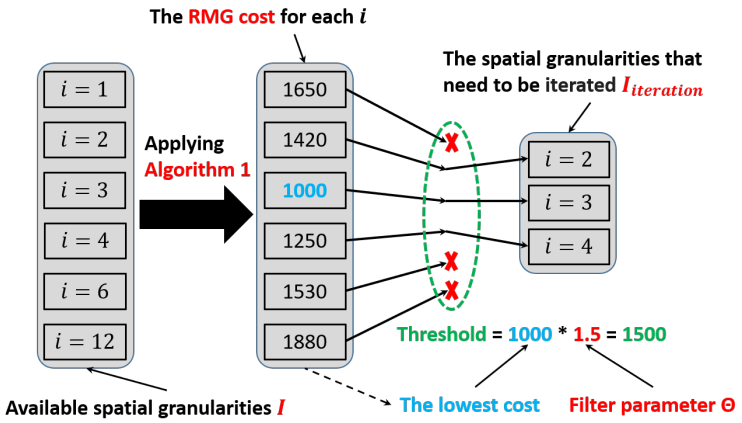

Figure 4.1: Example of the selection of the spatial granularities that need to be iterated.

the best spatial granularity and its corresponding assignment of all the connection requests.

SA heuristic algorithm

The ILP-SA model proposed in Section 4.1.2 is used to assign the spectrum resource. Since we consider the planning phase of the network, which can be performed offline, a few hours of runtime is generally acceptable. Indeed, the ILP-SA model is computationally tractable for the sizes of realistic backbone networks. As shown in Section 4.3, for a realistic 14-node, 42-link NSF network with 12 spatial dimensions on each link and hundreds of Tbps-level connection requests, the ILP-SA model can yield good solutions within a reasonable amount of time.

4.2.2 KSP & FF-SA heuristic algorithm

For further larger problem instances, such as thousands of connection requests and complex networks with dozens of spatial dimensions on each link, the ILP-SA model above may struggle to find a good solution within a reasonable amount of time. In these cases, the classic KSP & FF-SA policy [52] combined with the SimAn iteration can be applied to solve the RMSSGA problem. However, according to our simulation experiments, the performance of KSP & FF-SA is 21.8% (on average) worse than that of the proposed RR-RMSG + ILP-SA heuristic algorithm for a realistic NSF network.

4.3 Simulations and performance evaluations

In this section, we evaluate the performances of the proposed ILP formulations and heuristic algorithm. For a fair comparison among the three SDM switching paradigms and the corresponding SpCh policies, regardless of the transmission medium and related performance constraints, a bundle of 6 or 12 (for different network sizes) independent SMFs is considered. We assume that the

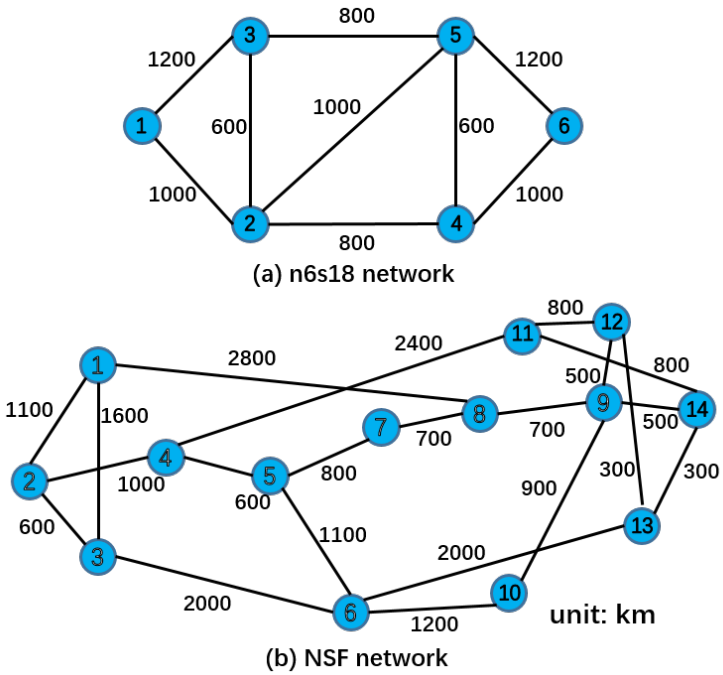

Figure 4.2: Illustration of network topologies: (a) 6-node n6s9 simple network and (b) 14-node NSF network.

granularity of the spectrum grid is 12.5 GHz [13], that the transceivers operate at a fixed baud rate of 32 Gbaud and that each transceiver transmits/receives an optical carrier that occupies 37.5 GHz (refers to Section 1.2.5 and Section 1.3.6). The transmission reach and bit-rates supported by a transceiver/optical carrier are shown in Table 1.1. Moreover, we consider that a guard-band of 6.25 GHz is allocated on both sides of all occupied spatial dimensions between two SpChs.

For all the proposed algorithms, we use $k = 3$ candidate paths for each source-destination node pair obtained via the KSP algorithm proposed in Ref. [52]. The results of the proposed RR-RMSG + ILP-SA (or KSP & FF-SA) heuristic algorithm are obtained after 1000 SimAn iterations (125 iterations per thread via multiprocessing). We use the GUROBI Optimizer 7.0.1 [138] to solve the ILP optimization models. The simulation experiments are performed using Microsoft Windows 10 on a computer with an Intel Xeon 4-core 8-thread 3.6 GHz CPU and 64 GB of memory.

4.3.1 Performance evaluations for different optimization goals

First, we rewrite the objective function Eq. (4.1) as follows:

$$\text{Minimize:} \qquad \alpha \cdot F_{max} + \beta \cdot S_{max} + \gamma \cdot L_{max} = \alpha \cdot (F_{max} + \frac{\beta}{\alpha} \cdot S_{max} + \frac{\gamma}{\alpha} \cdot L_{max})$$

Since α is a parameter which is given beforehand, the objective function above is mathematically

Table 4.3: Performance evaluations for different optimization goals in the simple n6s9 network.

W. Coef.		ILP-RMSSGA									ILP-RMSG + SA			RR-RMSG + ILP-SA				KSP & FF-SA		
$\omega_{s:f}$	$\omega_{l:f}$	N.F	N.L	N.W	N.i 1	2	3	6	Cost	Time	N.Hit	Gap	Time	N.Hit	Gap	Conf.	Time	N.Hit	Gap	Time
	0.001	20.6	115.5	93.2	0	75	9	16	20.849	8.3s	100	0.0%	1.5s	100	0.0%	0.27	7.7s	90	0.7%	12.9s
	0.005	20.6	115.4	93.2	0	75	9	16	21.310	10.4s	100	0.0%	1.8s	100	0.0%	0.27	7.5s	89	0.8%	12.9s
0.001	0.01	20.6	115.4	93.2	0	75	9	16	21.888	22.4s	100	0.0%	4.3s	100	0.0%	0.28	7.5s	88	1.0%	12.9s
	0.05	22.2	55.9	38.2	0	0	6	94	25.003	146.3s	100	0.0%	12.8s	100	0.0%	0.30	7.3s	90	1.7%	12.9s
	0.1	22.2	55.9	38.2	0	0	6	94	27.798	53.9s	100	0.0%	7.5s	100	0.0%	0.32	7.2s	98	1.7%	12.9s
	0.001	20.6	115.5	93.2	0	75	9	16	21.222	8.2s	100	0.0%	1.5s	100	0.0%	0.27	7.7s	88	0.8%	12.9s
	0.005	20.6	115.4	93.2	0	75	9	16	21.683	12.0s	100	0.0%	2.0s	100	0.0%	0.27	7.6s	87	1.1%	12.9s
0.005	0.01	20.6	115.4	93.2	0	75	9	16	22.261	34.0s	100	0.0%	4.6s	100	0.0%	0.28	7.6s	89	1.0%	12.8s
	0.05	22.2	55.9	38.2	0	0	6	94	25.156	113.6s	100	0.0%	9.7s	100	0.0%	0.30	7.5s	92	1.6%	12.9s
	0.1	22.2	55.9	38.2	0	0	6	94	27.951	57.7s	100	0.0%	6.2s	100	0.0%	0.32	7.3s	96	2.8%	12.9s
	0.001	20.6	115.5	93.2	0	75	9	16	21.688	9.6s	100	0.0%	1.6s	100	0.0%	0.27	7.7s	87	1.1%	12.9s
	0.005	20.6	115.4	93.2	0	75	9	16	22.150	16.4s	100	0.0%	3.3s	100	0.0%	0.28	7.7s	91	0.8%	12.8s
0.01	0.01	20.6	115.4	93.2	0	75	9	16	22.727	40.0s	100	0.0%	5.5s	100	0.0%	0.28	7.7s	89	1.1%	12.9s
	0.05	22.2	55.9	38.2	0	0	6	94	25.347	69.4s	100	0.0%	7.9s	100	0.0%	0.30	7.5s	86	2.6%	12.9s
	0.1	22.3	55.2	37.4	0	0	4	96	28.139	52.7s	100	0.0%	6.0s	100	0.0%	0.32	7.4s	98	2.8%	12.9s
	0.001	22.2	55.9	38.2	0	0	6	94	24.134	8.9s	100	0.0%	0.9s	100	0.0%	0.29	7.7s	88	2.1%	12.9s
	0.005	22.2	55.9	38.2	0	0	6	94	24.358	10.8s	100	0.0%	1.2s	100	0.0%	0.29	7.7s	87	2.0%	12.9s
0.05	0.01	22.2	55.9	38.2	0	0	6	94	24.637	12.1s	100	0.0%	1.5s	100	0.0%	0.29	7.7s	87	2.1%	12.9s
	0.05	22.2	55.9	38.2	0	0	6	94	26.873	32.2s	100	0.0%	2.9s	100	0.0%	0.31	7.6s	97	2.3%	12.9s
	0.1	22.4	53.7	36.0	0	0	0	100	29.584	34.4s	100	0.0%	2.8s	100	0.0%	0.32	7.5s	100	2.0%	12.9s
	0.001	22.2	55.9	38.2	0	0	6	94	26.042	6.3s	100	0.0%	0.8s	100	0.0%	0.29	7.6s	99	2.5%	12.9s
	0.005	22.2	55.9	38.2	0	0	6	94	26.266	8.0s	100	0.0%	1.1s	100	0.0%	0.30	7.6s	98	2.9%	12.9s
0.1	0.01	22.2	55.9	38.2	0	0	6	94	26.545	11.1s	100	0.0%	1.4s	100	0.0%	0.30	7.6s	94	3.1%	12.9s
	0.05	22.4	53.7	36.0	0	0	0	100	28.697	11.2s	100	0.0%	1.4s	100	0.0%	0.31	7.5s	100	1.7%	12.9s
	0.1	22.4	53.7	36.0	0	0	0	100	31.384	14.3s	100	0.0%	1.5s	100	0.0%	0.32	7.3s	100	2.4%	12.9s
1	≤1	22.4	53.7	36.0	0	0	0	100	-	<7.8s	100	0.0%	<0.9s	100	0.0%	-	<6.2s	100	≤1.3%	<13.5s
≤1	1	22.4	53.7	36.0	0	0	0	100	-	<87.6s	100	0.0%	<7.2s	100	0.0%	-	<5.8s	100	≤1.3%	<13.5s

equivalent to:

$$\text{Minimize:} \qquad F_{max} + \frac{\beta}{\alpha} \cdot S_{max} + \frac{\gamma}{\alpha} \cdot L_{max} = F_{max} + \omega_{s:f} \cdot S_{max} + \omega_{l:f} \cdot L_{max} \quad (4.18)$$

As shown in Eq. (4.18), $\omega_{s:f}$ / $\omega_{l:f}$ represents the relative cost ratio of a WSS / a pair of laser and one FS resources. Then, we evaluate the performances of the ILP model and heuristic algorithms under different settings of $\omega_{s:f}$ and $\omega_{l:f}$. For comparison, we also evaluate the performance of the KSP & FF-SA heuristic algorithm mentioned in Section 4.2.2.

Simulation experiments in n6s9 simple network

An n6s9 simple network topology (see Fig. 4.2.a), comprising 6 nodes and 18 directed links, with a bundle of 6 independent SMFs for all links, is considered in this part of the simulation experiments. The available spatial granularity i is considered to belong to $\{1, 2, 3, 6\}$. Note that nonuniform grouping (i.e., $\exists G \in \mathscr{G}_i : |G| \neq i$) of the spatial dimensions is allowed for all three algorithms. However, for a fair comparison, in the simulation experiments, we consider only the cases of uniform grouping (i.e., $\forall G \in \mathscr{G}_i : |G| = i$). The results are shown in Table 4.3.

We randomly generate 100 different traffic matrices which compose a set denoted as R_{set}. For each traffic matrix, one unidirectional connection request r exists between each node pair (s, d). The bit-rates of connection requests follow a normal distribution with an average of 1000 Gbps and a fixed standard deviation of 150 Gbps (ranging from 426 Gbps to 1470 Gbps) referring to the settings in Ref. [28] and [49]. Both $\omega_{s:f}$ and $\omega_{l:f}$ are considered ranging from 0.001, 0.005, to a maximum of 1. For a fair comparison, the R_{set} above is considered for each combination of $\omega_{s:f}$ and $\omega_{l:f}$, and the results in Table 4.3 represent the averages over 100 traffic matrices. Moreover, the filter parameter Θ for "RR-RMSG" (see Section 4.2.1) is set to 1.6.

In Table 4.3, "N.F", "N.L" and "N.W" represent the numbers of required FSs, laser pairs and WSSs in the network, respectively. "N.i" represents the number of times that the spatial granularity i is chosen as the best spatial granularity for the traffic matrices $R \in R_{set}$. For example, N.2 = 75 indicates that there are 75 generated traffic matrices $R \in R_{set}$ have chosen the spatial granularity i = 2 as the best spatial granularity to serve the connection requests in R. "N.Hit" represents the number of times that the other three algorithms select the same best spatial granularity as that of the optimal solution (given by "ILP-RMSSGA") as the result. Note that we generated 100 traffic matrices in R_{set}; thus, both the sum of "N.i" and the maximum of "N.Hit" are equal to 100. Moreover, "Cost" represents the value of the RMSSGA objective function Eq. (4.18), and "Gap" represents the average percentage gap of the "Cost" between the optimal solutions which are obtained by the "ILP-RMSSGA" and those of the other three algorithms. "Time" represents the runtime of the algorithms. For all ILP formulations, the values returned by the 'RunTime' parameter given by AMPL/GUROBI [138] are used as the measured runtimes. Finally, "Conf." represents the 95% confidence intervals (over 100 traffic matrices) regarding the value of the objective function of the proposed "RR-RMSG + ILP-SA" algorithm.

As shown in Table 4.3, different combinations of $\omega_{s:f}$ and $\omega_{l:f}$ result in different decisions regarding the best spatial granularity. When $\omega_{s:f}$ or $\omega_{l:f}$ is very small (e.g., $\omega_{s:f}, \omega_{l:f}$ = 0.001), the algorithms tend to conserve spectrum resources while allowing further usage of laser pairs and WSSs. Therefore, in these cases, a smaller spatial granularity $i = 2$ is selected 75 times as the best granularity over 100 traffic matrices, while $i = 3$ and $i = 6$ are selected only 9 and 16 times, respectively. When $\omega_{s:f}$ or $\omega_{l:f}$ increases (e.g., $\omega_{s:f}, \omega_{l:f}$ = 0.05), the largest spatial granularity $i = 6$ is selected 94 times to reduce the usage of WSSs and laser pairs. Finally, when either $\omega_{s:f}$ or $\omega_{l:f}$ is equal to 1, the largest spatial granularity $i = 6$ is always selected as the best one.

Even though a smaller spatial granularity can reduce the number of guard-bands between SpChs, more contiguous FSs are required in the selected spatial dimension group G. Note that F_{max} is calculated by the (maximal index of) required FSs in the network. Therefore, when several connection requests inevitably share a common spatial dimension group on a common link, the assignment of large numbers of contiguous FSs (due to the smaller spatial granularity) will increase the value of

F_{max}. For example, in Fig. 1.24 of Section 1.3.6, if a new connection with the same FS requirement is considered, for the smallest spatial granularity $i = 1$, F_{max} will increase to 26, regardless of the spatial dimensions selected to serve the new connection request. In contrast, in this case, the larger spatial granularity $i = 2$ and largest spatial granularity $i = 4$ require only 21 FSs and 20 FSs, respectively. Overall, in most cases, a relatively smaller spatial granularity can reduce the usage of FSs by decreasing the number of guard-bands. However, the largest spatial granularity is not always able to reduce the usage of FSs (depending on the network features and the traffic matrix R). This is the reason why $i = 1$ is never selected and why $i = 6$ is still selected for some traffic matrices, even if $\omega_{s:f}$ or $\omega_{l:f}$ is very small, as shown in Table 4.3.

As a result, when the importance of FSs and that of WSSs or laser pairs are similar (i.e., $\omega_{s:f}$ or $\omega_{l:f}$ close to 1), J-Sw (Spa SpCh) is always the best choice for serving the connection requests. From a comparison of the first row (smaller spatial granularities are selected in most cases) and the last row (the largest spatial granularity is always selected) in Table 4.3, the required FSs do not change obviously. However, the numbers of required WSSs and laser pairs are significantly reduced. In addition, as analyzed above, even in the cases where a single FS has more value than a WSS and a pair of laser, a smaller spatial granularity is not always the best decision.

Table 4.3 shows that compared to the optimal solutions given by "ILP-RMSSGA", the "ILP-RMSG + SA" and "RR-RMSG + ILP-SA" algorithms can achieve the same performance, with a 0.0% average gap regarding the optimization objective and 100% hit rates regarding the spatial granularity decisions, but with less runtime required. Therefore, in Table 4.3, we do not provide details regarding the spatial granularity decisions (the assignment of FSs, laser pairs, and WSSs) of the two algorithms, as the results are the same as the optimal solutions. Moreover, since 1000 iterations are carried out for "RR-RMSG + ILP-SA" and "KSP & FF-SA", the runtime of each exceeds that of "ILP-RMSG + SA". Finally, "KSP & FF-SA" clearly yields relatively worse solutions than those of the proposed algorithms.

Simulation experiments in the NSF network

The NSF network topology (see Fig. 4.2.b) [147] comprising 14 nodes and 42 directed links, with a bundle of 12 independent SMFs for all links, is considered. The available spatial granularity i is considered to belong to $\{1, 2, 3, 4, 6, 12\}$. We randomly generate 10 different traffic matrices which compose a set denoted as R_{set}. For each traffic matrix $R \in R_{set}$, one unidirectional connection request r exists between each node pair (s, d) (182 connection requests exist in the NSF network). The average bit-rate per connection request is also set as 1000 Gbps with a fixed standard deviation of 150 Gbps (ranging from 517 Gbps to 1511 Gbps). Both $\omega_{s:f}$ and $\omega_{l:f}$ are considered ranging from 0.001, 0.005, to a maximum of 0.1. The filter parameter Θ for "RR-RMSG" is set to 1.2 in this part of the simulation experiments.

Table 4.4: Performance evaluations for different optimization goals in the NSF network.

W. Coef.		ILP-RMG + SA									RR-RMG + ILP-SA								KSP & FF-SA	
$\omega_{s:f}$	$\omega_{l:f}$	N.i 2	3	4	6	12	ILP-RMG L.Bound	Cur.Cost	ILP-SA Cost	Time	N.i 3	4	6	12	RR-RMG Cost	Time	ILP-SA Cost	Conf.	Time	Cost	Time
	0.001	5	1	4	0	0	51.75	55.86	57.97	3.4	6	4	0	0	58.32	161.5	58.72	0.78	0.3	72.23	389.6
	0.005	1	0	6	3	0	53.89	59.40	62.90	15	3	7	0	0	61.20	172.1	61.20	0.43	0.4	75.95	388.6
0.001	0.01	0	1	8	1	0	58.35	62.14	65.64	12.3	0	10	0	0	64.38	177.0	64.38	0.38	0.5	79.48	388.4
	0.05	0	0	0	3	7	69.92	81.16	82.46	246.4*	0	0	3	7	82.00	146.9	82.80	0.99	211.9*	100.21	388.8
	0.1	0	0	0	0	10	84.06	93.74	95.64	300.0*	0	0	0	10	94.34	103.0	95.14	1.52	232.3*	113.24	389.4
	0.001	3	3	4	0	0	52.76	57.28	62.48	1.2	4	6	0	0	59.61	170.7	59.61	0.36	0.3	73.69	389.9
	0.005	0	0	5	5	0	55.68	60.65	61.85	118.9*	0	9	1	0	62.21	175.2	62.21	0.43	0.8	77.83	388.9
0.005	0.01	0	0	4	6	0	58.95	63.53	64.13	71.8*	0	6	4	0	65.12	177.7	65.12	0.47	1.7	81.40	388.7
	0.05	0	0	0	2	8	73.64	81.71	83.21	247.1*	0	0	1	9	82.40	144.9	83.20	1.08	238.2*	100.91	388.5
	0.1	0	0	0	0	10	78.82	94.08	96.18	300.0*	0	0	0	10	94.74	101.1	95.64	1.29	249.4*	114.79	388.5
	0.001	0	2	7	1	0	54.91	58.73	60.83	32.3*	1	9	0	0	60.84	173.2	61.34	0.81	0.5	76.64	389.3
	0.005	0	3	6	1	0	57.65	61.20	64.00	2.9	0	8	2	0	62.94	174.9	62.94	0.58	1.5	78.64	388.6
0.01	0.01	0	0	3	7	0	60.51	64.58	65.08	160.5*	0	7	3	0	66.27	175.5	66.27	0.80	1.7	81.67	388.3
	0.05	0	0	0	3	7	76.18	82.06	83.56	247.5*	0	0	2	8	82.92	138.0	83.82	1.03	221*	101.78	388.6
	0.1	0	0	0	0	10	84.94	94.50	96.20	300.0*	0	0	0	10	95.19	102.0	95.89	1.28	204.9*	115.17	388.9
	0.001	0	0	1	9	0	66.25	67.87	68.67	171.9*	0	1	9	0	69.77	168.5	69.77	0.67	3.2	87.24	388.8
	0.005	0	0	0	10	0	68.07	69.66	70.46	217.2*	0	0	10	0	71.78	166.4	71.78	0.75	2.9	88.02	388.5
0.05	0.01	0	0	0	10	0	70.15	71.92	72.82	202.3*	0	0	10	0	73.76	167.0	73.76	0.93	3.4	91.14	388.8
	0.05	0	0	0	0	10	81.37	85.88	87.88	300.0*	0	0	0	10	86.49	127.3	87.39	1.32	247.7*	105.78	388.0
	0.1	0	0	0	0	10	96.89	97.86	99.96	300.0*	0	0	0	10	98.67	97.4	99.67	1.45	254*	117.23	388.0
	0.001	0	0	0	10	0	75.52	76.43	76.93	240.8*	0	0	7	3	78.16	152.2	78.36	0.69	71.9*	96.42	388.0
	0.005	0	0	0	5	5	76.72	78.18	79.38	219.9*	0	0	4	6	79.26	144.5	79.76	1.01	157.4*	97.49	387.9
0.1	0.01	0	0	0	4	6	78.38	79.93	81.63	272*	0	0	2	8	80.79	142.0	81.69	1.09	230.5*	99.29	388.3
	0.05	0	0	0	0	10	88.73	90.08	92.48	300.0*	0	0	0	10	90.69	101.5	91.89	1.08	247.1*	110.57	388.6
	0.1	0	0	0	0	10	101.21	102.06	104.06	280.3*	0	0	0	10	102.67	93.1	103.77	1.18	276*	121.87	387.7

Time*: the $*$ represents that for all the applied 10 traffic matrices, the running time of the ILP-SA formulation has reached the bound of the limited running time of 300 seconds at least once.

Table 4.4 presents the results obtained for the NSF network. "ILP-RMSSGA" becomes unable to produce good solutions within a reasonable amount of time for the NSF network. This outcome means that we cannot obtain the optimal solutions in these cases. Therefore, we cannot provide the hit rates ("N.Hit") and the performance gaps ("Gap") of the other algorithms. For each traffic matrix $R \in R_{set}$, the results for "ILP-RMSG + SA" are obtained by stopping the optimization of "ILP-RMSG" and "ILP-SA" after 1 hour and 5 minutes of runtime (i.e., the 'RunTime' of GUROBI), respectively. Similarly, the runtime of "ILP-SA" in "RR-RMSG + ILP-SA" is also restricted to 5 minutes. In fact, for most (55.6%) inputs (i.e., $\omega_{s:f}$, $\omega_{l:f}$ and R), "ILP-SA" can be solved within 5 minutes; for the other inputs, it can also obtain good solutions with a less than 2.5% average 'MIPGap' (given by GUROBI) after 5 minutes, which indicates the high convergence efficiency of "ILP-SA". In contrast, the computational time of "ILP-RMSG" for all $\omega_{s:f}$ and $\omega_{l:f}$ values have exceeded the limitation of 1 hour. Note that the optimal solution to "ILP-RMSG" is the lower bound of the joint RMSSGA problem. Therefore, the 'BestBound' (given by GUROBI) of "ILP-RMSG" after 1 hour can be treated as a more relaxed lower bound of the joint RMSSGA problem, which is represented by "L.Bound" in Table 4.4.

From Table 4.4, the results are clearly similar to those in Table 4.3, which were obtained for the n6s9 simple network. When $\omega_{s:f}$ and $\omega_{l:f}$ are very small (e.g., $\omega_{s:f}, \omega_{l:f} = 0.001$), the algorithms tend to conserve the spectrum resources, resulting in smaller spatial granularities ($i = 2, 3, 4$) being selected more often. Then, as $\omega_{s:f}$ or $\omega_{l:f}$ increases, relatively larger spatial granularities are selected more often. Furthermore, when $\omega_{s:f}$ and $\omega_{l:f}$ are equal to 0.1, the largest spatial granularity ($i = 12$) is always selected.

Moreover, both the "ILP-RMSG + SA" and "RR-RMSG + ILP-SA" algorithms yield much better solutions than those of "KSP & FF-SA", which are close to the lower bound (i.e., "L.Bound"). The gaps between the "RR-RMSG + ILP-SA" and "KSP & FF-SA" algorithms range from 8.4% to 31.4%, with an average of 21.8% over all the inputs. Additionally, comparing the results obtained by the RMSG algorithms (i.e., "Cur.Cost" of "ILP-RMSG" with a 1-hour runtime limitation and "Cost" of "RR-RMSG") with their corresponding results after SA (i.e., "Cost" of "ILP-SA"), decomposing the RMSSGA problem into RMSG and SA subproblems is shown to not have significant effects (within a 3% average gap) on the final results, even though we limited the runtime of "ILP-SA" to 5 minutes and considered hundreds of Tbps-level connection requests.

Table 4.5: Average numbers of required FSs, laser pairs and WSSs in the cases of $\omega_{s:f}, \omega_{l:f}$ equal to 0.001 and 0.1.

W. Coef.		ILP-RMSG + SA			RR-RMSG + ILP-SA		
$\omega_{s:f}$	$\omega_{l:f}$	N.F	N.L	N.W	N.F	N.L	N.W
0.001	0.001	56.7	878.1	386.4	57.7	718.0	302.4
0.1	0.1	71.7	239.6	84.0	71.2	241.7	84.0

Finally, we present the average numbers of required FSs, laser pairs and WSSs of the "ILP-RMSG + SA" and "RR-RMSG + ILP-SA" algorithms when $\omega_{s:f}$ and $\omega_{l:f}$ equal to 0.001 (smaller spatial granularities are selected more often) and 0.1 (the largest spatial granularity is always selected) in Table 4.5. From Table 4.5, comparing the results of the two cases, the selection of the largest granularity is shown to not have an obvious effect on the number of required FSs. In contrast, the numbers of required laser pairs and WSSs clearly change. Hence, the largest granularity is always the best decision when the importance of FSs and that of WSSs or laser pairs are similar.

4.3.2 Impact of guard band width on the decision regarding the best spatial granularity

The key advantage of a smaller spatial granularity is that the number of guard-bands in all occupied spatial dimensions between neighboring SpChs can be reduced. As a negative effect, more WSSs and laser pairs are required. Therefore, the advantage of a smaller spatial granularity is more pronounced when the guard-band becomes wider. In contrast, a larger spatial granularity is more appropriate for a narrower guard-band to reduce the usage of WSSs and laser pairs. In this subsection,

we analyze the impact of guard-band width on the decision regarding the best spatial granularity. Since we cannot obtain the optimal decisions regarding the best spatial granularity in the NSF network, the n6s9 simple network is considered in the simulation experiments. Moreover, for a fair comparison, the same set of (100) traffic matrices R_{set} used in Section 4.3.1 is considered in these simulation experiments. $\omega_{s:f}$ and $\omega_{l:f}$ are fixed to 0.001, as in this case, various spatial granularities are selected (see Table 4.3). The guard-band widths considered ranging from 6.25 GHz to 25 GHz with a 6.25-GHz step. The results are shown in Table 4.6.

Table 4.6: Impact of the guard bandwidth on the decision regarding spatial granularities for a 6-node, 18-link simple network.

W.GB	ILP-RMSSGA				ILP-RMSG + ILP-SA		RR-RMSG + ILP-SA	
[GHz]	N.1	N.2	N.3	N.6	N.Hit	Gap	N.Hit	Gap
6.25	0	75	9	16	100	0%	100	0%
12.50	0	88	9	3	100	0%	100	0%
18.75	0	88	9	3	100	0%	100	0%
25.00	0	100	0	0	100	0%	100	0%

As shown in Table 4.6, as "W.GB" (denoting the guard-band width) becomes wider, the smaller granularities are selected more often. When "W.GB" increases to 25 GHz, for all 100 traffic matrices, spatial granularity $i = 2$ is selected. Clearly, the results are consistent with the theoretical analysis above. Moreover, both "ILP-RMSG + SA" and "RR-RMSG + ILP-SA" achieve the same performance (100% hit rate and 0% average gap regarding the optimization objective) comparing to the optimal solutions.

4.3.3 Impact of average traffic volume of conncetion requests on the decision regarding the best spatial granularity

In the simulation experiments of the previous subsection, we changed the guard-band width and analyzed its influence on the choice regarding the best spatial granularity. From another perspective, since the traffic volume of the connection requests are not changed (i.e., the same R_{set} used), we change the ratio between the FSs used for data transmission and the FSs occupied by the guard-band. Therefore, if the guard-band is fixed, a smaller granularity should be more suitable for the traffic matrices with the smaller traffic volume of connection requests. Thus, we now analyze the effect of the average traffic volume of connection requests on the choice regarding the best spatial granularity. Similarly, we consider an n6s9 simple network with $\omega_{s:f}$ and $\omega_{l:f}$ fixed at 0.001. For a fair comparison, we further consider 10 sets of 100 traffic matrices based on the original R_{set} used in Section 4.3.1. For the 10 new sets, the traffic volume of each connection request is considered to be 0.5, 0.75, 1.25, up to a maximum of 3 times the volume of the original one in R_{set}, respectively. That is, the average bit-rate per connection request in the new sets is changed to 500 Gbps, 750

Gbps, 1250 Gbps, up to a maximum of 3000 Gbps, respectively. The results are shown in Table 4.7.

Table 4.7: Impact of the average traffic volume [Gbps] of connection request on the decision regarding spatial granularities for a 6-node, 18-link simple network.

Av.Volume r	ILP-RMSSGA				ILP-RMSG + ILP-SA		RR-RMSG + ILP-SA	
[Gbps]	N.1	N.2	N.3	N.6	N.Hit	Gap	N.Hit	Gap
500	0	100	0	0	100	0%	100	0%
750	0	94	6	0	100	0%	100	0%
1000	0	75	9	16	100	0%	100	0%
1250	0	58	17	25	100	0%	100	0%
1500	0	14	12	74	100	0%	98	0.1%
1750	0	12	6	82	100	0%	100	0.3%
2000	0	4	3	93	100	0%	99	0.6%
2250	0	1	0	99	100	0%	100	0.3%
2500	0	0	1	99	100	0%	100	0.5%
2750	0	0	0	100	100	0%	100	0.6%
3000	0	0	0	100	100	0%	100	0.2%

As shown in Table 4.7, as the average bit-rate of the connection request ("Av.Volume r") increases, the larger spatial granularities are selected more often. As mentioned above, regardless of whether the traffic volume of the connection requests increases or the guard-band width decreases, we actually increase the ratio between the FSs used for data transmission and the FSs occupied by the guard-band. Thus, larger spatial granularities are selected more often. Similarly, both the "ILP-RMSG + SA" and "RR-RMSG + ILP-SA" algorithms achieve very similar performances compared to those for the optimal solutions.

Chapter 5

Conclusion and Future Work

This Ph.D. thesis addressed the resource allocation problems several generations of optical networks, from the traditional WDM-based optical networks to the EONs, and further to the spectrally & spatially flexible SDM-EONs. The conclusion of this thesis are per chapter summarized as follows:

- In Chapter 1, we introduced the evolutions of the optical networks in recent years from the traditional WDM-based optical networks to the spectrally & spatially flexible SDM-EONs. We also introduced opportunities on the resource allocation brought by the evolutions of the optical networks and discussed the challenges of these problems. In addition, we summarized our contribution to the research field of resource allocation in optical networks.

- In Chapter 2, we addressed the RMSTA problem in elastic optical networks. The key point of the RMSTA problem is that solving it would allow transceivers to be used more flexibly in elastic optical networks. The problem objective seeks to minimize the cost of network operations by making a trade-off between spectrum usage and transceiver usage. We proposed an ILP model and an efficient heuristic algorithm (i.e., GVNA) to solve the static RMSTA problem. The results of simulation experiments on representative network topologies and realistic networking scenarios indicate that, compared to algorithms that do not consider flexible use of transceivers (for the RMSA problem), the proposed algorithm achieved significant performance improvements on the 17-node NSF-East and the 28-node EON-RT networks. Moreover, compared to the previous algorithm that considered the flexible use of transceivers(i.e., the MCLOD algorithm), the proposed algorithm achieved better results, as well as remarkable savings of computational time on NSF-East and EON-RT networks. Such a computational time difference would be enlarged further if a larger network were considered. Overall, the proposed algorithm is more suitable for large networks.

- In Chapter 3, we addressed the static RSCA problem with XT management in SDM-EONs connected by MCFs. We first proposed a node-arc-based ILP model that assigns lightpath,

core, and the corresponding spectrum simultaneously for each connection request. In the proposed ILP model, we considered the XT in the worst interference scenario similar to previous works. The simulation results showed that the proposed ILP model can increase dozens or more than one hundred times in terms of convergence efficiency compared with the existing ILP models, and significantly reduce the required variables and constraints. We next proposed two XT-aware-based approaches that consider XT strictly: an MILP model, which is the extension of the proposed ILP model above, and a heuristic algorithm. The simulation results showed that the two XT-aware-based approaches can cope well with the cases of different XT-thresholds and/or different geographical sizes of the networks. Moreover, the simulation results demonstrated that the proposed heuristic algorithm can obtain effective solutions within an acceptable time even for large-scale problem instances (in 40 s for 1000 requests in 28-node 34-link EON network), which are more approximate to the optimal solutions or the lower-bounds of the problem than the existing approaches.

- In Chapter 4, we introduced the RMSSGA problem. The objective was to minimize the network CAPEX considering spectrum (FS), WSS and laser resources in spectrally & spatially flexible SDM-EONs. To solve this problem, we presented various algorithms, ranging from the optimal ILP-RMSSA model and the decomposed ILP-RMSG + SA models to an RR-based heuristic algorithm combined with a simulated annealing metaheuristic. We found that the decision of the best spatial granularity is related to the network resources to which network operators attach more importance. When the importance of FSs and that of WSSs or lasers are similar (the cost ratio $\omega_{s:f}$ or $\omega_{l:f}$ is close to 1), the largest spatial granularity is always the best decision. In contrast, a smaller spatial granularity is a better decision when the cost related to the unit FS is much larger than that of the WSS and laser. We also analyzed the impact of GB width and the size of connection requests on the decision regarding the best spatial granularity. We observed that for both a wider GB and smaller size of connection requests, a smaller spatial granularity is a better decision in most cases, while a larger spatial granularity is more suitable for both a narrower GB width and larger size of connection requests. Moreover, the simulation results indicate that compared with the optimal solutions (lower-bounds), the proposed decomposed ILP-RMG + SA formulation and the RR-based heuristic algorithm can achieve similar performances regarding the optimization objective, with a high hit rate for the best spatial granularity decision, with a lower runtime.

Future works can be inferred by following the research lines stated in this thesis. As we stated before, in the past few decades, the architecture of the optical network has undergone significant changes from the earliest WDM-based network to SDM-EONs, and such changes in network architecture will simultaneously present the challenges of resource allocation in optical networks.

Considering an approximately 40% compound annual growth rates of the client interface speed, the router interface rate is expected to reach 10 Tbps by 2024 in order to achieve Pbps level optical transmission networks. Assuming that a 32 GBaud DP-QPSK subchannel supports 100 Gbps transmission and occupies the bandwidth of 3 FSs equaling 37.5 GHz, there are only a few years left until the entire C-band of one SMF can only accommodate one super-channel for such a 10 Tbps traffic volume. The massive SDM era implemented by massive parallel SMFs or MCFs is upcoming and the wavelength switching layer is no longer necessary by then. For this reason, a new-generation network named spatial channel network (SCN) which achieves growable, reliable, and cost-effective optical cross-connects has been recently proposed in Ref. [149], and it is considered as a promising and cost-efficient solution in future network planning. As the same as what happened heretofore, the evolutions of network architecture always introduce opportunities and challenges. Therefore, a specially designed algorithm is essential to address the resource assignment problem in the newly designed SCN architecture, which we will focus on in our future work.

Appendix

Publications in Journals

1. **M. Yang***, Q. Wu, K. Guo, Y. Zhang, "Evaluation of Device Cost, Power Consumption, and Network Performance in Spatially and Spectrally Flexible SDM Optical Networks", *Journal of Lightwave Technology*, vol. 37, no. 20, pp. 5259–5272, Oct. 2019.

2. **M. Yang***, Q. Wu, Y. Zhang, "Joint Assignment of Spatial Granularity, Routing, Modulation, and Spectrum in SDM-EONs: Minimizing the Network CAPEX Considering Spectrum, WSS, and Laser Resources", *Journal of Lightwave Technology*, vol. 36, no. 18, pp. 4153–4166, Jul. 2018.

3. **M. Yang***, K. Guo, Y. Zhang, Y. Ji, "Routing, modulation level, spectrum, and transceiver assignment in elastic optical networks", *IEICE Transactions on Communications*, vol. 101, no. 5, pp. 1197–1209, May 2018.

4. **M. Yang***, Y. Zhang, Q. Wu, "Routing, spectrum, and core assignment in SDM-EONs with MCF: Node-arc ILP/MILP methods and an efficient XT-aware heuristic algorithm", *Journal of Optical Communication and Networking*, vol. 10, no. 3, pp. 195–208, Mar. 2018.

5. **M. Yang***, K. Guo, Y. Zhang, "Cooperative Data Caching for Cloud Data Servers", *EAI Transactions on Scalable Information Systems*, vol. 3, no. 8, pp. e3, Aug. 2016.

Publications in Conferences

1. **M. Yang***, Q. Wu, K. Guo, Y. Zhang, "Evaluation of Network CAPEX and Performance in SDM Optical Networks", in *2019 International Conference on Optoelectronics and Communications (OECC)*, pp. WP4-F8, Jul. 2019.

Bibliography

[1] S. Arnon, J. Barry, G. Karagiannidis, R. Schober, and M. Uysal, *Advanced optical wireless communication systems*. Cambridge university press, 2012.

[2] R. Ramaswami, K. Sivarajan, and G. Sasaki, *Optical networks: a practical perspective*. Morgan Kaufmann, 2009.

[3] G. Shen and M. Zukerman, "Spectrum-efficient and agile CO-OFDM optical transport networks: architecture, design, and operation," *IEEE Communications Magazine*, vol. 50, no. 5, pp. 82–89, 2012.

[4] B. Zhu, L. Leng, A. Gnauck, M. Pedersen, D. Peckham, L. Nelson, S. Stulz, S. Kado, L. Gruner-Nielsen, R. Lingle, *et al.*, "Transmission of 3.2 Tb/s (80× 42.7 Gb/s) over 5200 km of ultrawave^{TM} fiber with 100-km dispersion-managed spans using RZ-DPSK format," in *2002 28th European Conference on Optical Communication*, vol. 5, pp. 1–2, IEEE, 2002.

[5] H. Zang, J. P. Jue, B. Mukherjee, *et al.*, "A review of routing and wavelength assignment approaches for wavelength-routed optical WDM networks," *Optical Networks Magazine*, vol. 1, no. 1, pp. 47–60, 2000.

[6] R. Ramaswami and K. N. Sivarajan, "Routing and wavelength assignment in all-optical networks," *IEEE/ACM Transactions on Networking*, vol. 3, no. 5, pp. 489–500, 1995.

[7] D. Banerjee and B. Mukherjee, "A practical approach for routing and wavelength assignment in large wavelength-routed optical networks," *IEEE Journal on Selected Areas in Communications*, vol. 14, no. 5, pp. 903–908, 1996.

[8] A. E. Ozdaglar and D. P. Bertsekas, "Routing and wavelength assignment in optical networks," *IEEE/ACM Transactions On Networking*, vol. 11, no. 2, pp. 259–272, 2003.

[9] I. Chlamtac, A. Ganz, and G. Karmi, "Lightpath communications: An approach to high bandwidth optical WAN's," *IEEE Transactions on Communications*, vol. 40, no. 7, pp. 1171–1182, 1992.

[10] Cisco, "White paper: Cisco VNI Forecast and Methodology, 2017-2022," Available: http://www.cisco.com, 2017.

[11] M. Jinno, H. Takara, B. Kozicki, Y. Tsukishima, Y. Sone, and S. Matsuoka, "Spectrum-efficient and scalable elastic optical path network: architecture, benefits, and enabling technologies," *IEEE Communications Magazine*, vol. 47, no. 11, pp. 66–73, 2009.

[12] O. Gerstel, M. Jinno, A. Lord, and S. B. Yoo, "Elastic optical networking: A new dawn for the optical layer?," *IEEE Communications Magazine*, vol. 50, no. 2, pp. s12–s20, 2012.

[13] ITU-T, "Extension of Rec. G.694.1," 2011.

[14] W. Shieh and C. Athaudage, "Coherent optical orthogonal frequency division multiplexing," *Electronics letters*, vol. 42, no. 10, pp. 587–589, 2006.

[15] J. Armstrong, "OFDM for optical communications," *Journal of Lightwave Technology*, vol. 27, no. 3, pp. 189–204, 2009.

[16] W. Shieh and I. Djordjevic, *OFDM for Optical Communications*. Academic Press, 2009.

[17] J. Armstrong and A. Lowery, "Power efficient optical OFDM," *Electronics Letters*, vol. 42, no. 6, pp. 1, 2006.

[18] W. Shieh, H. Bao, and Y. Tang, "Coherent optical OFDM: theory and design," *Optics Express*, vol. 16, pp. 841–859, Jan 2008.

[19] T. Keller and L. Hanzo, "Orthogonal frequency division multiplex synchronisation techniques for wireless local area networks," in *1996 International Symposium on Personal, Indoor, and Mobile Communications*, vol. 3, pp. 963–967, IEEE, 1996.

[20] B. Lin, J. Li, H. Yang, Y. Wan, Y. He, and Z. Chen, "Comparison of DSB and SSB transmission for OFDM-PON," *Journal of Optical Communications and Networking*, vol. 4, no. 11, pp. B94–B100, 2012.

[21] G. Bosco, V. Curri, A. Carena, P. Poggiolini, and F. Forghieri, "On the performance of Nyquist-WDM terabit superchannels based on PM-BPSK, PM-QPSK, PM-8QAM or PM-16QAM subcarriers," *Journal of Lightwave Technology*, vol. 29, no. 1, pp. 53–61, 2010.

[22] R. Schmogrow, S. Wolf, B. Baeuerle, D. Hillerkuss, B. Nebendahl, C. Koos, W. Freude, and J. Leuthold, "Nyquist frequency division multiplexing for optical communications," in *CLEO: Science and Innovations*, pp. CTh1H–2, OSA, 2012.

[23] P. C. Schindler, R. Schmogrow, S. Wolf, B. Baeuerle, B. Nebendahl, C. Koos, W. Freude, and J. Leuthold, "Full flex-grid asynchronous multiplexing demonstrated with Nyquist pulse-shaping," *Optics Express*, vol. 22, pp. 10923–10937, May 2014.

[24] R. Rudnick, A. Tolmachev, D. Sinefeld, O. Golani, S. Ben-Ezra, M. Nazarathy, and D. M. Marom, "Sub-banded / single-sub-carrier drop-DEMUX and flexible spectral shaping with a fine resolution photonic processor," in *2014 The European Conference on Optical Communication (ECOC)*, pp. 1–3, Sep. 2014.

[25] A. Bocoi, M. Schuster, F. Rambach, M. Kiese, C. A. Bunge, and B. Spinnler, "Reach-dependent capacity in optical networks enabled by OFDM," in *2009 Conference on Optical Fiber Communication (OFC)*, pp. 1–3, IEEE, 2009.

[26] M. Klinkowski and K. Walkowiak, "On performance gains of flexible regeneration and modulation conversion in translucent elastic optical networks with superchannel transmission," *Journal of Lightwave Technology*, vol. 34, no. 23, pp. 5485–5495, 2016.

[27] M. Klinkowski and K. Walkowiak, "A heuristic algorithm for routing, spectrum, transceiver and regeneration allocation problem in elastic optical networks," in *2016 18th International Conference on Transparent Optical Networks (ICTON)*, pp. 1–4, IEEE, 2016.

[28] P. S. Khodashenas, J. M. Rivas-Moscoso, D. Siracusa, F. Pederzolli, B. Shariati, D. Klonidis, E. Salvadori, and I. Tomkos, "Comparison of spectral and spatial super-channel allocation schemes for SDM networks," *Journal of Lightwave Technology*, vol. 34, no. 11, pp. 2710–2716, 2016.

[29] M. Klinkowski, P. Lechowicz, and K. Walkowiak, "Survey of resource allocation schemes and algorithms in spectrally-spatially flexible optical networking," *Optical Switching and Networking*, vol. 27, pp. 58–78, 2018.

[30] P. S. Khodashenas, J. M. Rivas-Moscoso, B. Shariati, D. M. Marom, D. Klonidis, and I. Tomkos, "Investigation of spectrum granularity for performance optimization of flexible Nyquist-WDM-based optical networks," *Journal of Lightwave Technology*, vol. 33, no. 23, pp. 4767–4774, 2015.

[31] K. Yonenaga, F. Inuzuka, S. Yamamoto, H. Takara, B. Kozicki, T. Yoshimatsu, A. Takada, and M. Jinno, "Bit-rate-flexible all-optical OFDM transceiver using variable multi-carrier source and DQPSK/DPSK mixed multiplexing," in *2009 Conference on Optical Fiber Communication (OFC)*, pp. 1–3, IEEE, 2009.

[32] N. Sambo, P. Castoldi, A. D'Errico, E. Riccardi, A. Pagano, M. S. Moreolo, J. M. Fabrega, D. Rafique, A. Napoli, S. Frigerio, *et al.*, "Next generation sliceable bandwidth variable transponders," *IEEE Communications Magazine*, vol. 53, no. 2, pp. 163–171, 2015.

[33] M. Dallaglio, N. Sambo, F. Cugini, and P. Castoldi, "Control and management of transponders with NETCONF and YANG," *Journal of Optical Communications and Networking*, vol. 9, pp. B43–B52, March 2017.

[34] N. Sambo, A. Giorgetti, F. Cugini, and P. Castoldi, "Sliceable transponders: Pre-programmed OAM, control, and management," *Journal of Lightwave Technology*, vol. 36, pp. 1403–1410, April 2018.

[35] M. S. Moreolo, J. M. Fabrega, L. Nadal, F. J. Vílchez, A. Mayoral, R. Vilalta, R. Muñoz, R. Casellas, R. Martínez, M. Nishihara, T. Tanaka, T. Takahara, J. C. Rasmussen, C. Kottke, M. Schlosser, R. Freund, F. Meng, S. Yan, G. Zervas, D. Simeonidou, Y. Yoshida, and K. Kitayama, "SDN-enabled sliceable BVT based on multicarrier technology for multiflow rate/distance and grid adaptation," *Journal of Lightwave Technology*, vol. 34, pp. 1516–1522, March 2016.

[36] R. W. Hamming, "Error detecting and error correcting codes," *The Bell System Technical Journal*, vol. 29, no. 2, pp. 147–160, 1950.

[37] M. Klinkowski and K. Walkowiak, "Routing and spectrum assignment in spectrum sliced elastic optical path network," *IEEE Communications Letters*, vol. 15, no. 8, pp. 884–886, 2011.

[38] Y. Wang, X. Cao, Q. Hu, and Y. Pan, "Towards elastic and fine-granular bandwidth allocation in spectrum-sliced optical networks," *Journal of Optical Communications and Networking*, vol. 4, no. 11, pp. 906–917, 2012.

[39] A. Cai, G. Shen, L. Peng, and M. Zukerman, "Novel node-arc model and multi-iteration heuristics for static routing and spectrum assignment in elastic optical networks," *Journal of Lightwave Technology*, vol. 31, no. 21, pp. 3402–3413, 2013.

[40] Y. Liu, N. Hua, X. Wan, X. Zheng, and Z. Liu, "A spectrum-scan routing scheme in flexible optical networks," in *2011 Asia Communications and Photonics Conference and Exhibition*, pp. 83100B, OSA, 2011.

[41] J. Zhang, B. Chen, Y. Zhao, H. Chen, W. Zhang, X. Li, J. P. Jue, S. Huang, and W. Gu, "Minimized spectrum resource consumption with rescaled failure probability constraint in

flexible bandwidth optical networks," *Journal of Optical Communications and Networking*, vol. 5, no. 9, pp. 980–993, 2013.

[42] R. Almeida, A. F. D. Santos, K. Assis, H. Waldman, and J. M. Filho, "Slot assignment strategy to reduce loss of capacity of contiguous-slot path requests in flexible grid optical networks," *Electronics Letters*, vol. 49, no. 5, pp. 359–361, 2013.

[43] G. Raybon, A. Adamiecki, P. J. Winzer, S. Randel, L. Salamanca, A. Konczykowska, F. Jorge, J. Y. Dupuy, L. L. Buhl, S. Chandrashekhar, "High symbol rate coherent optical transmission systems: 80 and 107 Gbaud," *Journal of Lightwave Technology*, vol. 32, no. 4, pp. 824–831, 2013.

[44] E. Pincemin, M. Song, J. Karaki, O. Zia-Chahabi, T. Guillossou, D. Grot, G. Thouenon, C. Betoule, R. Clavier, A. Poudoulec, M. V. D. Keur, Y. Jaouën, R. L. Bidan, T. L. Gall, P. Gravey, M. Morvan, B. D. Feris, M. L. Moulinard, and G. Froc, "Multi-band OFDM transmission at 100 Gbps with sub-band optical switching," *Journal of Lightwave Technology*, vol. 32, pp. 2202–2219, Jun 2014.

[45] J. Zhao and A. D. Ellis, "A novel optical fast OFDM with reduced channel spacing equal to half of the symbol rate per carrier," in *2010 Optical Fiber Communication Conference (OFC)*, pp. OMR1, OSA, 2010.

[46] N. P. Diamantopoulos, B. Shariati, and I. Tomkos, "On the power consumption of MIMO processing and its impact on the performance of SDM networks," in *2017 Optical Fiber Communications Conference and Exhibition (OFC)*, pp. 1–3, IEEE, 2017.

[47] D. Siracusa, F. Pederzolli, P. Khodashenas, J. M. Rivas-Moscoso, D. Klonidis, E. Salvadori, and I. Tomkos, "Spectral vs. spatial super-channel allocation in SDM networks under independent and joint switching paradigms," in *2015 European Conference on Optical Communication (ECOC)*, pp. 1–3, IEEE, 2015.

[48] B. Shariati, D. Klonidis, J. M. Rivas-Moscoso, and I. Tomkos, "Evaluation of the impact of spatial and spectral granularities on the performance of spatial superchannel switching schemes," in *2016 International Conference on Transparent Optical Networks (ICTON)*, pp. 1–4, IEEE, 2016.

[49] B. Shariati, D. Klonidis, D. Siracusa, F. Pederzolli, J. M. Rivas-Moscoso, L. Velasco, and I. Tomkos, "Impact of traffic profile on the performance of spatial superchannel switching in SDM networks," in *2016 European Conference on Optical Communication (ECOC)*, pp. 1–3, VDE, 2016.

[50] F. Pederzolli, D. Siracusa, B. Shariati, J. M. Rivas-Moscoso, E. Salvadori, and I. Tomkos, "Improving performance of spatially joint-switched space division multiplexing optical networks via spatial group sharing," *Journal of Optical Communications and Networking*, vol. 9, no. 3, pp. B1–B11, 2017.

[51] F. Heismann, "System requirements for WSS filter shape in cascaded ROADM networks," in *2010 Optical Fiber Communication Conference (OFC)*, p. OThR1, OSA, 2010.

[52] K. Christodoulopoulos, I. Tomkos, and E. A. Varvarigos, "Elastic bandwidth allocation in flexible OFDM-based optical networks," *Journal of Lightwave Technology*, vol. 29, no. 9, pp. 1354–1366, 2011.

[53] G. Zhang, M. D. Leenheer, A. Morea, and B. Mukherjee, "A survey on OFDM-based elastic core optical networking," *IEEE Communications Surveys & Tutorials*, vol. 15, no. 1, pp. 65–87, 2012.

[54] B. C. Chatterjee, N. Sarma, and E. Oki, "Routing and spectrum allocation in elastic optical networks: A tutorial," *IEEE Communications Surveys & Tutorials*, vol. 17, no. 3, pp. 1776–1800, 2015.

[55] K. Christodoulopoulos, P. Soumplis, and E. Varvarigos, "Planning flexible optical networks under physical layer constraints," *Journal of Optical Communications and Networking*, vol. 5, no. 11, pp. 1296–1312, 2013.

[56] F. M. Madani, "Scalable framework for translucent elastic optical network planning," *Journal of Lightwave Technology*, vol. 34, no. 4, pp. 1086–1097, 2016.

[57] X. Wang, M. Brandt-Pearce, and S. Subramaniam, "Impact of wavelength and modulation conversion on translucent elastic optical networks using MILP," *Journal of Optical Communications and Networking*, vol. 7, pp. 644–655, Jul 2015.

[58] C. Rottondi, M. Tornatore, A. Pattavina, and G. Gavioli, "Routing, modulation level, and spectrum assignment in optical metro ring networks using elastic transceivers," *Journal of Optical Communications and Networking*, vol. 5, no. 4, pp. 305–315, 2013.

[59] M. Yang, K. Guo, Y. Zhang, and Y. Ji, "Routing, modulation level, spectrum and transceiver assignment in elastic optical networks," *IEICE Transactions on Communications*, vol. E101.B, no. 5, pp. 1197–1209, 2018.

[60] D. Richardson, J. Fini, and L. E. Nelson, "Space-division multiplexing in optical fibres," *Nature Photonics*, vol. 7, no. 5, p. 354, 2013.

[61] A. Chralyvy, "Plenary paper: The coming capacity crunch," in *2009 European Conference on Optical Communication (ECOC)*, pp. 1–1, IEEE, 2009.

[62] P. J. Winzer, "High-spectral-efficiency optical modulation formats," *Journal of Lightwave Technology*, vol. 30, no. 24, pp. 3824–3835, 2012.

[63] G. Li, N. Bai, N. Zhao, and C. Xia, "Space-division multiplexing: The next frontier in optical communication,"

[64] P. J. Winzer, "Spatial multiplexing: The next frontier in network capacity scaling," in *Proceeding of IET Conferences*, The Institution of Engineering & Technology, 2013.

[65] P. J. Winzer, "Making spatial multiplexing a reality," *Nature Photonics*, vol. 8, no. 5, p. 345, 2014.

[66] P. J. Winzer and D. T. Neilson, "From scaling disparities to integrated parallelism: A decathlon for a decade," *Journal of Lightwave Technology*, vol. 35, no. 5, pp. 1099–1115, 2017.

[67] P. J. Winzer, D. T. Neilson, and A. R. Chraplyvy, "Fiber-optic transmission and networking: The previous 20 and the next 20 years," *Optics Express*, vol. 26, no. 18, pp. 24190–24239, 2018.

[68] P. J. Winzer, "Optical networking beyond WDM," *IEEE Photonics Journal*, vol. 4, no. 2, pp. 647–651, 2012.

[69] H. Takara, A. Sano, T. Kobayashi, H. Kubota, H. Kawakami, A. Matsuura, Y. Miyamoto, Y. Abe, H. Ono, K. Shikama, *et al.*, "1.01-Pb/s (12 SDM/222 WDM/456 Gb/s) crosstalk-managed transmission with 91.4-b/s/Hz aggregate spectral efficiency," in *2012 European Conference and Exhibition on Optical Communication (ECOC)*, pp. Th–3, OSA, 2012.

[70] B. Li, L. Gan, S. Fu, Z. Xu, M. Tang, W. Tong, and P. P. Shum, "The role of effective area in the design of weakly coupled MCF: Optimization guidance and OSNR improvement," *IEEE Journal of Selected Topics in Quantum Electronics*, vol. 22, no. 2, pp. 81–87, 2015.

[71] T. Hayashi, T. Taru, O. Shimakawa, T. Sasaki, and E. Sasaoka, "Characterization of crosstalk in ultra-low-crosstalk multi-core fiber," *Journal of Lightwave Technology*, vol. 30, no. 4, pp. 583–589, 2011.

[72] J. Sakaguchi, B. J. Puttnam, W. Klaus, Y. Awaji, N. Wada, A. Kanno, T. Kawanishi, K. Imamura, H. Inaba, K. Mukasa, *et al.*, "305 Tb/s space division multiplexed transmission using homogeneous 19-core fiber," *Journal of Lightwave Technology*, vol. 31, no. 4, pp. 554–562, 2012.

[73] R. Ryf, A. Sierra, R. J. Essiambre, A. Gnauck, S. Randel, M. Esmaeelpour, S. Mumtaz, P. J. Winzer, R. Delbue, P. Pupalaikis, *et al.*, "Coherent 1200-km 6× 6 MIMO mode-multiplexed transmission over 3-core microstructured fiber," in *2011 European Conference and Exposition on Optical Communications (ECOC)*, pp. Th–13, OSA, 2011.

[74] R. Ryf, R. Essiambre, A. Gnauck, S. Randel, M. A. Mestre, C. Schmidt, P. J. Winzer, R. Delbue, P. Pupalaikis, A. Sureka, *et al.*, "Space-division multiplexed transmission over 4200 km 3-core microstructured fiber," in *2012 National Fiber Optic Engineers Conference (NFOEC)*, pp. PDP5C–2, OSA, 2012.

[75] R. Ryf, N. Fontaine, B. Guan, R. J. Essiambre, S. Randel, A. Gnauck, S. Chandrasekhar, A. Adamiecki, G. Raybon, B. Ercan, *et al.*, "1705-km transmission over coupled-core fibre supporting 6 spatial modes," in *2014 European Conference on Optical Communication (ECOC)*, pp. 1–3, IEEE, 2014.

[76] R. Ryf, N. Fontaine, B. Guan, B. Huang, M. Esmaeelpour, S. Randel, A. Gnauck, S. Chandrasekhar, A. Adamiecki, G. Raybon, *et al.*, "305-km combined wavelength and mode-multiplexed transmission over conventional graded-index multimode fibre," in *2014 European Conference on Optical Communication (ECOC)*, pp. 1–3, IEEE, 2014.

[77] N. K. Fontaine, R. Ryf, H. Chen, A. V. Benitez, J. A. Lopez, R. A. Correa, B. Guan, B. Ercan, R. P. Scott, S. B. Yoo, *et al.*, "30× 30 MIMO transmission over 15 spatial modes," in *2015 Optical Fiber Communication Conference (OFC)*, pp. Th5C–1, OSA, 2015.

[78] R. Ryf, S. Randel, A. H. Gnauck, C. Bolle, A. Sierra, S. Mumtaz, M. Esmaeelpour, E. C. Burrows, R.-J. Essiambre, P. J. Winzer, *et al.*, "Mode-division multiplexing over 96 km of few-mode fiber using coherent 6 *times* 6 MIMO processing," *Journal of Lightwave technology*, vol. 30, no. 4, pp. 521–531, 2011.

[79] S. Randel, R. Ryf, A. Sierra, P. J. Winzer, A. H. Gnauck, C. A. Bolle, R. J. Essiambre, D. W. Peckham, A. McCurdy, and R. Lingle, "6× 56-Gb/s mode-division multiplexed transmission over 33-km few-mode fiber enabled by 6× 6 MIMO equalization," *Optics Express*, vol. 19, no. 17, pp. 16697–16707, 2011.

[80] T. Hayashi, T. Nagashima, K. Yonezawa, Y. Wakayama, D. Soma, K. Igarashi, T. Tsuritani, and T. Sasaki, "6-mode 19-core fiber for weakly-coupled mode-multiplexed transmission over uncoupled cores," in *2016 Optical Fiber Communication Conference (OFC)*, pp. W1F–4, OSA, 2016.

[81] R. V. Uden, R. A. Correa, E. A. Lopez, F. Huijskens, C. Xia, G. Li, A. Schülzgen, H. D. Waardt, A. Koonen, and C. Okonkwo, "Ultra-high-density spatial division multiplexing with a few-mode multicore fibre," *Nature Photonics*, vol. 8, no. 11, p. 865, 2014.

[82] B. Shariati, J. M. Rivas-Moscoso, M. Dan, S. Ben-Ezra, D. Klonidis, L. Velasco, and I. Tomkos, "Impact of spatial and spectral granularity on the performance of SDM networks based on spatial superchannel switching," *Journal of Lightwave Technology*, vol. PP, no. 99, pp. 1–1, 2017.

[83] H. Tode and Y. Hirota, "Routing, spectrum and core assignment for space division multiplexing elastic optical networks," in *2014 International Telecommunications Network Strategy and Planning Symposium*, pp. 1–7, IEEE, 2014.

[84] Y. Hirota, Y. Hatada, T. Watanabe, and H. Tode, "Dynamic spectrum allocation based on connection alignment for elastic optical networks," in *2015 Asia-Pacific Symposium on Information and Telecommunication Technologies*, pp. 1–3, IEEE, 2015.

[85] B. Shariati, P. S. Khodashenas, J. M. Rivas-Moscoso, S. Ben-Ezra, D. Klonidis, F. Jiménez, L. Velasco, and I. Tomkos, "Evaluation of the impact of different SDM switching strategies in a network planning scenario," in *2016 Optical Fiber Communication Conference (OFC)*, pp. Tu2H–4, OSA, 2016.

[86] F. Pederzolli, D. Siracusa, J. M. Rivas-Moscoso, B. Shariati, E. Salvadori, and I. Tomkos, "Spatial group sharing for SDM optical networks with joint switching," in *2016 International Conference on Optical Network Design and Modeling (ONDM)*, pp. 1–6, IEEE, 2016.

[87] J. M. Rivas-Moscoso, B. Shariati, A. Mastropaolo, D. Klonidis, and I. Tomkos, "Cost benefit quantification of SDM network implementations based on spatially integrated network elements," in *2016 European Conference on Optical Communication (ECOC)*, pp. 1–3, VDE, 2016.

[88] R. Rumipamba-Zambrano, J. Perelló, J. M. Gené, and S. Spadaro, "Capacity quantification of joint-switching-enabled flex-grid/SDM optical backbone networks," in *2017 Optical Fiber Communications Conference and Exhibition (OFC)*, pp. 1–3, IEEE, 2017.

[89] D. Siracusa, F. Pederzolli, D. Klonidisz, V. Lopezy, and E. Salvadori, "Resource allocation policies in SDM optical networks," in *2015 International Conference on Optical Network Design and Modeling (ONDM)*, pp. 168–173, IEEE, 2015.

[90] K. Morita and K. Hirata, "Dynamic spectrum allocation method for reducing crosstalk in multi-core fiber networks," in *2017 International Conference on Information and Networking (ICOIN)*, pp. 686–688, IEEE, 2017.

[91] Y. Tan, R. Zhu, H. Yang, Y. Zhao, J. Zhang, Z. Liu, Q. Qu, and Z. Zhou, "Crosstalk-aware provisioning strategy with dedicated path protection for elastic multi-core fiber networks," in *2016 International Conference on Optical Communications and Networks (ICOCN)*, pp. 1–3, IEEE, 2016.

[92] Y. Zhao and J. Zhang, "Crosstalk-aware cross-core virtual concatenation in spatial division multiplexing elastic optical networks," *Electronics Letters*, vol. 52, no. 20, pp. 1701–1703, 2016.

[93] S. Fujii, Y. Hirota, H. Tode, and K. Murakami, "On-demand spectrum and core allocation for multi-core fibers in elastic optical network," in *2013 Optical Fiber Communication Conference (OFC)*, pp. OTh4B–4, OSA, 2013.

[94] S. Fujii, Y. Hirota, and H. Tode, "Dynamic resource allocation with virtual grid for space division multiplexed elastic optical network," in *2013 European Conference and Exhibition on Optical Communication (ECOC)*, pp. 1–3, IET, 2013.

[95] A. Muhammad, G. Zervas, D. Simeonidou, and R. Forchheimer, "Routing, spectrum and core allocation in flexgrid SDM networks with multi-core fibers," in *2014 International Conference on Optical Network Design and Modeling (ONDM)*, pp. 192–197, IEEE, 2014.

[96] S. Fujii, Y. Hirota, H. Tode, and K. Murakami, "On-demand spectrum and core allocation for reducing crosstalk in multicore fibers in elastic optical networks," *Journal of Optical Communications and Networking*, vol. 6, pp. 1059–1071, Dec 2014.

[97] S. Fujii, Y. Hirota, T. Watanabe, and H. Tode, "Dynamic spectrum and core allocation with spectrum region reducing costs of building modules in AoD nodes," in *2014 International Telecommunications Network Strategy and Planning Symposium*, pp. 1–6, IEEE, 2014.

[98] A. Muhammad, G. Zervas, G. Saridis, E. H. Salas, D. Simeonidou, and R. Forchheimer, "Flexible and synthetic SDM networks with multi-core-fibers implemented by programmable ROADMs," in *2014 European Conference on Optical Communication (ECOC)*, pp. 1–3, IEEE, 2014.

[99] Y. Li, N. Hua, and X. Zheng, "Routing, wavelength and core allocation planning for multi-core fiber networks with MIMO-based crosstalk suppression," in *2015 Opto-Electronics and Communications Conference (OECC)*, pp. 1–3, IEEE, 2015.

[100] A. Muhammad, G. Zervas, and R. Forchheimer, "Resource allocation for space-division multiplexing: Optical white box versus optical black box networking," *Journal of Lightwave Technology*, vol. 33, no. 23, pp. 4928–4941, 2015.

[101] P. M. Moura and N. L. D. Fonseca, "Routing, core and spectrum assignment based on connected component labelling for SDM optical networks," in *2016 IEEE International Conference on Communications (ICC)*, pp. 1–6, IEEE, 2016.

[102] L. Zhang, N. Ansari, and A. Khreishah, "Anycast planning in space division multiplexing elastic optical networks with multi-core fibers," *IEEE Communications Letters*, vol. 20, no. 10, pp. 1983–1986, 2016.

[103] R. Zhu, Y. Zhao, H. Yang, Y. Tan, H. Chen, J. Zhang, and J. P. Jue, "Dynamic virtual optical network embedding in spectral and spatial domains over elastic optical networks with multicore fibers," *Optical Engineering*, vol. 55, no. 8, p. 086108, 2016.

[104] R. Zhu, Y. Zhao, J. Zhang, H. Yang, Y. Tan, and J. P. Jue, "Multi-dimensional resource virtualization in spectral and spatial domains for inter-datacenter optical networks," in *2016 Optical Fiber Communications Conference and Exhibition (OFC)*, pp. 1–3, IEEE, 2016.

[105] H. Tode and Y. Hirota, "Routing, spectrum and core assignment on SDM optical networks," in *2016 Optical Fiber Communications Conference and Exhibition (OFC)*, pp. 1–3, IEEE, 2016.

[106] Y. Li, Y. Li, N. Hua, and X. Zheng, "Shared backup path protection in multi-core fiber networks with MIMO-based crosstalk suppression," in *2016 Optical Fiber Communication Conference (OFC)*, pp. Tu2H–7, OSA, 2016.

[107] R. Rumipamba-Zambrano, J. Perelló, A. Pagès, J. M. Gené, and S. Spadaro, "Influence of the spatial super channel guard-band width on the performance of dynamic flex-grid/SDM optical core networks," in *2016 International Conference on Transparent Optical Networks (ICTON)*, pp. 1–4, IEEE, 2016.

[108] R. Zhu, Y. Zhao, H. Yang, Y. Tan, X. Yu, G. Gao, J. Zhang, N. Wang, and J. P. Jue, "Crosstalk-aware virtual optical network embedding (VONE) in spatial division multiplexing enabled elastic optical networks with multi-core fibers," in *2016 European Conference on Optical Communication (ECOC)*, pp. 1–3, VDE, 2016.

[109] A. Muhammad, M. Furdek, G. Zervas, and L. Wosinska, "Filterless networks based on optical white boxes and SDM," in *2016 European Conference on Optical Communication (ECOC)*, pp. 1–3, VDE, 2016.

[110] M. N. Dharmaweera, L. Yan, M. Karlsson, and E. Agrell, "Nonlinear-impairments-and crosstalk-aware resource allocation schemes for multicore-fiber-based flexgrid networks," in *2016 European Conference on Optical Communication (ECOC)*, pp. 1–3, VDE, 2016.

[111] Z. Shi, Y. Zhao, X. Yu, Y. Li, J. Zhang, C. Liu, G. Zhang, and Z. Liu, "Contaminated area-based RSCA algorithm for super-channel in flex-grid enabled SDM networks," in *2016 Asia Communications and Photonics Conference*, pp. ATh2E–4, OSA, 2016.

[112] Q. Yao, H. Yang, Y. Zhao, R. Zhu, J. Zhang, and J. Wu, "Crosstalk-aware routing, spectrum, and core assignment in elastic optical networks with multi-core fibers," in *2016 Asia Communications and Photonics Conference*, pp. ATh2C.1, OSA, 2016.

[113] Y. Tan, H. Yang, R. Zhu, Y. Zhao, J. Zhang, Z. Liu, Q. Ou, and Z. Zhou, "Distance adaptive routing, core and spectrum allocation in space division multiplexing optical networks with multi-core fibers," in *2016 Asia Communications and Photonics Conference*, pp. AF2A–159, OSA, 2016.

[114] H. Tode and Y. Hirota, "Routing, spectrum, and core and/or mode assignment on space-division multiplexing optical networks," *Journal of Optical Communications and Networking*, vol. 9, no. 1, pp. A99–A113, 2017.

[115] Y. Zhao, R. Tian, X. Yu, J. Zhang, and J. Zhang, "An auxiliary graph based dynamic traffic grooming algorithm in spatial division multiplexing enabled elastic optical networks with multi-core fibers," *Optical Fiber Technology*, vol. 34, pp. 52–58, 2017.

[116] C. Rottondi, P. Boffi, P. Martelli, M. Tornatore, and A. Pattavina, "Optimal resource allocation in distance-adaptive few-modes backbone networks with flexible grid," in *2015 Asia Communications and Photonics Conference*, pp. AS4H–2, OSA, 2015.

[117] H. Huang, S. Huang, S. Yin, M. Zhang, J. Zhang, and W. Gu, "Virtual network provisioning over space division multiplexed optical networks using few-mode fibers," *Journal of Optical Communications and Networking*, vol. 8, no. 10, pp. 726–733, 2016.

[118] C. Rottondi, P. Boffi, P. Martelli, and M. Tornatore, "Routing, modulation format, baud rate and spectrum allocation in optical metro rings with flexible grid and few-mode transmission," *Journal of Lightwave Technology*, vol. 35, no. 1, pp. 61–70, 2016.

[119] Y. Yang, X. Chen, H. Yan, B. Hua, J. Li, Y. Hao, Z. Chen, and Y. He, "A scattered-spectrum-scan routing and spectrum allocation scheme for spatial-division-multiplexing optical networks based on blocking OXCs," in *2016 Asia Communications and Photonics Conference*, pp. ATh2E–2, OSA, 2016.

[120] Y. Li, N. Hua, and X. Zheng, "A capacity analysis for space division multiplexing optical networks with MIMO equalization," in *2017 Optical Fiber Communication Conference (OFC)*, pp. Th2A–15, OSA, 2017.

[121] S. Randel, P. J. Winzer, M. Montoliu, and R. Ryf, "Complexity analysis of adaptive frequency-domain equalization for MIMO-SDM transmission," in *2013 European Conference and Exhibition on Optical Communication (ECOC)*, pp. 1–3, IET, 2013.

[122] M. Jinno, "Spatial channel network (SCN): Opportunities and challenges of introducing spatial bypass toward the massive SDM era," *Journal of Optical Communications and Networking*, vol. 11, no. 3, pp. 1–14, 2019.

[123] R. Rumipamba-Zambrano, F. J. Moreno-Muro, J. Perelló, P. Pavón-Mariño, and S. Spadaro, "Space continuity constraint in dynamic flex-grid/SDM optical core networks: An evaluation with spatial and spectral super-channels," *Computer Communications*, vol. 126, pp. 38–49, 2018.

[124] K. Imamura, Y. Tsuchida, K. Mukasa, R. Sugizaki, K. Saitoh, and M. Koshiba, "Investigation on multi-core fibers with large Aeff and low micro bending loss," *Optics Express*, vol. 19, no. 11, pp. 10595–10603, 2011.

[125] T. Hayashi, T. Nagashima, O. Shimakawa, T. Sasaki, and E. Sasaoka, "Crosstalk variation of multi-core fibre due to fibre bend," in *2010 European Conference on Optical Communication (ECOC)*, pp. 1–3, IEEE, 2010.

[126] T. Hayashi, T. Taru, O. Shimakawa, T. Sasaki, and E. Sasaoka, "Low-crosstalk and low-loss multi-core fiber utilizing fiber bend," in *2011 Optical Fiber Communication Conference and Exposition, and the National Fiber Optic Engineers Conference (OFC/NFOEC)*, pp. 1–3, IEEE, 2011.

[127] T. Hayashi, T. Taru, O. Shimakawa, T. Sasaki, and E. Sasaoka, "Ultra-low-crosstalk multi-core fiber feasible to ultra-long-haul transmission," in *2011 National Fiber Optic Engineers Conference (NFOEC)*, p. PDPC2, OSA, 2011.

[128] T. Hayashi, T. Taru, O. Shimakawa, T. Sasaki, and E. Sasaoka, "Design and fabrication of ultra-low crosstalk and low-loss multi-core fiber," *Optics Express*, vol. 19, no. 17, pp. 16576–16592, 2011.

[129] K. Takenaga, Y. Arakawa, S. Tanigawa, N. Guan, S. Matsuo, K. Saitoh, and M. Koshiba, "Reduction of crosstalk by trench-assisted multi-core fiber," in *2011 Optical Fiber Communication Conference (OFC)*, p. OWJ4, OSA, 2011.

[130] K. Takenaga, Y. Arakawa, S. Tanigawa, G. Ning, S. Matsuo, K. Saitoh, and M. Koshiba, "An investigation on crosstalk in multi-core fibers by introducing random fluctuation along

longitudinal direction," *IEICE Transactions on Communications*, vol. 94, no. 2, pp. 409–416, 2011.

[131] M. Yang, Y. Zhang, and Q. Wu, "Routing, spectrum, and core assignment in SDM-EONs with MCF: Node-arc ILP/MILP methods and an efficient XT-aware heuristic algorithm," *Journal of Optical Communications and Networking*, vol. 10, no. 3, pp. 195–208, 2018.

[132] R. D. Rumipamba Zambrano, "Contributions to network planning and operation of flex-grid/SDM optical core networks," 2019.

[133] J. M. Rivas-Moscoso, S. Ben-Ezra, P. S. Khodashenas, D. M. Marom, D. Klonidis, P. Zakynthinos, and I. Tomkos, "Cost and power consumption model for flexible super-channel transmission with all-optical sub-channel add/drop capability," in *2015 International Conference on Transparent Optical Networks (ICTON)*, pp. 1–4, IEEE, 2015.

[134] S. Randel, "Space-division multiplexed transmission," in *2013 Optical Fiber Communication Conference and National Fiber Optic Engineers Conference (OFC/NFOEC)*, pp. OW4F.1, 2013.

[135] M. Jinno, "Elastic optical networking: Roles and benefits in beyond 100-Gb/s era," *Journal of Lightwave Technology*, vol. 35, no. 5, pp. 1116–1124, 2017.

[136] P. J. Winzer, "Scaling optical fiber networks: Challenges and solutions," *Optics and Photonics News*, vol. 26, no. 3, pp. 28–35, 2015.

[137] M. Yang, Q. Wu, and Y. Zhang, "Joint assignment of spatial granularity, routing, modulation, and spectrum in SDM-EONs: Minimizing the network CAPEX considering spectrum, WSS, and laser resources," *Journal of Lightwave Technology*, vol. 36, no. 18, pp. 4153–4166, 2018.

[138] Online, "AMPL Gurobi" Available: Http://www.gurobi.com, 2016.

[139] H. Thomas, E. Charles, L. Ronald, and S. Clifford, *Introduction to Algorithms, Third Edition*, pp. 359–370. Massachusetts Institute of Technology, 2009.

[140] É. Archambault, D. O'Brien, C. Tremblay, F. Gagnon, M. P. Bélanger, and É. Bernier, "Design and simulation of filterless optical networks: Problem definition and performance evaluation," *Journal of Optical Communications and Networking*, vol. 2, no. 8, pp. 496–501, 2010.

[141] A. Morea, J. Perelló, S. Spadaro, D. Verchère, and M. Vigoureux, "Protocol enhancements for "greening" optical networks," *Bell Labs Technical Journal*, vol. 18, no. 3, pp. 211–230, 2013.

[142] L. Song and B. Mukherjee, "Accumulated-downtime-oriented restoration strategy with service differentiation in survivable WDM mesh networks," *Journal of Optical Communications and Networking*, vol. 1, no. 1, pp. 113–124, 2009.

[143] S. D. Maesschalck, D. Colle, I. Lievens, M. Pickavet, P. Demeester, C. Mauz, M. Jaeger, R. Inkret, B. Mikac, and J. Derkacz, "Pan-European optical transport networks: An availability-based comparison," *Photonic Network Communications*, vol. 5, no. 3, pp. 203–225, 2003.

[144] W. D. Grover, *Mesh-based survivable networks: Optionsand strategies for optical, MPLS, SONET, and ATM Networking*. PTR Prentice Hall, 2004.

[145] J. Perelló, J. M. Gené, A. Pagès, J. A. Lazaro, and S. Spadaro, "Flex-grid/SDM backbone network design with inter-core XT-limited transmission reach," *Journal of Optical Communications and Networking*, vol. 8, no. 8, pp. 540–552, 2016.

[146] W. Klaus, B. J. Puttnam, R. S. Luís, J. Sakaguchi, J. M. D. Mendinueta, Y. Awaji, and N. Wada, "Advanced space division multiplexing technologies for optical networks," *Journal of Optical Communications and Networking*, vol. 9, no. 4, pp. C1–C11, 2017.

[147] B. G. Bathula and J. M. H. Elmirghani, "Constraint-based anycasting over optical burst switched networks," *Journal of Optical Communications and Networking*, vol. 1, no. 2, pp. A35–A43, 2009.

[148] L. Velasco, A. Jirattigalachote, M. Ruiz, P. Monti, L. Wosinska, and G. Junyent, "Statistical approach for fast impairment-aware provisioning in dynamic all-optical networks," *Journal of Optical Communications and Networking*, vol. 4, no. 2, pp. 130–141, 2012.

[149] M. Jinno, "Spatial channel network (SCN) architecture employing growable and reliable spatial channel cross-connects toward massive SDM era," in *2018 Photonics in Switching and Computing (PSC)*, pp. 1–3, IEEE, 2018.